TAMPEREEN TEKNILLINEN YLIOPISTO
TAMPERE UNIVERSITY OF TECHNOLOGY

Kirsi Katariina Holli

Texture Analysis as a Tool for Tissue Characterization in Clinical MRI

Julkaisu 988 • Publication 988

Tampere 2011

Tampereen teknillinen yliopisto. Julkaisu 988
Tampere University of Technology. Publication 988

Kirsi Katariina Holli

Texture Analysis as a Tool for Tissue Characterization in Clinical MRI

Thesis for the degree of Doctor of Science in Technology to be presented with due permission for public examination and criticism in Sähkötalo Building, Auditorium S4, at Tampere University of Technology, on the 28th of October 2011, at 12 noon.

Tampereen teknillinen yliopisto - Tampere University of Technology
Tampere 2011

Supervisors

Professor Hannu Eskola
Department of Biomedical Engineering, Tampere University of Technology
Tampere, Finland
Medical Imaging Centre, Pirkanmaa Hospital District
Tampere, Finland

Professor Seppo Soimakallio
Medical Imaging Centre, Pirkanmaa Hospital District
Tampere, Finland
Faculty of Medicine, University of Tampere
Tampere, Finland

ISBN 978-952-15-2656-5 (printed)
ISBN 978-952-15-2698-5 (PDF)
ISSN 1459-2045

To Mom and Dad

If you can imagine it, you can achieve it;
if you can dream it, you can become it.
- William Arthur Ward

ABSTRACT

Magnetic resonance imaging (MRI) is a valuable tool for medical diagnosis, as it is a non-invasive technique that allows superior visualisation of soft tissues. Because of the vast growth of the acquired information from medical images the development of new computer-aided diagnosis (CAD) systems has become increasingly important. The application of texture analysis (TA) in the diagnostic interpretation of MR images has become a rapidly expanding field of research. The goal of this thesis was to test the feasibility of texture analysis methods in diagnostic radiology.

In this dissertation, texture analysis was applied to three different clinical materials. This study investigates whether the texture could be used to discriminate breast cancer and visible and non-visible changes in brain MRI of mild traumatic brain injuries and multiple sclerosis patients and, if so, which is the optimal texture analysis method for these applications.

This study showed that TA could provide a quantitative method to aid radiologists in the detection and classification of pathological findings. A case-specific selection of the texture parameters from histogram-, co-occurrence-, run-length- and wavelet- based methods would be the optimal solution for the evaluated clinical applications. However, larger study samples are needed to further validate these findings. Another conclusion was that the texture analysis process should be simplified considerably and implemented in other CAD systems to be considered for clinical use in the future.

ACKNOWLEDGEMENTS

The work presented in this thesis was performed at the Department of Radiology, Medical Imaging Centre, Tampere University Hospital, and the Department of Biomedical Engineering, Tampere University of Technology from 2008-2011. This study was supported by the Jenny and Antti Wihuri Foundation, the Instrumentarium Science Foundation, Competitive Research Funding of the Tampere University Hospital, Pirkanmaa Hospital District and the Science Foundation of the City of Tampere.

Though only my name appears on the cover of this thesis, a great many people have contributed to its production with their help, support and guidance. I owe my gratitude to all those people who have made this dissertation possible.

I want to express my most sincere gratitude to my supervisors, Professor Hannu Eskola and Professor Seppo Soimakallio, for giving me the opportunity to prepare this thesis as a member of the Tissue Characterization Research group and for providing me with this opportunity to work in such excellent research facilities. I am thankful for their encouragement, guidance and support from the initial to the final stages, which enabled me to develop an understanding of the subject.

I am especially grateful to Docent Prasun Dastidar and Anna-Leena Lääperi, MD for their endless encouragement, guidance and insightful comments throughout this dissertation process. I would also like to thank hospital physicist Pertti Ryymin for his guidance and for carefully reading and commenting on my manuscripts.

I would like to express my sincerest gratitude to all co-authors of the original articles cited in this thesis for their professional help. My sincere thanks go to Minna Wäljas, MSc, for her help and valuable advice during my work. I also thank Tiina Luukkaala, MSc, for her help with the statistics. Warm thanks also go to Ms. Marjut Keskivinkka, and the personnel of the Department of Radiology, Medical Imaging Centre, and all participating departments for their assistance with data collection and radiological imaging. I also warmly thank all of the participants who volunteered for these studies.

I thank the official reviewers, Professors Hannu Manninen and Andrzej Materka, for their excellent commentary on this thesis.

Getting through my dissertation required more than just academic support, and I have many people to thank for listening to me and helping me over the past years. I wish to give a special thanks to my great friends and colleagues at Komentokeskus: Lara Harrison, MSc, MD, Minna Sikiö, MSc and Maija Rossi, MSc, who provided their friendship and often some much-needed humour to get through this process. I would also like to thank all my friends in ballet for offering an escape from the scientific world. My warm thanks go to all my friends: thanks for being there!

Most importantly, none of this could have happened without my family. I owe them the deepest gratitude for their understanding and support. I would especiallylike to express my heartfelt gratitude to my parents Kaija and Heimo for being a constant source of love and for their support and strength throughout this process. I also thank my brother Kimmo and his fiancée Tiina for their encouragement and support.

And finally, I would like to thank Magnus for his support, encouragement, patience and unwavering love. And thank to my beloved son Jerry, the light of my life, who has been an infinite source of energy and motivation.

Tampere, October 2011

Kirsi Holli

TABLE OF CONTENTS

LIST OF SYMBOLS AND ABBREVIATIONS

ACC	Average correlation coefficients
AD	Alzheimer's disease
ADC	Apparent diffusion coefficient
ANN	Artificial neural network
AR	Autoregressive
AUC	Area under the curve
BIRADS	Radiology Breast Imaging Reporting and Data System
BMRI	Breast magnetic resonance imaging
CAD	Computer-aided diagnosis
CC	Corpus callosum
COM	Co-occurrence matrix
COST	European Cooperation in Science and Technology
CSF	Cerebrospinal fluid
CT	Computed tomography
DCE-MRI	Dynamic contrast-enhanced MR imaging
DCIS	Ductal carcinoma in situ
DICOM	Digital imaging and communications in medicine file format
DTI	Diffusion tensor imaging
DWI	Diffusion-weighted imaging
EUSOMA	European Society of Breast Cancer Specialists
F	Fisher coefficient
FA	Fractional anisotropy
FFE	Fast field echo
FID	Free induction decay
fMRI	Functional magnetic resonance imaging
FLAIR	Fluid attenuated inversion recovery
FSE	Fast spin echo
DTPA	Diethylenetriaminepentaacetic acid

GCS	Glasgow Coma Scale
GE	General Electric
GLCM	Grey level co-occurrence matrix
GRASS	Gradient acquisition in a steady state
GRE	Gradient echo sequence
HS	Hippocampal sclerosis
IDC	Invasive ductal carcinoma
ILC	Invasive lobular carcinoma
IR	Inversion recovery
k-NN	k-nearest neighbour
LCIS	Lobular carcinoma in situ
LDA	Linear discriminant analysis
LRA	Linear regression analysis
MI	Mutual information
MPR	Magnetization prepared gradient echo/Multi-Planar Reconstruction
MRI	Magnetic resonance imaging
MRS	Magnetic resonance spectroscopy
MS	Multiple sclerosis
MTBI	Mild traumatic brain injury
MTLE	Mesial temporal lobe epilepsy
NAWM	Normal-appearing white matter
NDA	Non-linear discriminant analysis
NMR	Nuclear magnetic resonance
PCA	Principal component analysis
PD	Spin density
POE	Classification error probability
RDA	Raw data analysis
RF	Radiofrequency
RLM	Run-length matrix
ROC	Receiver operating characteristic
ROI	Region of interest
SPGR	Spoiled gradient-recalled echo
SE	Spin echo

SGLD	Spatial grey level dependency
SPECT	Single-photon emission computed tomography
STIR	Short TI inversion recovery
TA	Texture analysis
TBI	Traumatic brain injury
TE	Echo time
TR	Repetition time
TSE	Turbo spin echo
T1	Longitudinal relaxation time
T2	Transverse relaxation time
T2*	T2*-relaxation time
WM	White matter
2D	Two-dimensional
3D	Three-dimensional
4D	Four-dimensional

LIST OF ORIGINAL PUBLICATIONS

This Thesis is based on the following original articles, referred to in the text by their Roman numerals (I-V).

I Holli KK, Lääperi A-L, Harrison L, Dastidar P, Soimakallio S, Eskola H. *Detection of characteristic texture parameters in breast MRI*. IFBME Proceedings. 4th European Conference of the International Federation for Medical and Biological Engineering, Antwerp, Belgium. 2008; 22: 517-520.

II Holli KK, Lääperi A-L, Harrison L, Luukkaala T, Toivonen T, Ryymin P, Dastidar P, Soimakallio S, Eskola H. *Characterization of breast cancer types by texture analysis of magnetic resonance images.* Acad Radiol. 2010;17(2): 135-141.

III Holli KK, Harrison L, Dastidar P, Wäljas M, Liimatainen S, Luukkaala T, Öhman J, Soimakallio S, Eskola H. *Texture analysis of MR images of patients with mild traumatic brain injury*. BMC Med Imaging. 2010; (12)10:8.

IV Holli KK, Wäljas M, Harrison L, Liimatainen S, Luukkaala T, Ryymin P, Eskola H, Soimakallio S, Öhman J, Dastidar P. *Mild traumatic brain injury tissue texture analysis correlated to neuropsychological and DTI findings.* Acad Radiol. 2010; 17(9):1096-1102.

V Harrison LC, Raunio M, Holli KK, Luukkaala T, Savio S, Elovaara I, Soimakallio S, Eskola HJ, Dastidar P. *MRI texture analysis in multiple sclerosis: toward a clinical analysis protocol.* Acad Radiol. 2010; 17(6):696-707.

The author's contribution

The author has performed the texture data collection, data classification, analyzing the results and drafted the publications I-IV. The studies were designed with a co-operation with co-worker Lara Harrison. In publication V the author participated in technical aspects of texture analysis and participated in manuscript modifications. When writing the publications the author received valuable comments from all co-authors.

1. INTRODUCTION

Medical imaging has become a crucial part of the biomedical sciences, not only for diagnosis but also for treatment planning and follow-up. Just 50 years ago, imaging of the human body was very limited. Since then, with the advancement of computers and technology, we now have a wide range of techniques for examining different aspects of the human body in exceptional detail. Computer-aided visualisation methods for medical imaging are being continually developed to fully exploit the information that has been acquired. The capacity to extract quantitative information from images is becoming increasingly important.

Magnetic resonance imaging (MRI) is an imaging technique used primarily in medical settings to produce high-quality images of the inside of the human body (Hornak, 2002). MRI is a unique and powerful tool for medical diagnosis because it is a non-invasive technique that allows visualisation of soft tissues that is superior to other modalities. The basic theory of magnetic resonance (MR) was introduced in the mid-1940s by Felix Bloch and Edward Mills Purcell (Bloch, 1952; Purcell, 1952). In the beginning of the 1970s, Lauterbur and associates presented methods that made producing MR images possible and led to applications of magnetic resonance in medical imaging. Later, Mansfield further developed the utilisation of gradients in the magnetic field and showed how the signals could be mathematically analysed, thus making it possible to develop a useful diagnostic imaging technique. Recent technologies offer a continuous development of imaging accuracy and quality. MRI is now a routine method within medical diagnostics and is used to examine almost all organs of the body.

There is a growing interest in using MRI for early detection of many diseases, such as breast cancer and neurological disorders. A qualitative analysis of MR images is based on the expert radiologist's skills to identify the parameters that characterise and classify the lesion on the basis of visual inspection. A further classification method, called quantitative analysis, consists of the use of mathematical models to quantify and characterise the region of interest. Until recently, little attention had been paid to the diagnostic potential of texture analysis in MR images. Texture analysis (TA) of MR images is a quantitative method that can be used to detect and qualify structural abnormalities in different tissues (Lerski et al., 1993). TA may be sensitive enough to detect subtle changes in MRIs and to extract more information than from visual assessment. In this thesis, we concentrate on evaluating texture analysis as a supplementary method for diagnostic radiology.

2. METHODOLOGICAL BACKGROUND

2.1 Magnetic resonance imaging

MRI enables non-invasive imaging of patient anatomy through the measurement of emitted nuclear magnetic resonance (NMR) signals. MRI measures the spatial distribution of specific nuclear spins in the body. Electrical signals from the spins are measured using precessional motion of the proton spins after they are excited by the radio frequency (RF) irradiated in a static magnetic field. In the presence of the external magnetic field, atomic nuclei possessing a magnetic dipole moment will precess around the external magnetic field. The frequency of this precessing motion is called the Larmor frequency. Nuclei with different gyromagnetic ratios will precess with different Larmor frequencies if placed in the same magnetic field. The sum of the nuclei precessing around the direction of the external field is equivalent to a single magnetic moment, called the net magnetisation. Following the RF pulse, the net magnetisation is tipped away from its axis, creating a vector rotating at the Larmor frequency. This rotating magnetic vector causes a small current to flow in the detector coil, giving rise to the MRI signal. The phase and frequency of the signal are a direct consequence of the local magnetic field experienced by the nuclei. By superimposing a magnetic field gradient on the external magnetic field, the frequency of the MRI signal will shift in accordance with its position along the gradient; therefore, its position in space is defined. Gradient magnetic fields are normally generated by passing an electric current through specially wound electric coils that reside within the main magnetic field, which can produce linearly varying magnetic fields. These gradients are oriented in directions *x*, *y*, and *z* to define the volume elements that resonate at known frequencies. To obtain a complete picture, the local conditions are superimposed in programmed sequences, which are stored. These sequences define the application times of the gradients, the excitation times of the nuclei by the RF pulses and the reading or acquisition times of the image data.

2.1.1 Relaxation times

The duration of the return to equilibrium of the overall magnetic moment of a considered region and the decrease of the signal are dependent on two important factors: the recovery of the longitudinal magnetisation, described by the time constant T1 and called the spin-lattice relaxation; and the decay of transverse magnetisation – the

magnetisation that is flipped into the transverse plane, which is described by the time constant T2 or T2* and is called the transverse relaxation or the T2-decay (Hendrick, 2008). Different tissues will have different relaxation times because of their different chemical constitutions and different physical states. The T1 constant indicates how quickly the spinning nuclei will emit their absorbed RF into the surrounding tissue. The T1 time is a contrast-determining tissue parameter. T2 describes the lifetime of the spin echo signal and is usually used to distinguish pathological tissue from normal tissue. T2* describes the decay rate of free induction decay (FID) (Weishaupt et al., 2008; Brown and Semelka, 2010). MRI is applicable in diagnosing various diseases because T1 and T2 of pathological tissue generally become longer than in normal tissues. Tissues with long T1 values are dark on T1-weighted images, whereas tissues with long T2 values appear bright on T2-weighted images (Weishaupt et al., 2008).

2.1.2 NMR signal

There are two types of NMR signal generally used in MRI: free induction decay (FID) and spin echo (SE). FID is the simplest signal obtained from an MR sequence. The FID signal is produced by the freely rotating, decaying transverse magnetisation immediately following a 90º RF pulse. This decay is dominated by T2*, which makes the FID very short in general. The SE is a way of recovering the T2 information that is masked by T2*. It eliminates the influence of T2*; therefore, an image based on the signal height of the echo is said to be T2-weighted. In this sequence, a 180° pulse is applied some time after the original 90° pulse, and some of the signal, originally lost after the FID, is recovered as a type of echo that comes and goes (Brown and Semelka, 2010).

2.1.3 Pulse sequences

The development of new and faster imaging sequences has enabled more detailed visualisation of different anatomical structures and pathologies. Each sequence is a combination of RF pulses and gradients. The main sequence families are spin echo (SE) sequences, inversion recovery (IR) sequences and gradient echo sequences (GRE) with their several variations (Weishaupt et al., 2008).

One of the most important measuring techniques in clinical diagnosis is the spin echo sequence, in which 90° and 180° RF pulses produce the spin echo signal. In addition, gradients are used in the x, y, and z directions to localise the signal. This technique allows measurement of the three relevant MRI tissue parameters: spin density (PD) and relaxation times T1 and T2, which are the most responsible for tissue contrast and texture. Different types of images include T1-, T2-, PD-weighted images, and fluid-attenuated inversion recovery (FLAIR) images. By controlling the acquisition

parameters of the scan, different image weightings may be obtained, allowing for different and improved image contrast between different types of tissue. The duration, frequency and the repetition times (TR), echo time (TE) and the energy of the RF pulse can be adjusted to generate the basic MR imaging types. These imaging parameters are used to control contrast between tissues. TR is the time between successive applications of RF excitation pulses. It affects T1 contrast, scanning time, minimum echo time and the number of slices in multi-slice imaging. The TR controls the extent of recovery of the longitudinal magnetisation. TE is the time between the excitation pulse and the formation of the echo. It affects T2 contrast, the minimum possible value for TR, the minimum bandwidth, and the sensitivity to dephasing. A long TE allows more transverse relaxation to occur before measuring the signal. In clinical use, the SE sequence is often performed as a fast spin echo (FSE) sequence, where multiple spin echoes are collected during the same TR period. This makes the sequence faster than the conventional SE sequence.

Inversion recovery pulse sequences are used to give heavy T1-weighting. They are generally applied in T1-weighted or fat-suppressed imaging (Weishaupt et al., 2008). An IR sequence is an SE sequence with an additional 180° inversion pulse. By applying this 180° pulse at the beginning of a sequence, it is possible to invert the alignment of the spins from being aligned with the magnetic field to being anti-aligned. If the spins are then left to themselves, they return back to equilibrium, which is the aligned position. As a consequence, the magnetisation goes from negative, through zero, to positive; thus, the magnetisation recovers from inversion (and hence the name inversion recovery). Two IR techniques are widely used in clinical applications: short TI inversion recovery (STIR) and FLAIR sequences (Weishaupt et al., 2008). The STIR (Tofts, 2003) sequence can be used for fat suppression, where a relatively short inversion time is used to null the fat signal while maintaining water and soft tissue signals. The main disadvantage of this sequence is the low signal-to-noise ratio because the magnetisation of all the other tissues is also close to zero. With an additional radio frequency pulse and additional manipulation of the magnetic gradients, a T2 sequence can be converted to a FLAIR sequence, in which free water is now dark, but oedematous tissues remain bright. FLAIR is used to achieve heavy T2 weighting without signal from the cerebrospinal fluid (CSF). The aim of a FLAIR sequence is to suppress liquid signals by inversion-recovery at an adapted TI. Damaged tissues tend to develop oedemas, which makes a T2 sequence sensitive for pathology; thus, one is generally able to distinguish pathological tissue from normal tissue (Tofts, 2003). With an additional radio frequency pulse, and additional manipulation of the magnetic gradients, a T2 sequence can be converted to a FLAIR sequence, in which free water is now dark, but oedematous tissues remain bright. This sequence is a particularly good approach for evaluating the brain for demyelinating diseases (Hori et al., 2003), such as multiple sclerosis, as the whitest voxels correspond to demyelinated white matter.

GRE sequences utilise FID signal and are characterised by the sequence parameters TR, TE and flip angle. GRE sequence is also known as fast field-echo (FFE) sequence (Weishaupt et al., 2008). The gradient echo sequence is the simplest type of MRI sequence. The gradient echo sequence differs from the spin echo sequence in regard to the flip angle, which is usually below 90°, and the absence of a 180° RF rephasing pulse. The echo is produced by applying a frequency-encoding gradient with negative polarity to destroy the phase coherence of the precessing spins (Weishaupt et al., 2008). The gradient is then reversed, and the spins rephrase to form an echo. A flip angle lower than 90° decreases the amount of magnetisation tipped into the transverse plane. The effect of a low-flip angle excitation and the absence of the 180° refocusing pulse allow for a shorter TR/TE and thus decrease the scan time.

One of the confusing aspects of MRI is the variety of pulse sequences available. All of these main sequences, SE, IR and GRE, have a number of variations. In addition, similar sequences may be known by a variety of names depending of the manufacturer. Some of the common names for regularly applied pulse sequences in clinical use by different manufacturers are presented in Table 1.

Table 1. *Common names for regularly applied pulse sequences in clinical use by three manufacturers (Siemens, GE and Philips).*

	Siemens	GE	Philips
Spin echo pulse sequences	Single spin echo	Spin echo	Spin echo
	Double echo	Multi-echo multiplanar	Modified spin echo
	Turbo spin echo (TSE)	Variable echo multiplanar Fast spin echo (FSE)	Multiple spin echo Turbo spin echo (TSE)
	Half Fourier acquisition turbo spin echo	Single-shot FSE	Ultrafast spin echo
Gradient echo pulse sequences	Fast low-angle shot (FLASH)	Spoiled gradient-recalled acquisition in a steady state (GRASS), fast spoiled GRASS, multiplanar spoiled GRASS, fast multiplanar spoiled GRASS	T1-contrast-enhanced fast-field echo (FFE)
	Fast imaging with steady-state precession	GRASS, fast GRASS, multiplanar GRASS, fast multiplanar GRASS, fast imaging employing steady-state acquisition	FFE
	Turbo FLASH, magnetisation prepared rapid acquisition gradient echo (MPR)	IR-prepared fast GRASS	T2 contrast enhanced FFE Turbo field echo
Inversion recovery pulse sequences	Standard inversion recovery	Multiplanar IR	IR, IR turbo spin echo
	Echo train inversion recovery	Fast multiplanar IR	
	Interleaved excitation	Nonsequential (standard)	
	Magnitude reconstruction Phase sensitive reconstruction	Absolute value, magnitutude	Modulus real

(Brown and Semelka, 2010)

2.1.4 Techniques for special applications

Breast MRI (BMRI) has emerged as a promising technique for detecting, diagnosing, and staging breast cancer. In recent years, it has gained great importance as a valuable adjunct to both mammography and ultrasound in the detection of primary and recurrent breast cancer.

The application of MRI to detect breast cancer was first reported in the 1980s, but at the time, it was concluded that there was very little clinical usability for MRI in detecting or diagnosing breast cancer. When Heywang and colleagues (Heywang et al., 1986) published the application of contrast agents in breast imaging, it changed the thinking and revealed that breast cancers, when compared to normal breast tissue, were enhanced significantly with standard gadolinium contrast agents. Additionally, Kaiser and Zeitler (Kaiser and Zeitler, 1989) found contrast-enhanced magnetic resonance images useful in breast cancer diagnosis but by using a very different technique. The work performed by Heywang and Kaiser established that contrast-enhanced MRI was able to distinguish benign from malignant breast tissue. In the 1990s, Harms and Kuhl (Harms and Flamig, 1993; Kuhl et al., 1999) also published additional reports on the subject. Two basic camps were established: one focusing on the rapid acquisition of images of both breasts after contrast injection (the high temporal resolution of the so-called dynamic school), and the other focusing on three-dimensional gradient echo imaging with thin slices through one breast (the high spatial resolution of the so-called static school). Currently, most authorities agree that both high temporal and high spatial resolution are important in gaining information about both the pharmacokinetics and morphology of breast lesions.

Dynamic-enhanced MR imaging (DCE-MRI) offers great potential in cancer diagnosis and tumour classification (Jansen et al., 2008; Schelfout et al., 2004; Rodenko et al., 1996). With DCE-MRI, the morphologic and haemodynamic features of the entire breast tissue can be evaluated. DCE-MRI takes advantage of the network of microvascular structures associated with cancerous tumours (Taylor et al., 1999). The process of angiogenesis (i.e., the growth of new blood vessels) is part of malignant tumour growth and development. In normal tissue, the angiogenesis process stops after sufficient blood flow exists to supply the tissue with oxygen and nutrients. Some tumours have the capacity to leave the angiogenesis process active, which leads to exponential formation of microvascular structures; the resulting vascular growth leads to exponential tumour growth, as oxygen and nutrients are in abundant supply. A paramagnetic contrast agent, such as Gadolinium-DTPA, is administered intravenously (Padhani, 2002). DCE-MRI is used to evaluate various enhancement characteristics of the lesion by acquiring baseline images prior to contrast agent injection and multiple post-contrast images. The dynamic acquisition of data allows for the determination of vascular permeability. Normal tissue has a diffusion permeability characteristic that serves as a baseline. This baseline vascular permeability is compared to the vascular

permeability of the tissue of interest to determine whether the tissue is non-malignant or malignant. In areas with increased microvascular growth and increased vascular leakage, more contrast agent moves from the vascular system to the tumour tissue. The paramagnetic properties of the contrast agent increase the local magnetisation, which results in a stronger signal intensity in a defined image sequence. This enhancement causes tumour tissue to increase in image signal intensity over time, while normal tissue remains at the same signal intensity, thereby making tumour tissue appear brighter than normal tissue in the image.

A variety of imaging techniques are available with MR imaging, and different protocols are favoured by different investigators on the basis of available hardware and software, clinical indications, desired results, and personal experience (Harms and Flamig, 1993; Kuhl et al., 1999; Heywang et al., 1989; Boetes et al., 1994). In 2003, the 4th edition of the manual for the American College of Radiology Breast Imaging Reporting and Data System (BIRADS®) included a section dedicated to the performance and reporting of breast MRI (BIRADS Atlas, 2003). The committee acknowledged that no single method of image acquisition had been proven superior to others, but that reporting from breast MRIs should include field strength, pre-contrast and post-contrast sequences used, method of fat suppression, and post-processing performed (e.g., subtractions, axial, sagittal, and coronal reconstructions, and/or maximum intensity projections).

In recent years, much research has been conducted on the improvement of pulse sequences, artefact removal, coil technology, and methods for evaluating contrast enhancement and washout kinetics for maximising sensitivity and improving specificity (Turnbull, 2009; Desmond et al., 2007; Martel et al., 2008; Morrell, 2006; Rausch and Hendrick, 2006; Peng et al., 2005; Konyer et al., 2002). Although MRI has extremely high sensitivity for the diagnosis of breast cancer, varying from 89% to 100% for invasive cancers, the specificity is only moderate and varies widely based on the criteria used in the differentiation of malignant from benign lesions (Orel et al., 2006; Heywang-Koebrunner et al., 2001; Warren et al., 2005; Peters et al., 2008; Macura et al., 2006). An overlap between MR imaging findings for benign and malignant lesions persists, resulting in variable specificity (50% – 90%). This confounding overlap may make it impossible to make a differential diagnosis between benign and malignant lesions from conventional MR imaging features. To further increase the specificity of breast MRI and to overcome pitfalls, research on new MRI techniques, such as diffusion-weighted imaging (DWI) (Guo et al., 2002; Marini et al., 2007; Lo et al., 2009; Tozaki and Fukuma, 2009; Partridge et al., 2010; Partridge et al., 2009; Wenkel et al., 2007) and spectroscopy (Jacobs et al., 2005; Cecil et al., 2001; Tozaki and Fukuma, 2009) is being conducted. DWI is based on the translational movement or diffusion of water; it is able to quantify the random, microscopic motion of protons in tissues. DWI has been shown to be a promising quantitative method for use in differential diagnosis of enhancing lesions in breast MRI (Pereira et al., 2011; Partridge et al., 2009).

Additionally, computer-aided diagnosing (CAD) programs for MR imaging of the breast (Wood, 2005; Castellino, 2005; Dorrius et al., 2011; Muralidhar et al., 2011) have been developed. The term CAD is used to refer broadly to clinical decision support systems that assist in the interpretation of breast imaging studies. CAD systems for breast MRI assist radiologists by performing certain automated post-processing tasks, such as image analysis and visualisation. The primary aim for developing CAD for breast MRI is not to identify lesions but to assist the radiologist in identifying suspect features on the image and in determining which lesions are benign and which are malignant. The CAD systems provide automatic ways to evaluate the enhancement properties, providing additional discriminatory power to distinguish abnormalities from normal regions on an image (Behrens et al., 2007). The enhancement properties are extracted from the time contrast enhancement curve, which is a plot of the lesion intensity before and after the administration of the contrast agent versus time (Hendrick, 2008). The shape of the time-enhancement curve provides insight into the diagnosis of lesions. Because there can be a significant overlap in the washout kinetics of benign and malignant lesions, the enhancement curves are used in conjunction with morphological properties, such as lesion shape properties, for accurate cancer diagnosis. The enhancement curves can also be used for generating a colour overlay on the contrast-enhanced MR image that represents the contrast agent enhancement kinetics in the breast (Dorrius et al., 2011).

During the last years, there has been a rapid growth in neuroimaging methodology, resulting new, promising clinical applications. There have been several improvements in technology, methodology, and interpretation. Neuroimaging includes various techniques used to either directly or indirectly image the structure and function of the brain. The types of neuroimaging in MRI can be divided into functional and structural imaging. Functional neuroimaging in MRI is focused on the functions of the brain, using equipment that can register brain activity. Functional MRI (fMRI) is based on the increase in blood flow to the local vasculature that accompanies neural activity in the brain. fMRI can generate images in which different sections of the brain light up as they become active (Bandettini, 2009). Structural neuroimaging, however, is static and concentrates on the structure of the brain and the diagnosis of gross intracranial diseases, such as tumours, and injury. Computed tomography (CT) scanning and MRI both look at the structure of the brain. CT scanning uses a series of x-rays of the head taken from many different directions. CT is typically used for quickly viewing brain injuries or for identifying tumours in the brain that could interfere with function. An MRI of the human brain includes anatomical description and detection of lesions. MRI provides detailed images of brain and nerve tissues in multiple planes without obstruction from overlying bones. Brain MRI is the procedure of choice for most brain disorders. Additionally, it provides clear images of the brainstem and posterior brain, which are difficult to view on a CT scan.

Special techniques, such as diffusion-weighted imaging (DWI), diffusion tensor imaging (DTI), and spectroscopy, also provide information about the function and chemical metabolites of the brain. DWI is a method that is currently often implemented as a part of a routine protocol. It shows the diffusivity of water molecules and is based on the measurement of the Brownian motions of molecules (Mori and Barker, 1999). DTI is a bit more complex application of DWI that can detect in vivo anisotropic diffusion properties in white matter. Several diffusion indices can be derived from the tensor matrix that characterizes the size, shape and orientation of the diffusion tensor. These include the fractional anisotropy (FA) and the apparent diffusion coefficient (ADC) values. ADC describes the average diffusion of the media and has low values in white matter, while FA represents the magnitude of the diffusion tensor and has high values in white matter (Basser and Jones, 2002; Mori and Barker, 1999). DTI allows a view in anisotropic diffusion within white matter tracts but is still limited in demonstrating spatial and directional diffusion anisotropy. Therefore, new, sophisticated methods for demonstrating diffusion directions, such as fibre tracking, have been proposed (Mori and Van Zijl, 2002). Fibre tracking, or tractography, uses diffusion tensor data and allows 3D visualisation of specific white matter tracts (Basser and Jones, 2002). Diffusion-weighted imaging has been shown to be very useful in detecting early signs of ischaemia (Bochar, 2001; Mori and Barker, 1999); it is also increasingly used in the investigation of brain diseases, such as multiple sclerosis (Larsson et al., 1992; Sundgren et al., 2004), epilepsy (Sundgren et al., 2004; Arfanakis et al., 2002; Guo et al., 2002), trauma (Mayer et al., 2010; Lo et al., 2009) and brain tumours (Castillo et al., 2001; Sinha et al., 2002).

2.2 Texture analysis

Tissue characterization includes quantitative methods for characterizing and recognizing various tissues types beyond what is possible from visual interpretation of the source images. The aim of tissue characterization is to increase the diagnostic sensitivity and specificity of the applied radiological modality by (e.g., increasing the detectability of diseases) or to improve the differentiation between normal and pathologic tissues. Texture analysis (TA) is one method for tissue characterization. TA of medical MR images is a quantitative method that can be used to detect and qualify structural abnormalities in different tissues (Lerski et al., 1993). TA of medical images is an on-going field of research, with applications ranging from the segmentation of specific anatomical structures and the detection of lesions, to differentiation between pathological and healthy tissues in different organs.

There is no clear definition of texture in the literature. The reason for this is that textures often display contradicting properties, such as regularity versus randomness and uniformity versus distortion, which cannot be described in a unified manner. In a

general sense, the word texture refers to surface characteristics of an object given by the size, shape, density, arrangement, or proportion of its elementary parts. Texture can be regarded as a similarity grouping in an image. Texture is an image feature that corresponds to both brightness value and pixel locations. Examples of different types of image textures can be seen in Figure 1.

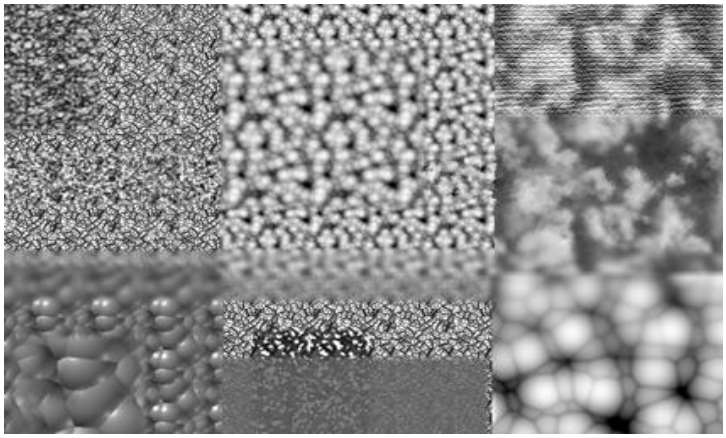

Figure 1. *Example image of different types of textures.*

Image texture is known to provide rich visual information; therefore, the analysis of texture parameters offers a useful way to increase the information obtainable from images. Texture analysis is the term used for methods developed to quantify image texture. TA methods evaluate the spatial location and signal intensity characteristics of the fundamental structural elements (i.e., pixels) of images. TA allows one to calculate mathematical patterns, or texture features, which can be used to characterise the underlying properties. (Castellano et al., 2004). TA plays an important role in many image analysis applications. TA was initially developed for the assessment of aerial photographs and satellite images (Haralick et al., 1973). Texture methods can also be used in applications, such as industrial visual inspection for the detection of defects and quality control (Xie, 2007; Weszka and Rosenfeld, 1976), biometric identification (Ma et al., 2003), content-based image retrieval (Zhang et al., 2000; Manjunath and Ma, 1996), document analysis (Bulacu and Schomaker, 2007; Jain and Zhong, 1996) and texture synthesis (Gui and Ma, 2010), just to name but a few. Texture analysis of medical images represents only a small section of all texture analysis applications. In the medical field, TA applications range from studying images of pathological samples (Farjam et al., 2007; Singh and Gupta, 2011) to diagnosing diseases and classifying pathological tissues from normal tissues in ultrasound (Chen et al., 2001; Bader et al., 2000), X-ray (Mavroforakis et al., 2006; Ganeshan et al., 2011), and, in recent years, MR images (Harrison et al., 2008; Gibbs and Turnbull, 2003; Mahmoud-Ghoneim et al., 2003).

The first steps toward computational texture analysis were led by Julesz et al. (Julesz et al., 1973). The main contributions resulting from their studies were the Julesz

conjecture and the texton theory, which can be conceptualised as the beginning of the two main streams of texture analysis approaches. The Julesz conjecture inspired the statistical approach to texture analysis, which characterizes a texture by the statistical features of the image; the texton theory led to a structural approach that extracts texture primitives as local features for texture description. Texture analysis can be roughly divided into four major application domains: texture classification, texture segmentation, shape from texture, and texture synthesis. The basis for all applications involves extracting the texture features from the image.

2.2.1 Texture feature extraction

Feature extraction involves computing a characteristic of an image that may numerically describe its texture properties. Several methods exist for extracting texture features from images; often, it is beneficial to combine some of these methods to obtain an optimal set of texture features. These methods are generally classified as statistical-based, structural-based, model-based and transform-based (Haralick, 1979; Tuceryan and Jain, 1998).

2.2.1.1 Statistical methods

The statistical approaches analyze the spatial distribution of grey values, computing local features at each point in the image, and deriving a set of statistics from the distributions of the local features (Haralick, 1979). With this method, the textures are described by statistical measures. Statistical methods include features derived from the histogram, gradient, autocorrelation function, run-length matrix and co-occurrence matrix. Depending on the number of pixels defining the local feature, the statistical methods can be classified into first-order (one pixel), second-order (two pixels) and higher-order (three or more pixels) statistics. Methods based on second-order statistics usually achieve higher discrimination indices than do the structural or transform methods. The most popular second-order statistical features for texture analysis are derived from a second-order joint conditional histogram called a co-occurrence matrix. Haralick texture analysis (Haralick, 1979; Haralick et al., 1973) is a form of statistical texture analysis that utilizes co-occurrence matrices to relay the joint statistics of neighbouring spatial or temporal voxels. The 14 textural features described by Haralick et al (Haralick, 1979) provide a wide range of parameters that can be used in medical imaging analysis. In addition grey level differences (Weszka and Rosenfeld, 1976) and their numerous modifications are commonly used. These modifications include signed differences (Ojala et al., 2001) and the Local Binary Pattern operator which incorporate occurrence statistics of simple local microstructures combining statistical and structural approaches in texture analysis.

2.2.1.2 Structural methods

The structural methods are based on the view that textures are made up of primitives with geometrical properties (Allen and Mills, 2004). For example, a square object is represented in terms of the straight lines or primitives that form its borders (Haralick, 1979). In these models, one may compute the statistical properties from the extracted texture elements and utilizes these as texture features or try to extract the placement rule that describes the texture. The advantage of these methods is that they provide a good symbolic description of the image.

2.2.1.3 Model-based methods

Model-based texture analysis techniques generate an empirical model of each pixel in the image based on a weighted average of the pixel intensities in its neighbourhood. These estimated parameters of the image models can then be used as textural feature descriptors. Model-based texture methods try to capture the process that has generated the texture. Popular random field modes used in TA include Markov Random Fields (Jain, 1989), fractals (Pentland, 1984; Mandelbrot, 1977), and multi-resolution autoregressive (AR) features (Haralick, 1979; Jain, 1989).

Random field models analyze spatial variations in two dimensions. They are able to capture the local (spatial) contextual information in an image. These models assume that the intensity at each pixel in the image depends on the intensities of only the neighbouring pixels. Global random field models treat the entire image as a realization of a random field, whereas local random field models assume relationships of intensities in small neighbourhoods. A widely applied class of local random field model types includes Markov random field models. The Markov random field model for texture assumes that the texture field is stochastic and stationary and satisfies a conditional independence assumption. Fractal-based texture analysis was introduced in the 1980' (Pentland, 1984). Fractals measure geometric complexity, which can be used to describe spatial patterns of textures. Fractals are generally set of self-similar functions characterized by so-called fractal dimension (Mandelbrot, 1977). Fractal dimension is the defining property in the study of texture analysis. The fractal dimension gives a measure of the roughness of a surface (Pentland, 1984). The auto-regressive model tries to find relationships between groups of neighbouring pixels so that the pixel grey level value is a weighted sum of the grey level values of the neighbouring pixels thus describing shapes within the image (Castellano et al., 2004) .

2.2.1.4 Signal processing methods

Signal processing methods perform frequency analysis of the textures. This can be achieved by using spatial filters or through filtering in the frequency domain. Some well-known signal processing methods are based on Law's Filter, Gabor filters, and

wavelet transforms (Allen and Mills, 2004; Qian and Chen, 1993; Russ, 2002). They describe the textural properties of an image by parameters that are derived from transformations used in signal processing. The Fourier transform is one of the best known among the various frequency transform types. When windowing a Fourier transform-, (i.e., using a short-time Fourier transform with Gaussian window function), the transform becomes a Gabor transform. The Gabor filter is a frequency- and orientation-selective filter (Tuceryan and Jain, 1998). Gabor filters provide ways for better spatial localisation, but their utility is limited in practice because there is usually no single filter resolution at which one can localize a spatial structure in natural textures. With wavelets, one can analyzes the frequency content of an image within different scales of that image (Castellano et al., 2004). Wavelet analysis produces a set of wavelet coefficients corresponding to different scales and frequency directions. Texture parameters can be computed from these coefficients.

2.2.2 Texture classification

Because some of the calculated features may be highly correlated and may contain irrelevant information, most of the classification methods involve feature extraction before the actual classification task. The classification algorithms generally use many features, without consideration of whether the features are effective for the discrimination task. Feature selection is used to select a subset of features from a given set of features. In some cases, the reduction of the feature set may increase the performance of the classification accuracy by reducing the dimensionality of the classification problem. There have been a number of feature selection and reduction methods proposed (Zhonker and Jain, 1996; Kudo and Sklansky, 2000; Dash and Liu, 1997), but probably the most common feature selection methods are principal component analysis (PCA), Fisher discriminant analysis, and a genetic algorithm-based approach (Jolliffe, 2005; Dash and Liu, 1997).

After feature extraction, the next stage is classification, in which classifiers are trained to determine the classification for each input texture based on obtained measures of selected features. The dataset used during construction of the classifier (i.e., the training set) is different from the sample used for evaluation (i.e., the test set). The textural features of the sample are compared to those of the training images with a classification algorithm, and the sample is assigned to the category with the best match.

In texture classification, the goal is to assign an unknown sample image to one of a set of known texture classes (Mao and Jain, 1992; Ojala et al., 1996). There are two main classification methods: supervised and unsupervised classification. A supervised classifier is trained using the set to learn a characterization for each texture class; unsupervised classification does not require prior knowledge and is able to automatically discover different classes from input textures (Ojala et al., 2001). In

supervised techniques, classifiers have been traditionally divided into two categories: parametric and non-parametric classifiers. The parametric classifiers make certain assumptions about the distribution of features, whereas non-parametric classifiers can be used with arbitrary feature distributions and with no assumptions about the forms of the underlying densities (Duda et al., 2001). Both classifiers require prior knowledge, such as training samples or parameters of the assumed feature distributions of the data. Among the most widely applied are parametric statistical classifiers derived from the Bayesian decision theory, nonparametric k-nearest neighbour classifiers and various neural networks. A k-nearest neighbour (k-NN) classifier determines the classification of a texture by computing distances to the k-nearest training cases. The distances are computed in a multi-dimensional feature space constructed from selected texture features (Ojala et al., 1996; Varma and Zisserman, 2003).

2.2.3 Texture segmentation

Texture segmentation (Reed and Dubuf, 1993; Hofmann et al., 1998; Mao and Jain, 1992) dissolves an image into different homogeneous regions based on certain texture properties. Segmentation has two objectives: to decompose the image into parts for further analysis, and to provide a more meaningful or a more efficient representation. Similar to classification, segmentation of texture also involves extracting features before the actual segmentation. Texture segmentation can also be supervised or unsupervised depending on if prior knowledge about the image texture is available. Supervised texture segmentation identifies and separates one or more regions that match texture properties shown in the training textures. In unsupervised segmentation (Hofmann et al., 1998; Manjunath and Chellappa, 1991; Ojala and Pietikäinen, 1999), one has to recover different texture classes from an image before separating them into regions. The two general approaches for texture segmentation are region-based and boundary-based approaches. In a region-based approach, the aim is to identify regions of the image that have a uniform texture. The regions having different textures are then considered to be segmented regions. The boundary-based approaches are based on the detection of differences in textures in adjacent regions (Tuceryan and Jain, 1998). Segmenting an image into homogeneous regions using texture is employed in a variety of medical applications (Sharma and Aggarwal, 2010; Woods et al., 2007).

2.2.4 Shape from texture

Shape from texture is a computer vision technique in which a 3D object is reconstructed from a 2D image. The basic principle is the distortion of the individual texels (i.e., the texture elements) which are the fundamental units of texture space. Measurement of their variation across the image allows the estimation of the shape of the observed

surface. The amounts of shape and gradient distortions can be measured from an image. The surface shape is reconstructed by calculating the surface orientation. Examples of uses of shape from texture include tasks for recovering true surface orientation (Warren and Mamassian, 2010), 3D scene analysis and reconstructing surface shapes (Tuceryan and Jain, 1998).

2.2.5 Texture synthesis

In computer graphics, texture synthesis is a technique to create large textures from generally small texture samples (Efros and Leung, 1999; Gui and Ma, 2010). The goal of texture synthesis is to reproduce a texture from an input texture. A synthetic texture should differ from the samples, but it should have perceptually identical texture characteristics. Examples of potential applications of texture synthesis include image de-noising (Buades et al., 2005), image editing, image completion and compression (Simoncelli, 1997).

2.2.6 Texture analysis of medical MR images

2.2.6.1 Texture analysis of breast MR images

Because of the increasing amount of data contained in acquired MR images, the manual processing and interpretation of breast MRI has become very laborious. To extract and emphasise information from the images, computer assistance is needed in processing the data. In an attempt to reduce the workload and to maximise the output from DCE-MRI examinations, many systems have been proposed. Chen and associates (Chen et al., 2006) developed a fuzzy c-means clustering-based technique in an attempt to automatically identify characteristic signal intensity-time curves obtained from a T1-weighted SPGR sequence. Artificial neural networks have also been used to characterise signal intensity-time curves obtained from breast masses by dynamic T1-weighted MRI (Lucht et al., 2001). Kelcz et al. (Kelcz et al., 1996) proposed a quantitative approach for fitting dynamic signal intensity data to distinguish benign from malignant lesions. Feature extraction included the measurements of the signal intensity of a lesion as a function of time. Tzacheva and associates (Tzacheva et al., 2003) proposed a method of automating the diagnosis of malignancy by classifying breast tissues as negative or positive for malignancy in gadolinium-enhanced dynamic MR images, using static region descriptors and a neural network classifier, and obtained 90% – 100% sensitivity, 91% – 100% specificity, and 91% – 100% accuracy. A paper by Twellmann et al. (Twellmann et al., 2005) described an approach for automatic localisation and characterisation of suspicious lesions in DCE-MRI data. Their method applied an artificial neural network (ANN) architecture, which combined unsupervised and

supervised techniques for voxel-by-voxel classification of temporal kinetic signals. They suggested that addition of textural features might increase the discriminative power of their classifier. TA has been utilised in X-ray mammography to assess suspicious masses (Gupta and Undrill, 1995) and the texture properties of the tissue surrounding microcalcification clusters (Karahaliou et al., 2008) and also to discriminate between glandular and fatty regions (Miller and Astley, 1992). Rangayyan et al. (Rangayyan et al., 2010) presented methods for the detection of architectural distortion in mammograms of interval cancer cases taken prior to the detection of breast cancer using Gabor filters, phase portrait analysis, fractal analysis, and texture analysis. Guo et al. (Guo et al., 2009) presented fractal-based methods for texture characterization of mammographic mass lesions and architectural distortion. The purpose of this study was to explore the use of fractal and lacunarity analysis for the characterisation and classification of both tumour lesions and normal breast parenchyma in mammography. TA has also been successfully used to differentiate benign from malignant lesions in ultrasound breast images (Bader et al., 2000; Chen et al., 2001).

The use of TA in MR images is a relatively new application; until recently, only a small number of studies had explored the efficacy of TA in breast MRI. So far, published studies have been retrospective by nature, and patient materials have been rather limited and diverse in size and age distributions. Gibbs and associates used TA to discriminate between benign and malignant regions by using the grey level co-occurrence matrix to post-contrast MR breast images. Significant differences between benign and malignant lesions were observed, and by using logistic regression analysis (LRA), a good diagnostic accuracy was obtained with a model requiring only three parameters (Gibbs and Turnbull, 2003). TA has also been used to detect simulated microcalcification susceptibility effects. In their study, James et al. used blurred fat-suppressed inversion recovery spin echo coronal images of the same coronal plane, with one image having readout in the superior-inferior direction, and the other image having readout in the medio-lateral direction, to detect and localise the simulated susceptibility effects. Using Haralick texture methods to detect localised directional blurring, they obtained rather high sensitivity and specificity (James et al., 2001). Chen and associates (Chen et al., 2007) investigated a volumetric texture analysis approach, extending the traditional 2D grey level co-occurrence matrix method. They applied their method for the characterisation of breast MR lesions in T1-weighted 3D-spoiled gradient echo sequence images; based on their study, it appeared that the classification performance of volumetric texture features might well be superior to that based on 2D analysis. Woods and associates (Woods et al., 2007) presented a study applying four-dimensional (4D) co-occurrence-based TA to distinguish between non-malignant and malignant tissues. They showed that texture analysis can be used to quantify variations in voxel intensities over time and can be used, along with a neural network, to segment malignant lesions from DCE-MRI data sets. This study showed promising results in malignant lesion segmentation; however, because the material consisted of images from only four

women, they recommended further studies with larger materials. Nie et al. (Nie et al., 2008) studied the quantitative morphology and texture features of breast lesions for diagnostic prediction and to explore the association of computerised features with lesion phenotype appearances on MRI. They included 28 histologically benign and 43 malignant lesions in their retrospective study. The lesions were segmented by a semi-automated method, and 8 morphological and 10 co-occurrence matrix texture features were extracted. The selected texture features for the analysis were grey level entropy, grey level sum average and homogeneity. Textural features were investigated slice by slice, and the averaged value was used to represent the whole lesion. For maximum discrimination capability, an artificial neural network was used to obtain the features. Their study showed that combining morphological and textural features improved the discrimination potential assessed with receiver operating characteristic (ROC) analysis, compared to the performance of separate groups of morphological and textural features. By using the same patient material as Nie and associates (Nie et al., 2008), McLaren et al. (McLaren et al., 2009) compared analytical methods for diagnostic feature selection and the performance of lesion classification for differentiating between malignant and benign lesions in patients. Eight morphologic parameters, 10 grey level co-occurrence matrix texture features, and 14 Laws texture features were obtained using automated lesion segmentation and quantitative feature extraction. An artificial neural network and logistic regression analysis were compared for the selection of the best predictors of malignant lesions among the normalised features. Newell et al. (Newell et al., 2010) investigated methods for the characterisation of both mass and non-mass lesions using morphological features, enhancement kinetic parameters and co-occurrence matrix texture parameters for 1.5T T1-weighted 3D gradient echo subtraction image data of malignant and benign mass and non-mass lesions. The results demonstrated that the CAD system used achieved high sensitivity and reasonable specificity in classifying mass lesions, but in cases of non-mass lesions, the results were moderate. In a very recent study, Karahaliou et al. (Karahaliou et al., 2010) investigated the feasibility of using texture analysis to quantify the heterogeneity of lesion enhancement kinetics to discriminate malignant from benign breast lesions using co-occurrence matrix texture analysis on initial enhancement, post-initial enhancement and signal enhancement ratio parametric maps. They obtained promising results, showing that the quantification of the heterogeneity of parametric maps that reflect lesion washout properties could contribute to the computer-aided diagnosis of breast lesions in DCE-MRI. A brief summary of the study questions and applied texture parameters and MRI sequences in the reviewed texture analysis of breast MR images articles is presented in Table 2.

Table 2. *A summary of the articles on texture analysis of breast MRI.*

Author	Study question	Data (malignant/benign)	Image sequences	TA parameters	Data analysis
James et al. (2001)	To detect simulated microcalcification susceptibility effects	2 healthy subjects	Coronal images (fat-suppressed inversion recovery spin echo), post-contrast	Co-occurrence matrix-based texture features	Neural network classifier
Gibbs et al. (2003)	To differentiate between benign and malignant lesions	45 / 34	Dynamic contrast enhanced images (multiplanar spoiled gradient-recalled-echo), post-contrast	Co-occurrence matrix-based texture features	Logistic regression analysis
Chen et al. (2007)	To evaluate volumetric TA for the characterization of breast MR lesions	77 / 44	Dynamic contrast enhanced MR images (T1-weighted 3D spoiled gradient echo sequence), post-contrast	Co-occurrence matrix-based texture features	Receiver operating characteristics (ROC) analysis
Woods et al. (2007)	To differentiate between non-malignant and malignant tissues with four-dimensional TA	4 / 2	Dynamic contrast-enhanced MR images (dynamic T1-weighted gradient-echo sequence), post-contrast	Co-occurrence matrix-based texture features	Model-free neural network-based classification
Nie et al. (2008)	To assesses the feasibility of using texture features for diagnostic prediction	43 / 28	Dynamic contrast enhanced MR images (T1-weighted 3D SPGR sequence), post-contrast	10 co-occurrence matrix- based texture features	Artificial neural network
Newell et al. (2009)	To differentiate between malignant and benign lesions	88 / 28	Dynamic contrast enhanced MR images (T1-weighted 3D gradient echo sequence), post-contrast	Co-occurrence matrix-based texture features	Artificial neural network
McLaren et al. (2009)	To differentiate between malignant and benign lesions	43 / 28	Dynamic contrast enhanced MR images (T1-weighted 3D SPGR sequence) , post-contrast	10 co-occurrence matrix- based texture features, and 14 Laws' texture features	Artificial neural network and logistic regression analysis
Karahaliou et al. (2010)	To differentiate between malignant and benign lesions	51 / 31	Dynamic contrast enhanced MR images	Co-occurrence matrix-based texture features	Least-squares minimum distance classifier

2.2.6.2 Texture analysis of MR images of central nervous systems and associated lesions

The earliest published works in MRI texture analysis were studies on brain tumours. Lerski et al. (Lerski et al., 1993) showed in preliminary clinical series that TA seemed to be a useful tool to characterise brain tissues and tumours, such as metastases and glioblastomas, in their general aspects (i.e., contrast, intensity, and homogeneity) or in their different constituents. Lerski et al. (Lerski et al., 1993) described how texture analysis could be used to classify tissues and showed that texture analysis could be used to segment brain regions from MR images using techniques based on a grey level co-occurrence matrix, run lengths and grey level distribution. Herlidou-Même et al. (Herlidou-Meme et al., 2003) performed a multicentre study of the usefulness of TA for the characterisation of healthy and pathologic human brain tissues. They used scans of test subjects (63 patients with intracranial tumours and 10 age- and sex-matched healthy referents), acquired in three sites with 1.5T scanners using centre-specific routine acquisition parameters. They found that MR brain images contained textural features suitable for tissue classification and image segmentation, even though the images were obtained from different sites and with different acquisition routine protocols. It has been suggested that the three-dimensional approach could provide a good tool for tumour grading, treatment follow-up, and for surgery or radiation therapy planning. Mahmoud-Ghoneim et al. (Mahmoud-Ghoneim et al., 2003) used the texture analysis approach based on a 3D co-occurrence matrix to improve brain tumour characterisation. With the 3D approach, they achieved better discrimination between necrosis and solid tumours and between oedema and solid tumours using the MR images of seven patients. Georgiadis et al. (Georgiadis et al., 2009) readdressed the question of the discrimination power of 2D versus 3D analyses with a larger patient sample set. In addition to co-occurrence matrix-based parameters, they also used parameters based on run-length matrices. Their results showed that classification of 3D features outperformed 2D features when discriminating primary tumours from metastatic tumours. However, the discrimination between benign and malignant tumours resulted in exact classification with both 2D and 3D features. Zacharaki et al. used TA to distinguish different types of brain tumours, such as primary gliomas from metastases, and to grade gliomas using images from 98 patients with diagnoses of brain neoplasms. They achieved rather high classification accuracy (an accuracy of 97.8% when distinguishing grade II glioma from metastases, and the lowest accuracy at 75% when distinguishing grade II from grade III glioma) by using tumour shape features, image intensity characteristics and texture features based on a Gabor filter (Zacharaki et al., 2009).

Texture analysis has also proved to be a potential tool for disease evaluation in many central nervous system-related diseases. Texture analysis has been successfully applied in studies of hippocampal sclerosis (HS) and epilepsy. Yu et al. (Yu et al., 2001) performed a study with patients with unilateral temporal lobe epilepsy characterised on

texture analysis of MR images by ipsilateral hippocampal sclerosis and an apparently normal contralateral hippocampus and showed that the apparently normal contralateral hippocampi could be classified into categories in terms of texture. TA has also been shown to be capable of detecting pathologically proven HS in preoperative MRI from patients with refractory mesial temporal lobe epilepsy (MTLE), which is often associated with HS (Bonilha et al., 2003; Jafari-Khouzani et al., 2010).

The value of TA as diagnostic marker and a measure of progression in Alzheimer's disease (AD) was evaluated by Freeborough et al. (Freeborough and Fox, 1998). By applying co-occurrence matrix textural parameters on MRI head scans of 40 normal subjects and 24 AD patients, they achieved a classification rate of 91%. Using TA, de Oliveira et al. (de Oliveira et al., 2011) attempted to find differences among patients with amnestic mild cognitive impairment and mild AD and normal-aging subjects. TA showed differences among the three groups for the corpus callosum (CC) and the thalamus. De Oliveira et al. (de Oliveira MS, 2010) also applied texture analysis to MR images of patients with Machado-Joseph disease. They studied images of 18 patients and 18 age- and sex-matched control subjects. They investigated subtle structural abnormalities in the CC, the thalamus, the putamen, and the caudate nucleus. The applied texture parameters showed differences between the two groups for all areas, except for the CC.

Texture analysis has been proposed as a method for identifying active multiple sclerosis (MS) lesions and monitoring disease progression. The capacity of TA to classify MS lesions vs. normal-appearing white matter (NAWM), MS lesions vs. white matter (WM) and NAWM vs. WM was evaluated by Zhang et al. (Zhang et al., 2008). Their study material consisted of 16 relapsing-remitting MS patients and 16 age- and sex-matched controls. They extracted feature sets from gradient matrix, run-length matrix (RLM), grey level co-occurrence matrix (GLCM), autoregressive (AR) model and wavelet analysis approaches and compared these results with results of GLCM-based features alone. Classification by 1-nearest neighbour (1-NN) and ANN was successful on the tissue pairs MS vs. NAWM and MS vs. WM with both feature sets; however, the combined set of features showed higher discrimination power when evaluated by the Fisher coefficient. Yu et al. (Yu et al., 1999) assessed the capacity of TA to discriminate between active and non-active lesions. They evaluated first- and second-order statistical textural features and performed linear discriminant analysis (LDA) to classify lesions into active and non-active groups. Their attempt to classify the level of activity using only co-occurrence matrices was unsuccessful, whereas TA performed using run-length matrices allowed the accurate classification of 88% of active lesions and 96% of non-active lesions. Texture analysis was applied to the spinal cord MR images of 40 patients with primary progressive, secondary progressive, relapsing-remitting, benign relapsing-remitting MS and 10 age- and sex-matched healthy referents in an attempt to quantify pathological changes that occur in MS (Mathias et al., 1999). Statistically significant differences in textures between normal

controls and MS patients were observed but not between disease subgroups. Theocharakis et al. developed a pattern recognition system for the discrimination between cerebral microangiopathy lesions and MS lesions based on the texture analysis of MR images. According to their findings, statistically significant differences exist in the values of the textural features (Theocharakis P, 2009).

In addition to TA of brain tumours and neurological disorders, TA has also been used to study the effects of gender and age on structural brain asymmetry (Kovalev et al., 2003) and texture anisotropy of brain white matter (Kovalev and Kruggel, 2007). Additionally, the impact of image dynamic range on texture classification of brain white matter when using the co-occurrence matrix approach has been investigated (Mahmoud-Ghoneim et al., 2008). They concluded that the dynamic range over which texture features are evaluated can influence the accuracy of classification of white matter regions.

A brief summary of the study questions, patient data and applied texture parameters and MRI sequences in the reviewed texture analysis of brain MR images articles is presented in Table 3.

Table 3. *A summary of the articles on texture analysis of MRI of central nervous systems and associated lesions.*

Author	Study question	Data (patients/controls)	Image sequences	TA parameters	Data analysis
Lerski et al. (1993)	To discriminate CSF, WM, GM, solid tumour, and oedema	12 / 0	T1- and T2-weighted spin-echo MR images	First-order histogram, gradient, and co-occurrence matrix based texture features	Stepwise discriminant analysis
Herlidou-Même et al. (2003)	To characterizate healthy and pathologic human brain tissues (a multicentre study)	63 /10	T2-weighted Fast Spin Echo MR images, T1-weighted Spoiled Grass SPGR MR images	Histogram, co-occurrence matrix, gradient matrix and run-length matrix based texture features	Hierarchical Ascending Classification and Mann-Whitney U test
Mahmoud-Ghoneim et al. (2003)	To characterizate solid tumour, necrosis, oedema and surrounding white matter	7 /0	T1-weighted gradient-echo MR images	Co-occurrence matrix based texture features (3D)	LDA
Georgiadis et al. (2008)	To discriminate benign, malignant and metastatic brain tissues with 3D textural features	67 / 0	3D T1-weighted contrast enhanced MR images (post-contrast images)	Co-occurrence matrix and run-length matrix based texture features	Support vector machine classifier
Zacharaki et al. (2009)	To distinguish different types and grades of brain tumours	98 / 0	3.0 Tesla MRI, FLAIR images and 3D contrast enhanced T1-weighted images	Gabor texture features	LDA with Fisher's Discriminant Rule, k-NN, and nonlinear SVMs
Yu et al. (2001)	To identify hippocampal abnormalities	23 / 9	0.28 Tesla MRI, Proton density-weighted images and T2-weighted images	Histogram, co-occurrence matrix, gradient matrix and run-length matrix based texture features	Discriminant analysis
Bonilha et al. (2003)	To detect hippocampal abnormalities	19 / 38	coronal IR-T1-weighted MR images	Histogram, co-occurrence matrix, gradient matrix and run-length matrix based texture features	ANOVA, MANOVA
Jafari-Khouzani et al. (2010)	To assess the efficacy of texture analysis for lateralizing mesial temporal lobe epilepsy	36 / 25	FLAIR images	Wavelet based texture features	Fisher linear discriminant analysis

Freeborough et al. (1998)	To test the value of texture as a diagnostic marker for Alzheimer's disease	24 /40	T1-weighted spoiled gradient-echo MR images	Co-occurrence matrix based texture features	Stepwise discriminant analysis
de Oliveira et al. (2011)	To differentiate amnestic mild cognitive impairment and mild Alzheimer disease (AD) and normal-aging subjects	17 amnestic mild cognitive impairment 16 (mild AD) / 16	2,0 tesla MRI,T1-weighted images	Co-occurrence matrix based texture features	Kruskal-Wallis test and Mann-Whitney U test
de Oliveira et al. (2010)	To investigate structural abnormalities of patients with Machado-Joseph disease	18 / 18	2,0 tesla MRI, Volumetric structural MRI: T1-weighted gradient-echo sequence	Co-occurrence matrix based texture features	t-test
Zhang et al. (2008)	To discriminate tissues between MS lesions, normal appearing white matter and white matter.	16 / 16	T2-weighted MR images (turbo spin echo sequence)	Gradient matrix, run-length matrix, grey level co-occurrence matrix, autoregressive model and wavelet based features	RDA, PCA, LDA, NDA and k-NN and ANN
Yu et al. (1999)	To discriminate between active and nonactive MS lesions	8 / 0	T2-weighted MR images	Run-length matrix, grey level co-occurrence matrix based features	LDA
Mathias et al. (1999)	To quantify pathological changes that occur in MS	40 / 10	T2-weighted MR images (IR-prepared fast spoiled gradient echo sequence)	First order statistical and co-occurrence matrix based features	Student's t-test
Theocharakis et al. (2008)	To discriminate multiple sclerosis from cerebral microangiopathy lesions	11 (MS) and 18 cerebral microangiopathy / 0	FLAIR images	Histogram, co-occurrence matrix and run-length matrix based texture features	LDA, the logistic regression and the PNN classifiers
Kovalev et al. (2003)	To study effects of gender and age on structural brain asymmetry	516 normal volunteers	T1-weighted 3D MR images	Co-occurrence matrix based texture features	Multivariate linear models
Kovalev et al. (2007)	To study specific texture properties of the brain's white matter	210 normal volunteers	3 Tesla MRI, high-resolution -weighted MRI	3D anisotropy histograms and co-occurrence matrix based texture features	Linear regression, pairwise t-test
Mahmoud-Ghoneim et al. (2008)	To investigate the impact of image dynamic range on texture classification of brain white matter.	10 / 0	3 Tesla MRI, 3D gradient echo	Co-occurrence matrix based texture features	LDA, The Area Under the ROC Curve (AUC)

2.3 Background for clinical applications

2.3.1 Breast cancer

Worldwide, breast cancer is the most common form of cancer and the second-most common cause of cancer deaths in females. An increased risk of breast cancer is associated with increasing age. Additionally, genetic, endocrine and reproductive factors, along with family histories, all contribute to assessing an individual's risk of developing breast cancer. There is also up to a ten-fold difference in breast cancer incidence depending on geography and socioeconomic background (Vainio and Bianchini, 2002).

The most common pathologic types of invasive breast cancer are invasive ductal carcinoma (IDC) and invasive lobular carcinoma (ILC). The terms 'ductal' and 'lobular' are used to describe the behaviour and growth pattern of the tumour. Although the names indicate that a ductal carcinoma would arise in the ductuli of the breast and a lobular carcinoma in the lobules, most tumours arise at the terminal ductal-lobular unit (Wellings, 2008). All IDC are characterised by the formation of tubules or ducts that infiltrate throughout the supporting breast parenchyma (Tavassoli, 1999; Rosen, 2001). The pathologic features of IDC are highly variable. Approximately 80% of IDC are called 'Not Otherwise Specified' ductal carcinomas; the rest are categorised into subtypes, such as tubular, medullary, mucinous, metaplastic, or papillary. Classic ILC is composed of small, uniform cells invading the supporting breast parenchyma in a linear, single-file arrangement or concentrically around benign ducts in a target-like fashion. Unlike ductal carcinomas, ILC has ill-defined margins and does not form microcalcifications, making it difficult to detect on screening mammography and ultrasound (Yeatman et al., 1995).

Diagnosis of breast cancer is usually based on clinical inspection and palpation, imaging with mammography and/or other imaging modalities, and histopathology verified by image-guided biopsy. Mammography may also be supplemented by breast ultrasound examination for the further evaluation of masses identified by mammography and other space-occupying lesions. Ultrasound is useful for differentiating solid from cystic breast lesions, but it can also be used to characterise solid breast masses (Esserman et al., 2002). The addition of ultrasound to mammography in the evaluation of breast lesions can improve the overall sensitivity of conventional breast imaging for the detection of breast cancer (Skaane, 1999). Mammography and ultrasound have their benefits as imaging methods. Mammography can be used to visualise calcifications deposited in the lumens of ducts or the necrotic centre of a mass, whereas ultrasound has the additional capacity to assess blood flow. However, the capacity for these techniques to discriminate malignancies within tissues

of similar density and low-density neoplastic processes, especially DCIS and invasive lobular cancer, in dense breast tissue is limited (Esserman et al., 2002).

Breast MRI offers a valuable adjunct to both mammography and ultrasound. Breast MRI has been investigated for its potential role in the detection of breast cancer in high-risk young women, the detection and the characterisation of invasive lobular cancer, the determination of the extent of DCIS, the detection of multifocal cancer, and the staging or characterization of locally advanced cancer and its response to chemotherapy (Saslow et al., 2007). Ten indications for breast MRI have been proposed by the working group of The European Society of Breast Cancer Specialists (EUSOMA) (Sardanelli et al., 2010). These indications include: staging before treatment planning; screening of high-risk women; evaluation of response to neoadjuvant chemotherapy; patients with breast augmentation or reconstruction; occult primary breast cancer; breast cancer recurrence; nipple discharge; characterization of equivocal findings at conventional imaging; inflammatory breast cancer; and male breast.

2.3.2 Mild traumatic brain injury

Mild traumatic brain injury (MTBI) represents 70 - 90% of all treated brain injuries (Cassidy et al., 2004). In MTBI, the damage to the brain is often found in grey matter and white matter (WM) at the site of impact and/or on the contralateral side. WM tracts, particularly in the corpus callosum (CC), brain stem, and subcortical WM regions, are vulnerable to axonal stretching and shearing which is often associated with the occurrence of diffuse axonal injury (Yuan et al., 2007). Even though the vast majority of MTBI patients have radiologically normal CT scans MTBI may cause a collection of physical, cognitive, emotional and sometimes sleep-related symptoms. Duration of symptoms may last from several minutes to days, weeks, months, or even longer in some cases. Numerous systems have been developed to classify traumatic brain injury (TBI) along a continuum from mild to severe. These systems usually rely on acute injury characteristics, such as Glasgow Coma Scale (GCS) scores (Belanger et al., 2007), loss of consciousness, post-traumatic amnesia, as well as findings from neuroimaging techniques. Even with recent improvements to MRI techniques that have become even more sensitive than standard MRI, such as diffusion-weighted MRI, DTI and new MRI sequences, the diagnosis of MTBI still remains a challenge.

2.3.3 Multiple sclerosis

Multiple sclerosis (MS) is the most common autoimmune disease of the central nervous system which includes inflammation, demyelination, axonal degeneration and neuronal loss. MS has a very wide range of symptoms including fatigue, visual problems, balance problems and altered sensations. The cause of the disease is not known, but genetic

changes are suspected to be a partial cause. Diagnostic evaluation of MS in MRI is commonly based on the McDonald criteria (McDonald et al., 2001; Polman et al., 2005.). The development of modern imaging techniques for early detection of brain inflammation and characterization of tissue specific injury is an important objective in MS research. Though there are promising research developments, at this time, no cure is known for this disease. Several treatment options are available, and allow for management of the disease. Despite this, most patients progress in disability over the course of their lives (Noseworthy et al., 2002).

3. AIM OF THE STUDY

The aim of this thesis was to test the applicability of MRI based texture analysis in three different clinical applications – breast cancer (Studies I and II), mild traumatic brain injuries (Studies III and IV) and multiple sclerosis (Study V) – by applying TA based on statistical, auto-regressive-model and wavelet-derived parameters to clinically obtained MR images. The objectives of this study include the following.

1) With the help of texture analysis evaluate whether it is possible to obtain information from MR images that is not necessarily visible to the human eye.

2) To identify the optimal texture analysis methods in the three clinical applications.

3) To give a starting point for texture analysis approaches that would render them rapid enough to be usable in a clinical setting.

4. MATERIALS AND METHODS

4.1 Patients

4.1.1 Breast cancer

The database consisted of MR images from 20 patients (mean age 50.6 ± SD 10.6; range 37 to 70 years) with biopsy-proven breast cancer who were appointed to preoperative contrast-enhanced breast MRI. A waiver of patient consent for this study was approved by the Ethics Committee of Tampere University Hospital because the study involved only retrospective review of existing MR images with known diagnoses.

Seven patients with histopathologically proven breast cancer were included in the preliminary study (Study I). Ten consecutive histopathologically typical invasive ductal cancers and ten typical invasive lobular cancers were included in retrospective TA of contrast-enhanced breast MRI (Study II).

4.1.2 Mild traumatic brain injury

For the TA studies (Studies III and IV) 42 consecutive patients (17 male, 25 female; mean age ± SD, 38.8 ± 13.6 years; range 18 to 60 years) with MTBI (GCS score 13-15) were included from a larger MTBI study. The patients for the MTBI study were recruited from the emergency room of the Tampere University Hospital from 2006-2007. Clinical examination on admission and CT examination on the day of the accident were conducted. The patient's degree of consciousness was assessed to determine the severity of brain injury using the GCS (Teasdale and Jennett, 1973). Possible loss of consciousness was recorded (length in minutes or hours) as along with post-traumatic amnesia (length in minutes or hours). To classify and assess the severity of the trauma neurological and neuropsychological examinations were performed within six weeks after injury and MRI was performed within three weeks from the day of admission. All patients met the criteria of MTBI according to the World Health Organisation Collaborating Centre for Neurotrauma Task Force on Mild Traumatic Brain Injury (Carrol et al., 2004). Exclusion criteria for this study were age under 18 or over 65, severe traumatic brain injury, previous brain trauma, other major cognitive disorder and history of major alcohol or drug abuse. All 42 patients had radiologically normal CT

and MRI scan. Ten healthy volunteers (4 male, 6 female; mean age ± SD, 39.8 ± 12.9 years; range 28 to 61 years) were recruited to form a control group. All patients and healthy volunteers gave written consent and the study was approved by the Ethics Committee of Tampere University Hospital.

4.1.3 Multiple sclerosis

Thirty-eight multiple sclerosis (MS) patients with definite diagnosis based on revised the McDonald' criteria (McDonald et al., 2001; Polman et al., 2005) were included in this TA study (Study V) (15 males, 23 females; mean age ± SD, 42 ± 12 years). Consecutive patients with multiple sclerosis were included over 1 year. The only exclusion criterion for this study was patients who had received cortisone treatment 8 weeks before the MRI examination. The Ethics Committee of Tampere University Hospital approved the study, and participants provided written informed consent.

4.2 MRI acquisition

4.2.1 Breast cancer

Imaging was performed on a 1.5 T MRI device (Siemens Magnetom Avanto, Erlangen, Germany) using a four-channel breast array coil. The sequences included in the breast MRI texture analysis are presented in Table 4.

Table 4. *The MRI sequences included in the breast cancer texture analysis.*

Sequence	TR	TE	T1	Slice thickness	Matrix	FOV	Flip angle
Axial T2 Turbo Inversion Recovery	9460	67	0	4.0	512x512	32-36	150
3D Transversal T1 Gradient Echo (dynamic)	11	4.76	0	2.0	512x512	32-35	25

The dynamic study consisted of six measurements. The first frame (pre-contrast) was acquired before injection of paramagnetic contrast agent (Gd, 0.1 mmol/kg body, Dotarem®), followed by 5 measurements. Un-enhanced images were subtracted from the contrast-enhanced images on a pixel-by-pixel basis, creating five subtraction series.

4.2.2 Mild traumatic brain injury

All 42 patients were studied on a 1.5 Tesla MRI machine (Siemens Magnetom Avanto, Erlangen, Germany). The sequences included in the MTBI texture analysis are presented in Table 5.

Table 5. *The MRI sequences included in the MTBI texture analysis.*

Sequence	TR	TE	T1	Slice/gap	Matrix	FOV	Flip angle
Sagittal T1 3D Turbo Flash	1910	3.1	1100	1.0/0	256x256	250	15
Axial FLAIR	9000	109	2500	5.0/1.5	256x256	230	-

4.2.3 Multiple sclerosis

Magnetic resonance imaging was performed on a 1.5 T MRI device (Siemens, Avanto, Erlangen, Germany). The sequences included in the MS texture analysis are presented in Table 6.

Table 6. *The MRI sequences included in the MS texture analysis.*

Sequence	TR	TE	T1	Slice thickness	Matrix	FOV	Flip angle
Axial T2 Inversion Recovery Turbo Spin Echo	8500	100	2500	5.0	256x224	230	150
T1-weighted 3D Magnetisation Prepared Gradient Echo sequence	1160	4.24	600	0.9	256x224	230	15
T1-weighted Gradient Echo sequence acquired with intra-venous contrast agent	1160	4.24	600	0.9	256x224	230	15

4.3 Texture analysis

Analysis of the DICOM-format images was made in a Microsoft Windows XP environment. A stand-alone DICOM viewer Osiris (Windows version 4.19, The Digital Imaging Unit of the Service for Medical Computing of the University Hospitals of Geneva, Switzerland), was used to select slices from image series for analysis. The

application used for TA was the MaZda MRI texture analysis software package. This software was developed at The Institute of Electronics in the Technical University of Lodz, Poland, within COST B11 European project "Quantitative Analysis of Magnetic Resonance Image Texture" and the subsequent COST B21 "Physiological modeling of magnetic resonance image formation". MaZda and integrated B11 software have a graphical user interface and work under Microsoft Windows 9x/NT/2k/XP operating systems (Hajek et al., 2006).

4.3.1 Texture features

The software allows computation of almost 300 texture features. Calculated parameters are based on statistical methods: *histogram* (mean, variance, skewness, kurtosis and percentiles), *gradient* (mean, variance, skewness, kurtosis and percentage of pixels with nonzero gradient), *co-occurrence matrix* (angular second moment, contrast, correlation, sum of squares, inverse difference moment, sum average), *run-length matrix* (run length non-uniformity, grey level non-uniformity, long-run emphasis, short-run emphasis and fraction of image in runs), *autoregressive model* (theta: model parameter vector, 4 parameters; sigma: standard deviation of the riving noise) and *wavelet*-derived (Haralick, 1979; Hajek et al., 2006). The texture features calculated by MaZda are presented in the following sections of this chapter. Mathematical notations of the parameters are presented in Appendix I.

4.3.1.1 Histogram-based parameters

The histogram-based approach to texture analysis is based on the intensity value concentrations of all or some parts of an image, presented as a histogram. The histogram of intensity levels is a simple summary of the statistical information contained in the image. The histogram can be easily computed from the image, and the shape of the histogram provides many clues to the characteristics of the image. For example, a narrowly distributed histogram indicates a low-contrast image. Different image features can be calculated from the histogram to describe the first-order statistical properties of the image. Common features include mean, variance, skewness and kurtosis. The mean gives an estimate of the average intensity level in the investigated region. Variance is a measure of the dispersion of region intensity, and it describes how far values lie from the mean. Histogram skewness is a measure of histogram symmetry about the mean. Kurtosis is a measure of the tail of the histogram, and it describes the relative flatness of the histogram compared to the normal distribution. The histogram-based percentiles give the highest grey level value under which a given percentage of the pixels in the image are contained.

4.3.1.2 Gradient-based parameters

The gradient measures the spatial variation of grey level values across the image. High gradient values correspond to states where the grey levels rapidly change from black to white, and low gradient values correspond to states where tone changes are smooth (Castellano et al., 2004). Based on the histogram of the image gradient a similar feature set is calculated for the image intensity distribution in MaZda software. The mean absolute gradient, is a measure of the mean grey level variation across the image, and its variance is a measure of how far from the mean these variations extent. Gradient skewness and kurtosis are functions of gradient asymmetry.

4.3.1.3 Run-length matrix -based parameters

The run-length matrix (RLM) contains higher-order statistics of the grey level histogram. The RLM contains information on the number of runs, with pixels of defined grey levels and run lengths in an image. The matrices can be calculated with different angles of runs. In MaZda software, there are four different run-length matrices computed for four directions of pixel runs: horizontal, vertical, at 45 º and at 135 º. There are five run-length matrix-based features computed for each of the matrices: short-run emphasis inverse moment, long-run emphasis moment, grey level non-uniformity, run length non-uniformity and fraction of image in runs. A grey level run consists of a set of consecutive collinear pixels in a given direction. Long- and short-run emphasis parameters give measures of proportions of runs with long and short lengths. Short-run emphasis is expected to be larger in coarser images, and long-run emphasis is expected to be larger for smoother images. Grey level non-uniformity calculates how uniformly runs are distributed among the grey levels; it has small values when the distribution of runs is uniform. Similarly, run-length non-uniformity measures the distribution of grey levels among the run lengths. Fraction of image in runs calculates the fraction of image pixels that are part of any runs available in a defined matrix.

4.3.1.4 Co-occurrence matrix -based parameters

A grey level co-occurrence matrix (COM) estimates image properties related to second-order statistics, which considers the relationships among pixels or groups of pixels. This method, first proposed by Haralick (Haralick, 1979), is based on the joint probability distributions of pairs of pixels. Co-occurrence matrices show how often each grey level occurs at a pixel located at a fixed geometric position relative to each other pixel as a function of the grey level. In the applied texture analysis software MaZda, the COM-based parameters are angular second moment, contrast, correlation, sum of squares, and various averages, variances, inverse moments and entropies. Angular second moment is a measure of homogeneity of an image. It measures the monotonicity of grey level transition in the image texture. A higher value for this feature indicates that the intensity

varies less in an image, and the image is homogenous. Contrast is a measure of local variations in the image. It is the difference between the highest and the lowest values of a contiguous set of pixels. Correlation measures the grey level linear dependencies in the image. For an image with large areas of similar intensities, correlation is much higher than for an image with uncorrelated intensities. Sum of squares defines the variance of the co-occurrence matrix. Inverse difference moment measures image homogeneity; a smooth image returns high values. Sum average gives the average of sums of two pixel values in the original image of interest. Sum variance is calculated based on the sum average. Entropy indicates the complexity and randomness within the region of interest. When the image is not texturally uniform, many COM elements have small values, which imply that entropy is very large. The highest value for entropy is reached when all probabilities are equal. Entropy is inversely correlated to second angular moment. Sum entropy is calculated similarly to the other sum- parameters. Difference variance and difference entropy are based on differences calculated between two pixel values (Hajek et al., 2006).

4.3.1.5 Autoregressive model -based parameters

An autoregressive model assumes a local interaction between image pixels and describes a pixel grey level value as a weighted sum of values of the neighbouring pixels. In MaZda, five autoregressive model-based parameters are calculated: coefficients for four neighbouring pixels and the standard error of noise (Hajek et al., 2006). For coarse textures, the coefficients of neighbouring pixels will be similar to each other; for fine textures, the coefficients will have wider variation.

4.3.1.6 Wavelet-based parameters

In wavelet transformations, the image signal is put through a low-pass and high-pass filter cascade; the signal is down-sampled and decomposed simultaneously to increase the spatial resolution. In MaZda, Energy of Haar wavelet sub-bands are calculated (Hajek et al., 2006; Kociołek et al., 2001). The discrete wavelet transform is a linear transformation that transforms a 2n×2n image matrix (where n is positive integer value) into a matrix of the same dimensions. The transposed input image is multiplied by the transform matrix; the result is transposed and multiplied once again by the same transform matrix. Half of the transform matrix rows may be considered as smoothing filter coefficients, while the other half are considered sharpening filter coefficients. For this reason, the obtained matrix consists of five square quarters.

4.3.2 Regions of interest

Regions of interest (ROI) were set manually by freehand drawing or by placing pre-

defined fixed size ROI boxes on a layer on the image. Grey level intensities were normalised in the range [μ-3σ, μ+3σ], where μ is the mean grey level value, and σ is the standard deviation.

In the breast cancer study, the ROIs were drawn on the basis of optimal representation of the largest tumour area. A standard quadratic 15x15 pixel ROI containing the cancer tissue was manually defined for each image. A similar ROI was placed in a reference area in a patient's healthy breast. A manually defined irregular ROI containing only the visible tumour was also defined on each image.

In the MTBI study, the ROIs were manually placed symmetrically on the left and right hemispheres on each level of interest. Three ROIs were placed on different segments of the CC. Freehand ROIs were placed on the cross-section of the mesencephalon; the sizes of the ROIs varied depending on the size of the mesencephalon. The ROIs on white matter and the CC were standard-size circular ROIs and were placed so that overlap with other structures and possibly observed microhaemorraghes, macroscopic hemosiderin deposits or hyperintensities would be avoided. However, no evidence of contusions was observed on any patients. The levels and regions of interest were selected based on a clinical knowledge of typical sites for lesions. The lesions were located on the corticospinal and pyramidal tracts.

In the MS study, both standard ROI boxes and freehand ROI were drawn on focal MS lesions; standard ROIs were used in white and grey matter. Based on anatomical landmarks and clinical knowledge on typical sites for focal MS lesions, two anatomical locations, the corona radiata-centrum semiovale and the basal ganglia, were used for analysis.

In all materials, ROI drawing was performed manually by an engineer of medical technology, and a professional radiologist confirmed all selected levels of interest and ROI locations.

4.3.3 Texture analysis protocol for the breast cancer study

In Study I, with the small data set of seven patients, we analysed the differences between cancer tissue from the affected breast and healthy tissue from the other breast and the differences between cancer tissue and healthy appearing tissue in a dynamic T1-weighted imaging series with and without the contrast media and an axial T2-weighted fat suppression turbo-inversion recovery sequence. In Study II, a larger data set and more imaging sequences were used. The images were the T1-weighted pre-contrast, two contrast-enhanced series (contrast first and contrast last) and their subtraction series (subtraction first and subtraction last). Analysis between different histological types of invasive breast cancer (ductal carcinoma vs. lobular carcinoma) was conducted; the classification for breast cancer tissue and healthy reference tissue was evaluated in this setting. The protocol for TA for breast cancer studies is presented in Figure 2.

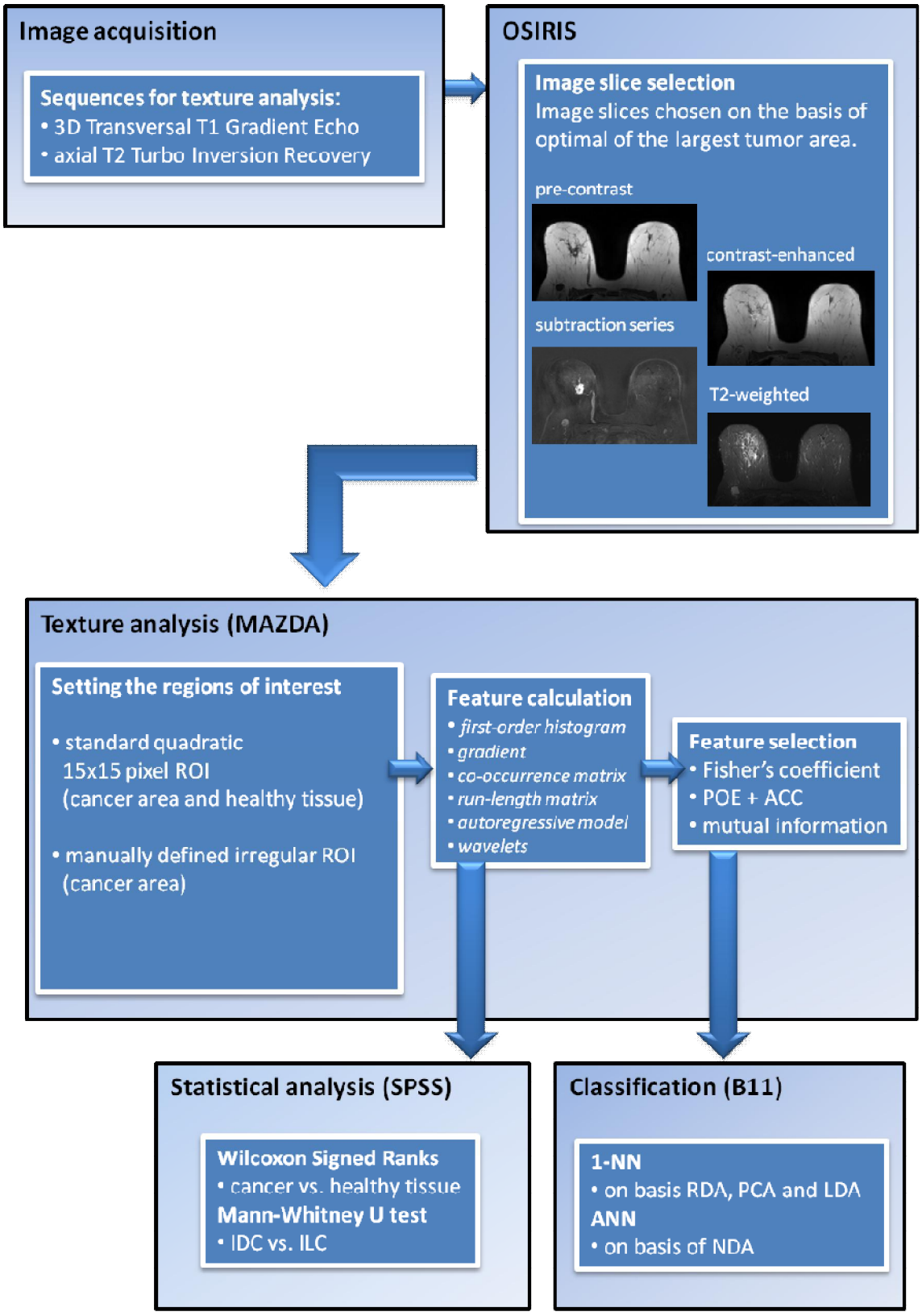

Figure 2. *Texture analysis protocol for the breast cancer study.*

4.3.4 Texture analysis protocol for the MTBI studies

In Study III, the raw texture parameters were tested to determine how many and which of the 277 parameters were statistically different between hemispheres in the mesencephalic area, WM on three different levels of interest and segments of the CC. For the TA study of MTBI (Study IV), two composite scores, a verbal memory composite score and a visual memory composite score, were created to study the correlation between obtained TA features and memory defects. These scores are thought to provide global estimates of a subject's verbal and visual memory in the acute post-injury phase. For the verbal memory composite score, total immediate recall, post-interference recall, and recognition with the Rey Auditory Verbal Learning Test (Lezak et al., 2004) and the Four-Word Short-Term Memory Test were measured (Morrow and Ryan, 2002). For the visual memory composite score, the total adjusted errors and the total adjusted errors for six shapes from the Cambridge Neuropsychological Test Automated Battery (CANTAB) (the Cambridge Neuropsychological Automated Testing Battery, 2004), the Paired Associates Learning subtest, and the Rey-Osterrieth Complex Figure Test immediate recall (Strauss et al., 2006) were used. All raw scores from neurocognitive tests were converted into *z*-scores and adjusted for age and education (Strauss et al., 2006). The composite scores for verbal and visual memory were calculated by averaging the standardised scores from the tests that assessed each domain. Additionally, diffusion parameter analyses were performed on 34 patients. Anisotropic diffusion can be visualised as ellipsoids, fractional anisotropy maps and tractography views. In the Tensor mode, FA, ADC, DWI, eigenvalues and low b maps can be visualised. In our study, ADC values and FA were measured symmetrically at the mesencephalon, the centrum semiovale and the CC (genu, body and splenium). The protocol for TA for the MTBI studies is presented in Figure 3.

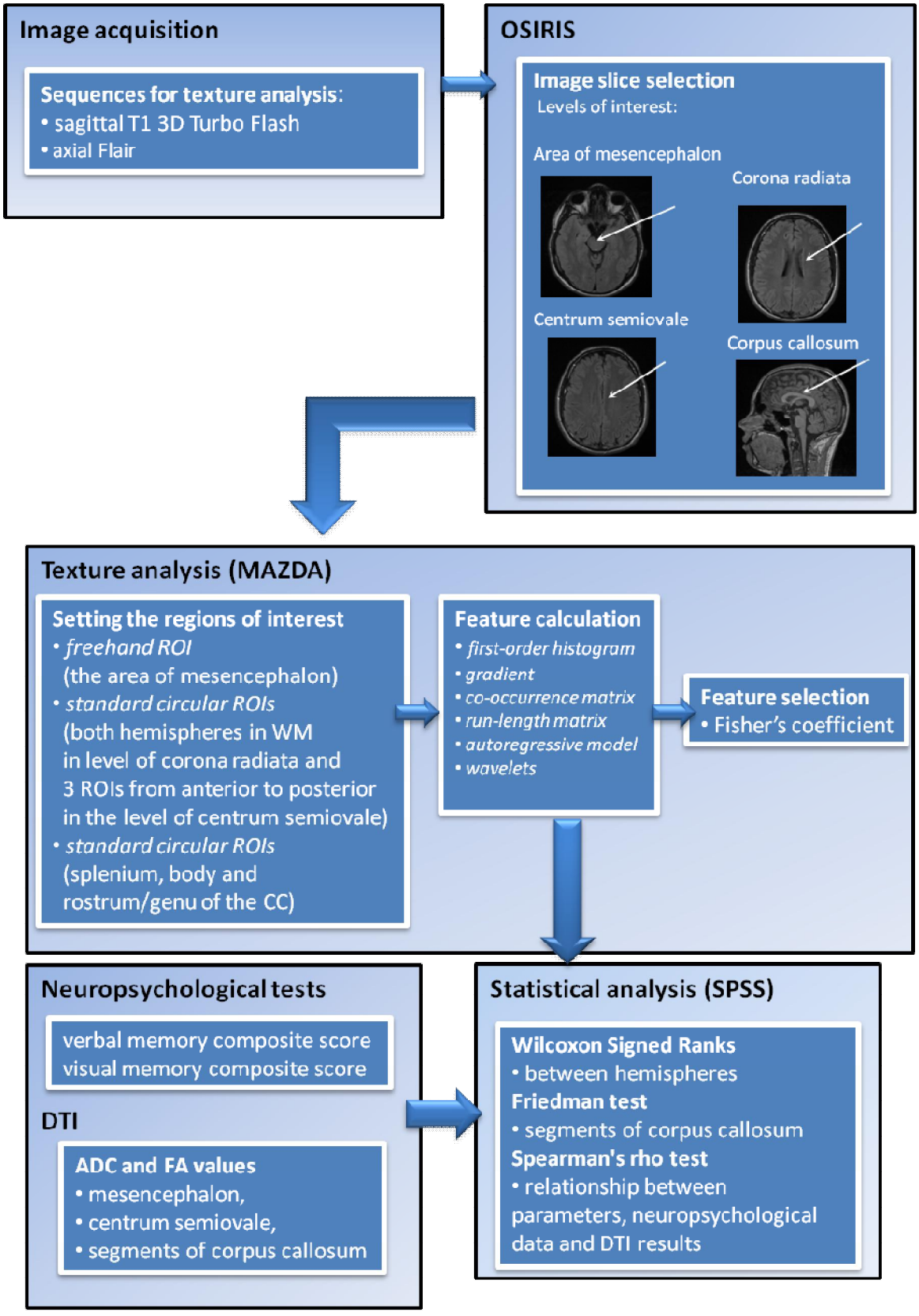

Figure 3. *Texture analysis protocol for the MTBI study.*

4.3.5 Texture analysis protocol for the MS study

In Study V, the classification of multiple sclerosis plaques from white matter and normal-appearing white matter close to the focal lesions was evaluated using freehand ROIs and standard-size ROIs. ROIs were defined on images from two anatomical locations on fixed axial imaging sequences, FLAIR and native T1-weighted magnetisation-prepared gradient echo with and without contrast agent. The protocol for the TA for the MS study is presented in Figure 4.

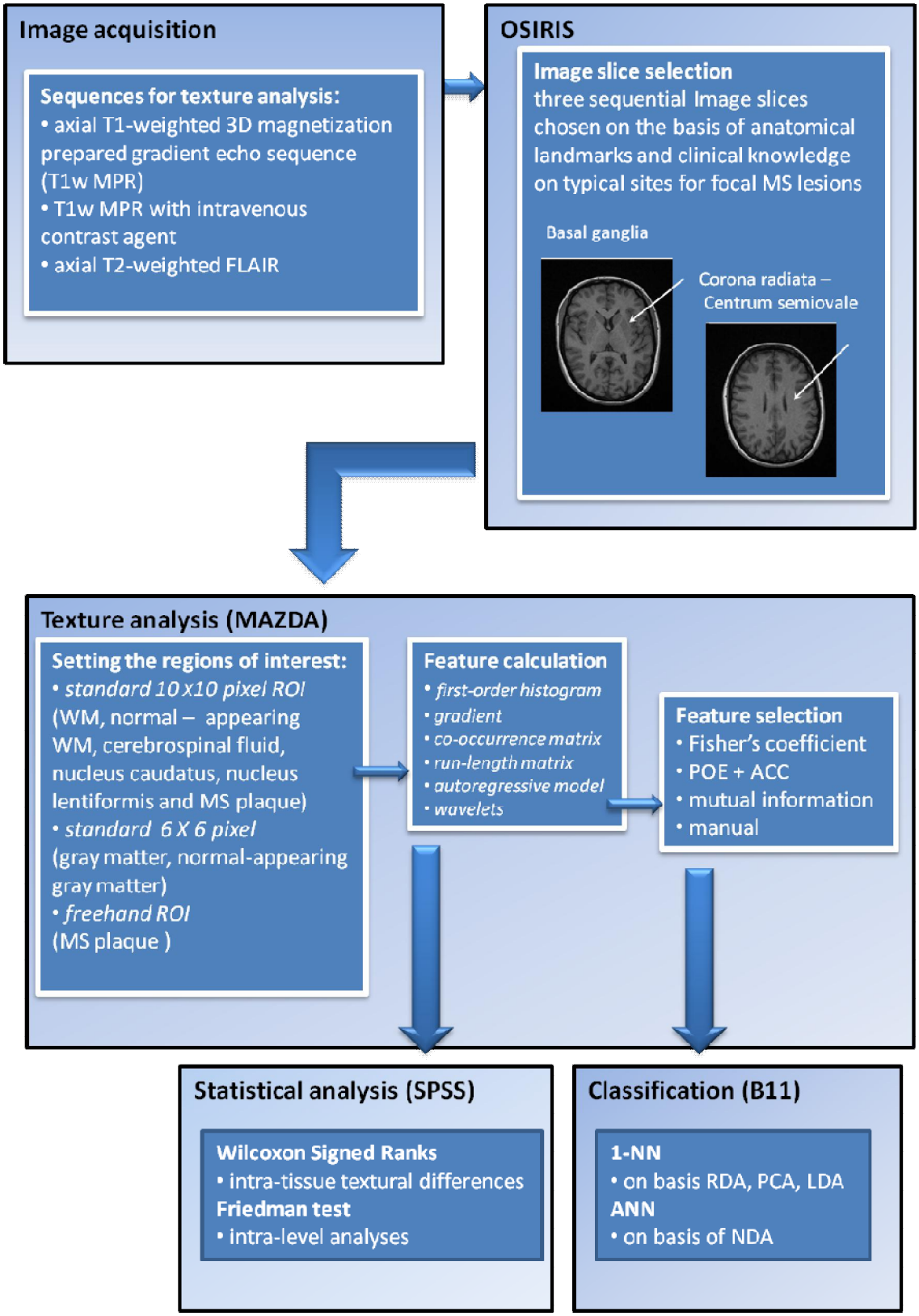

Figure 4. *Texture analysis protocol for the MS study.*

4.4 Data analysis and statistical methods

4.4.1 Feature selection

The B11 application integrated with MaZda was used for data analysis and classification. The MaZda software provides feature selection algorithms, such as the Fisher coefficient (F), classification error probability (POE) combined with average correlation coefficients (ACC), and mutual information (MI). The Fisher criterion usually produces a set of features that have a high discriminatory potential and that are also highly correlated with each other, while the heuristic POE+ACC technique consecutively seeks features that are best-suited for classification but are the least correlated with features that are already selected.

In the breast cancer Study I, the best features were selected by the Fisher and POE+ACC methods. In Study II, the combination of the feature selection algorithms MI, POE+ACC and F was used to determine 30 texture features. In the MS study (Study V), feature selection algorithms POE+ACC and F, in addition to manual selection, were used to determine texture features with the highest discriminative power for separation and classification.

4.4.2 Classification

The feature sets were set as an input in the integrated B11 application (version 4.5) for data analysis and classification. B11 investigates the capacity of these texture feature sets to distinguish various texture categories using statistical methods, such as principal component analysis (PCA), linear discriminant analysis (LDA), and nonlinear discriminant analysis (NDA), which can be run for each subset of images and chosen texture feature groups. Default neural network parameters in the B11 application were used for texture data analyses: the first hidden layer = 1; the second hidden layer = 2; backprop eta = 0.15; backprop iter. limit = 150 000 and optimisation iter. limit = 50. Classification tests on the input data was performed on Studies I, II and V using different classifiers: a k-nearest-neighbour (k-NN) classifier, which assigns an observation point in the data space to the class to which its k-NN belong, and the artificial neural network (ANN) classifier, which produces complex smooth hypersurfaces in the data space that separate clusters of points belonging to different classes. The k-NN classification was performed for the raw data (RDA), the most expressive features resulting from PCA and the most discriminative features resulting from LDA. ANN uses NDA to perform the feature classifications.

4.4.3 Statistics

4.4.3.1 Breast cancer

All calculated raw texture parameters were tested to determine how many and which differed statistically between regions. Differences between texture parameters between cancer tissue and healthy reference tissue were analysed by Wilcoxon signed-ranks, and the differences between texture parameters of the two histological types IDC and ILC were analysed by the Mann-Whitney U test. These analyses were performed by SPSS for Windows, version 16.0.2. (SPSS Inc., Illinois, USA). A p-value < 0.05 was considered to be statistically significant.

4.4.3.2 Mild traumatic brain injury

The calculated texture parameters were tested with Wilcoxon signed-rank test to find out how many and which parameters had statistically significant differences between hemispheres. The Friedman test was used for comparisons of tissue samples originating from the same hemisphere from different anatomical locations and samples from different segments of the CC (rostrum/genu, body and splenium). The tests were run separately for patients and healthy referents. Spearman's rho test was performed to evaluate relationships in patients between the composite scores for verbal and visual memory functions and the TA parameters. The DTI vs. TA results and the DTI findings vs. the composite scores were tested using a non-parametric Spearman's rho test. Statistically significant differences were defined by p-values < 0.05. Analyses were run in SPSS for Windows, version 14.0.2 (SPSS Inc., Illinois, USA).

4.4.3.3 Multiple sclerosis

The Wilcoxon signed-rank test was used in the analysis of intra-tissue textural variation between anatomical levels. We evaluated how many and which parameters had statistically significant differences between them. Statistically significant differences were defined by p-values < 0.05. The tests were run separately for each MR sequence. Intra-tissue textural variations between sequential image slices were run for T1-weighted images of a randomly sampled sub-population (N=23) by the Friedman test. The Wilcoxon signed-rank test and the Friedman test were performed using SPSS for Windows, version 16.0.2 (SPSS Inc., Illinois, USA).

5. RESULTS

5.1 Tissue discrimination

5.1.1 Classification of visible lesions

In Study I, with the small data set of seven patients and in Study II with a larger data set classifications between cancer tissue and the healthy tissue were conducted. TA was applied in different imaging sequences and ROI settings.

A summary of the classification results performed with 1-NN on the basis of PCA and LDA and ANN on the basis of features of NDA from both of the studies is presented in Table 7.

Table 7. *Summary of the classification results from Studies I and II.*
The classification percentages (from two separate studies) are presented for imaging sequences dynamic T1-weighted imaging series with (contrast first and last, and subtracted first and last) and without (pre-contrast) the contrast media and the axial T2-weighted fat suppression turbo inversion recovery sequence (T2T). Classification is based on methods included in the MaZda software package: 1- NN for principal component analysis (PCA) and linear discriminant analysis (LDA) features and ANN for non-linear discriminant analysis (NDA) features.

	MRI Sequence	**1-NN (PCA)**	**1-NN (LDA)**	**ANN (NDA)**
Cancer tissue vs. healthy tissue from patients other breast (standard ROIs) 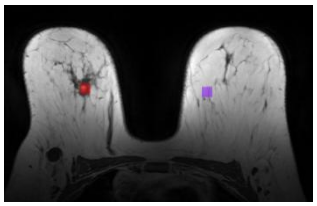	Pre-contrast	85 -90%	100 %	100%
	Contrast first	98 %	98%	95%
	Subtraction first	88-100%	100%	100%
	Contrast last	80%	100%	100%
	Subtraction last	98%-100%	100%	100%
	T2T	97 %	100 %	100 %
Cancer tissue vs. healthy tissue near the lesion (standard ROIs) 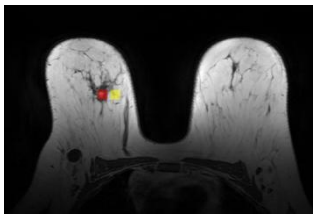	Pre-contrast	86 % - 97 %	86 %-93%	93 %
	Contrast first	-	-	-
	Subtraction first	100 %	100 %	100 %
	Contrast last	-	-	-
	Subtraction last	100 %	100 %	100 %
	T2T	79 %-89 %	89 %-93%	100 %
Cancer tissue vs. healthy tissue from patients other breast (free hand ROI) 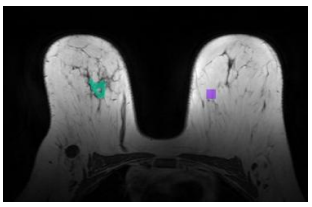	Pre-contrast	90 %	100 %	100 %
	Contrast first	90 %	100 %	100 %
	Subtraction first	100 %	100 %	100 %
	Contrast last	90 %	100 %	100 %
	Subtraction last	100 %	100 %	100 %
	T2T	-	-	-

The classification results varied slightly depending on the size of the applied patient material, ROI setting and feature selection method. The analyses with LDA and NDA performed well on the task of discriminating the breast cancer area from the healthy breast area, with 100% accuracy in all imaging sequences, regardless of the data size or whether a standard ROI box or a freehand ROI was used. The discrimination between

cancer tissue and healthy-appearing tissue next to the tumour could be considered good, especially with the subtracted images (accuracy of 100%).

Analysis between different histological types of invasive breast cancer (ductal carcinoma vs. lobular carcinoma) was conducted in Study II. Only irregular free-hand ROI was used in these analyses. A summary of the classification results performed with 1-NN on the basis of PCA and LDA and ANN on the basis of features of NDA is presented in Table 8.

Table 8. *Summary of the classification results between histological types from Study II. The classification percentages are presented for imaging sequences dynamic T1-weighted imaging series with (contrast first and last, and subtracted first and last) and without (pre-contrast) the contrast media. Classification is based on methods included in MaZda software package: 1- NN for features of principal component analysis (PCA) and Linear discriminant analysis (LDA) and ANN for non-linear discriminant analysis (NDA) features.*

	MRI Sequence	1-NN (PCA)	1-NN (LDA)	ANN (NDA)
Invasive ductal carcinoma vs. invasive lobular carcinoma 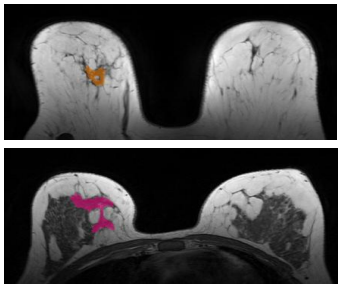	Pre-contrast	83 %	100 %	95 %
	Contrast first	78 %	100 %	100 %
	Subtraction first	83 %	100 %	100 %
	Contrast last	80 %	100 %	95 %
	Subtraction last	88 %	88 %	100 %

The classification accuracy between the two histological types (ILC and IDC) approached 100% in all images when results from LDA and NDA were combined.

In Study V, the classification of multiple sclerosis plaques from white matter and normal-appearing white matter close to the focal lesions from two anatomical locations was evaluated using FLAIR images and native T1-weighted magnetisation-prepared gradient echo images with and without contrast agent. A summary of classification results for tissue pairs from imaging level 1 (corona radiata-centrum semiovale), based on PCA and NDA, is presented in Table 9.

Table 9. *Summary of the classification results from Study V.*
The classification percentages are presented for imaging sequences T1-weighted magnetization preparedgradient echo (T1w MPR), previous with contrast agent (T1w MPR+C). Classification is based on methods included in MaZda software package: 1- NN for features of principal component analysis (PCA) and ANN for non-linear discriminant analysis (NDA) features.

ROIs	MRI Sequence	1-NN (PCA)	ANN (NDA)
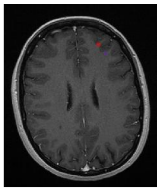 White matter vs. MS free hand ROI	T1w MPR	85 -98 %	100%
	T1w MPR + C	93 -100 %	100 %
	FLAIR	89 -100 %	100 %
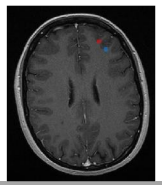 WM vs. MS standard ROI	T1w MPR	78 -96 %	98 -100%
	T1w MPR + C	82 -94 %	96 -100 %
	FLAIR	80 -86 %	96 -98 %
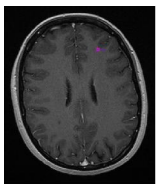 NAWM vs. MS freehand ROI	T1w MPR	86-98 %	100 %
	T1w MPR + C	90 -98 %	96 -100 %
	FLAIR	93 -100 %	100 %
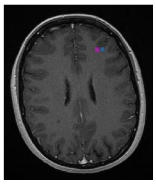 NAWM vs. MS standard ROI	T1w MPR	81 -90 %	98 %
	T1w MPR + C	81 -94 %	96 -100 %
	FLAIR	68 -81 %	96 – 98 %

WM, white matter; NAWM, normal appearing white matter; MS, multiple sclerosis

There were some differences in classification results depending on the method applied for feature selection, ROI type (standard-size or freehand ROI) and imaging sequence. All combinations of white matter and MS lesions gave rather accurate classification results in all image types, anatomical levels, and feature selection methods (NDA 96%–100%). The T1 MPR with contrast agent sequence exhibited slightly better overall classification than without contrast agent and than the FLAIR series. Separation of WM or NAWM from MS plaques was slightly better when the ROI of the plaque was hand-drawn and the white matter ROI was drawn apart from the MS lesion.

5.1.2 Distinguishing non-visible lesions

In studies of texture changes caused by MTBI (Studies III and IV), there were no visible lesions in MR images. Therefore, no classification analyses could be conducted because

the patients could not be categorised according to in which part of the head the damage may have occurred. Analysis of the texture differences between hemispheres was conducted. The number of texture parameters (n = 277) that were statistically significantly different (p<0.05) in the area of the mesencephalon between the hemispheres and in the WM in the level of corona radiata between the hemispheres and between segments of the CC of patients and healthy controls is presented in Table 10.

In Study IV, we compared the TA results with the memory composite scores using only COM parameters. The final number of subjects in this part of the analysis was 34 because eight subjects had dropped out of the neuropsychological examinations. The data regarding whether there were correlations found in the studied areas are also included in Table 10.

Table 10. *Summary of the results relating to Studies III and IV.*
Total number of significantly differing parameters between left and right side of analysed regions (mesencephalon, WM in level of corona radiate and corpus callosum) and correlations to the patient's neuropsychological composite scores are presented.

	MRI Sequence	**Group**	**Number of significantly differing parameters (left vs. right side)**		**Correlation to neuropsychological data (yes/no)**
Mesencephalon 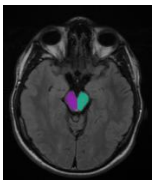	T2w FLAIR	Patients		107 / 277	yes
		Controls		37 / 277	
WM corona radiata 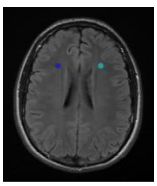	T2w FLAIR	Patients		63 / 277	no
		Controls		13 / 277	
corpus callosum 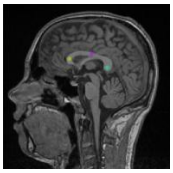	T1w MPR	Patients	rostrum/genu	6 / 277	yes
			body	49 /277	no
			splenium	5 / 277	no
		Controls	rostrum/genu	6 / 277	
			body	4 / 277	
			splenium	3 / 277	

The patients had clearly more differences in texture features between hemispheres than did the healthy controls. In the WM in the level of the corona radiata, there were clearly more significantly different parameters between hemispheres than in other studied levels in the WM. Significant correlations between texture parameters and memory composite scores were found in the mesencephalic area and in the genu of the CC. In the mesencephalic area, many textural parameters correlated significantly with results from the memory tests. The parameters sum of squares and the sum entropy were negatively correlated with verbal memory test scores on the right side, while on the left side, the sum of squares was negatively correlated and the inverse difference moment was positively correlated with verbal memory test scores. On the right side of the mesencephalon, there were no correlations between the textural parameters and visual memory tests. On the left side, a correlation was found between the sum average and the visual memory tests. Although the correlations were not very strong, they were consistent. Additionally, several parameters measured in the genu of the CC correlated with results from the visual memory tests. Correlations between texture parameters and the visual memory composite score were also observed in the genu of the corpus callosum.

For areas in which significant interactions were found between composite scores and TA parameters, comparisons between DTI results and TA results were also performed. Texture parameters and FA and ADC values were compared to determine whether the defined texture parameters and changes in DTI values were correlated. Statistically significant correlations were observed in patients on the left side of the mesencephalon, especially with FA values. The correlations between texture parameters and ADC values were in opposing directions but were of similar magnitudes. The inverse difference moment and angular second moment of the texture parameters were positively correlated with FA values, while entropy-based parameters were negatively correlated with FA values.

5.2 Discriminative parameters

In the breast cancer study (Study II), texture parameters were tested to determine how many and which parameters were statistically different ($p<0.05$) between regions of interest. Parameters were evaluated between cancer tissue and healthy reference tissue using standard and freehand ROIs and between two histological types of breast cancer.

In the MTBI study (Study III), texture parameters were again tested to determine how many and which parameters were statistically different ($p<0.05$) between brain hemispheres. We tested parameters between hemispheres in the mesencephalic area in different levels of WM and in segments of the CC. We also tested texture parameters between hemispheres in WM in different levels of interest to determine how many and

which parameters were statistically different. In the level of the corona radiata (level 2), there were clearly more significantly different parameters between hemispheres than in other levels in patients; additionally, there were fewer texture differences in controls when all analysed parameters were considered. The texture parameters of WM between different levels were analysed with the Friedman test to determine whether the textures differed in the same hemisphere between different levels of interest. Textural differences were observed between levels. Textural differences were also analysed in the anterior-posterior direction in the same hemisphere (front, middle and back) on level 3; it was observed that the texture parameters in the posterior region differed from the anterior and central regions in both hemispheres.

5.2.1 Histogram-based parameters

Results of the evaluation of histogram-based parameters between breast cancer lesion and healthy reference tissue using standard and freehand ROIs and the evaluation between IDC and ILC are presented in Figure 5.

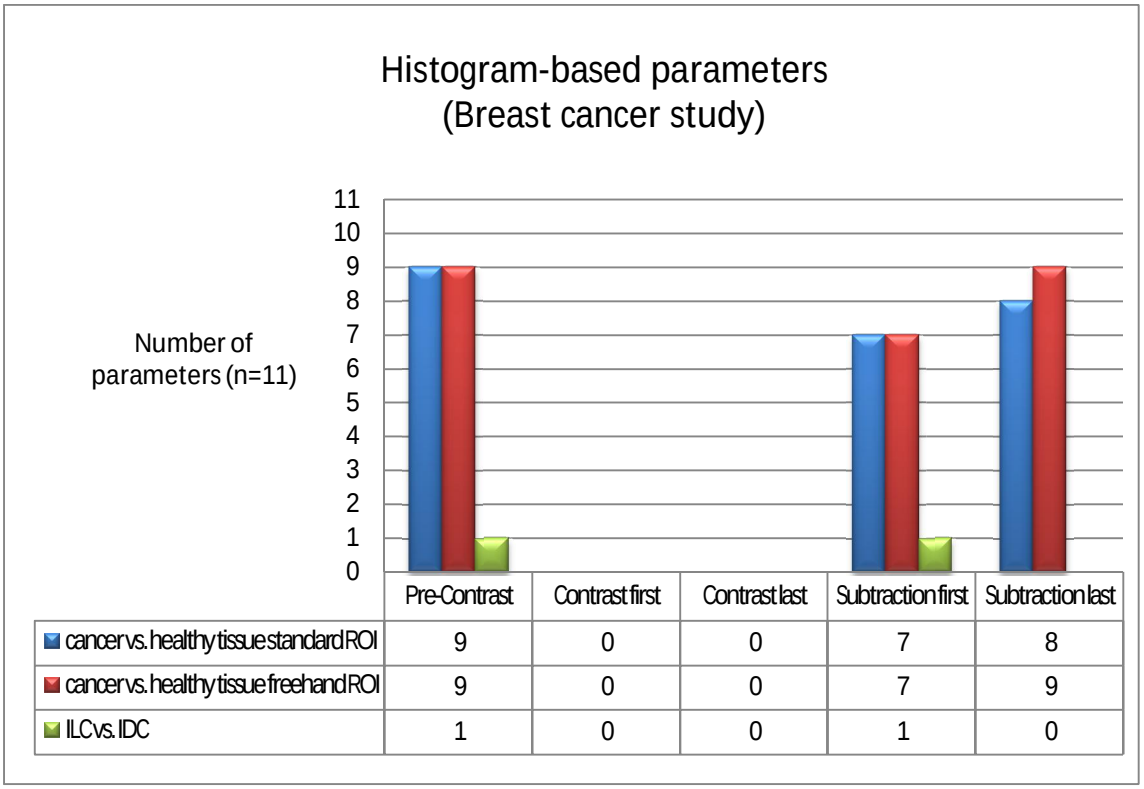

	Pre-Contrast	Contrast first	Contrast last	Subtraction first	Subtraction last
cancer vs. healthy tissue standard ROI	9	0	0	7	8
cancer vs. healthy tissue freehand ROI	9	0	0	7	9
ILC vs. IDC	1	0	0	1	0

Figure 5. *The numbers of statistically different histogram-based parameters ($p<0.05$) are presented, as analysed with the Wilcoxon signed-rank test for every tested imaging sequence between healthy tissue and cancer tissue (using standard and freehand ROIs) and between invasive lobular carcinoma (ILC) and invasive ductal carcinoma (IDC).*

No histogram-based parameters were significantly different in images from contrast sequences, while in images from subtraction sequences and pre-contrast sequences, almost all histogram-based parameters yielded significantly different values between the cancerous area and healthy tissue.

The numbers of statistically different histogram-based parameters in the mesencephalon, in WM and in the level of the corona radiata between hemispheres and between segments of the CC on patients and controls are presented in Figure 6.

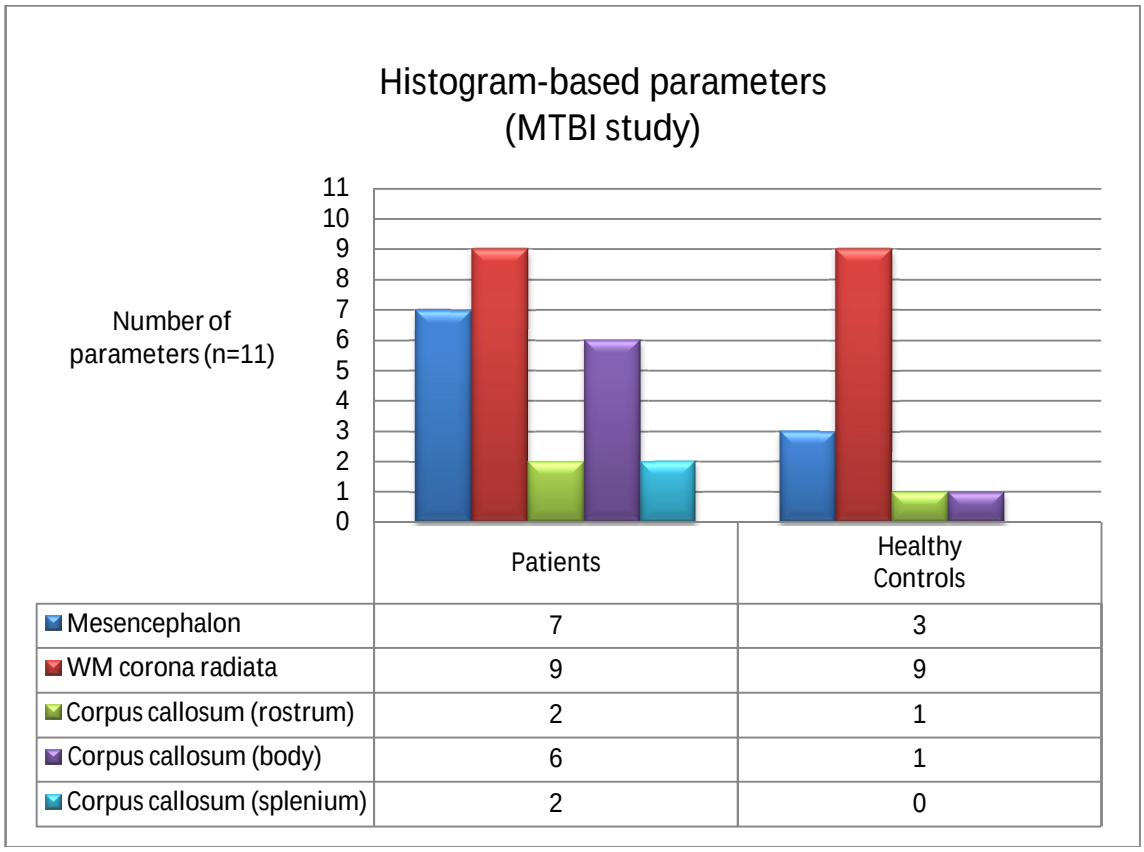

	Patients	Healthy Controls
Mesencephalon	7	3
WM corona radiata	9	9
Corpus callosum (rostrum)	2	1
Corpus callosum (body)	6	1
Corpus callosum (splenium)	2	0

Figure 6. *The numbers of statistically different histogram-based parameters ($p<0.05$) are presented, as analysed with the Wilcoxon signed-rank test for patients and controls between hemispheres in the mesencephalic area and the WM in the level of corona radiata and between segments of the CC.*

The patients had more differences in histogram-based texture features between hemispheres than did the healthy controls in the mesencephalon and in the segments of the CC, especially in the body of the CC. However, in the WM, in the level of the corona radiata, there were no observed differences in histogram-based parameters between patients and controls: both had 9 out of 11 differing parameters between hemispheres.

5.2.2 Gradient-based parameters

Only a few gradient-based parameters were significantly different between analysed areas, mainly because there were only 5 gradient-based parameters calculated. In the breast cancer study, 2/5 gradient-based parameters differed in subtracted images when using standard ROIs. Otherwise, there were no specific trends observed in the differing parameters. In the MTBI study, there were no differences in the gradient-based parameters between hemispheres or in the segments of the CC, either in patients or in controls.

5.2.3 Co-occurrence-based parameters

Many co-occurrence-based parameters were statistically different in all analysed imaging sequences in the breast cancer study. The results of the evaluation of the co-occurrence-based parameters between breast cancer lesions and healthy reference tissue using standard and freehand ROIs and the evaluation between IDC and ILC are presented in Figure 7.

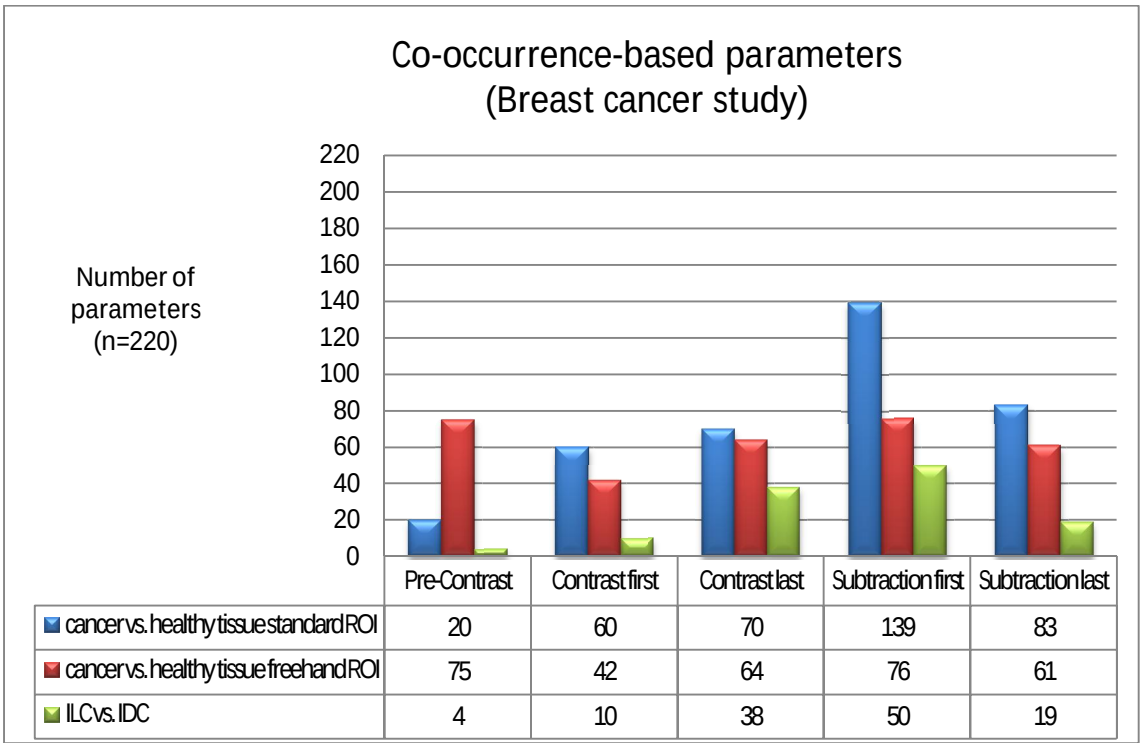

Figure 7. *The numbers of statistically different co-occurrence-based parameters ($p<0.05$) are presented, as analysed with the Wilcoxon signed-rank test for every tested imaging sequence between healthy tissue and cancer tissue (using standard and freehand ROIs) and invasive lobular carcinoma (ILC) and invasive ductal carcinoma (IDC).*

Most of the differing parameters were obtained when using standard ROIs in subtracted images. However, when using freehand ROIs, the results were more consistent than when using standard ROIs.

The numbers of statistically different co-occurrence-based parameters in the mesencephalon, in the WM in the level of the corona radiata between hemispheres and between segments of the CC in patients and healthy controls are presented in Figure 8.

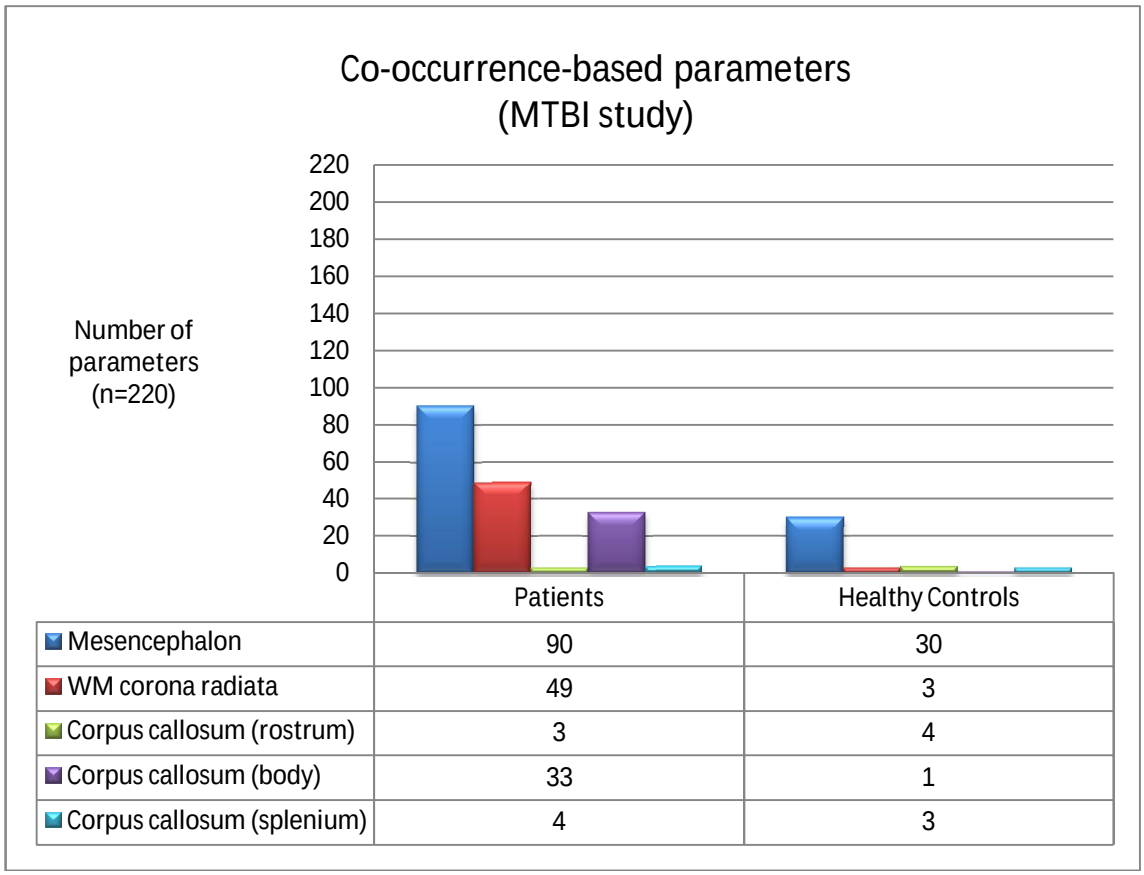

	Patients	Healthy Controls
Mesencephalon	90	30
WM corona radiata	49	3
Corpus callosum (rostrum)	3	4
Corpus callosum (body)	33	1
Corpus callosum (splenium)	4	3

Figure 8. *The number of statistically different co-occurrence-based parameters ($p<0.05$) are presented, as analysed with the Wilcoxon signed-rank test for patients and controls between hemispheres in the mesencephalic area and the WM in the level of the corona radiate and between segments of the CC.*

Most of the differences were obtained in the mesencephalic area. Also in the level of the corona radiata in the WM, there was a clear difference in the number of differing parameters between patients and controls. While analysing the segments of the CC, the body of the CC seemed to differ from the rostrum and splenium in patients.

5.2.4 Run-length matrix-based parameters

Many of the run-length matrix-based parameters were statistically different in all analysed imaging sequences in the breast cancer study. Results of the evaluation of run-length matrix-based parameters between breast cancer lesions and healthy reference tissues using standard and freehand ROIs and the evaluation between IDC and ILC are presented in Figure 9.

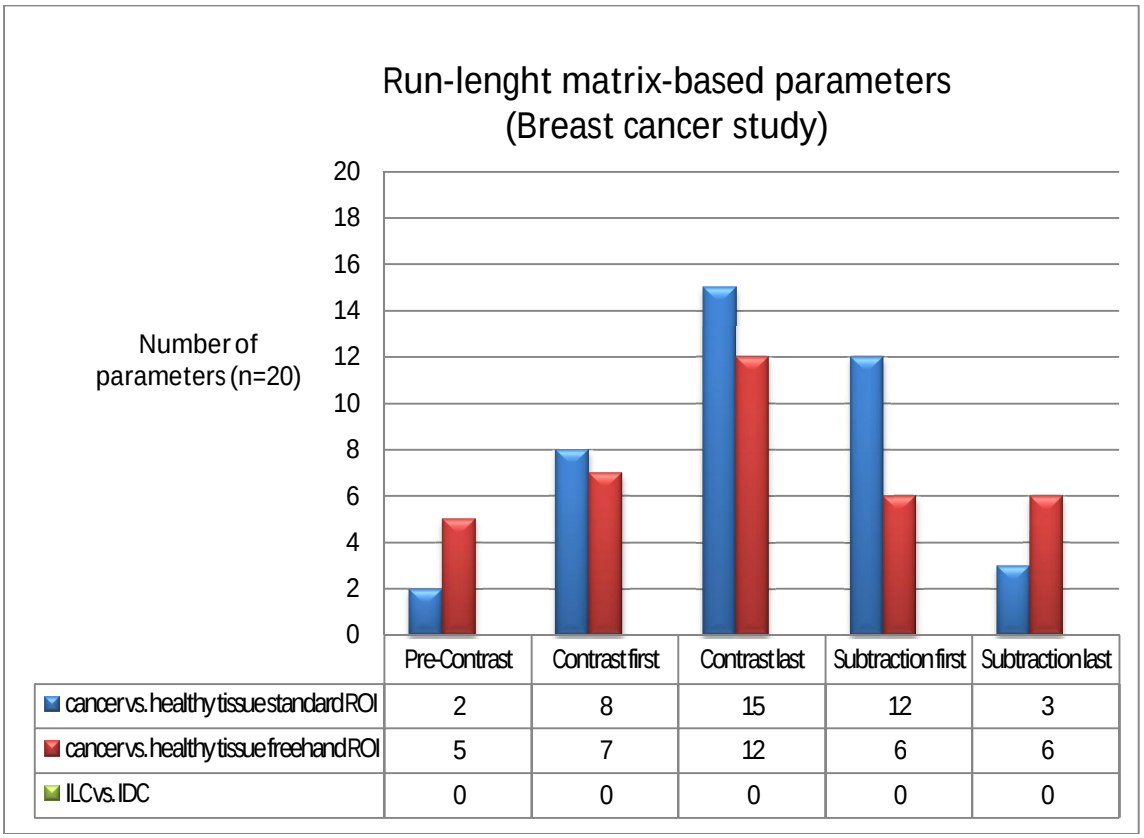

	Pre-Contrast	Contrast first	Contrast last	Subtraction first	Subtraction last
cancer vs. healthy tissue standard ROI	2	8	15	12	3
cancer vs. healthy tissue freehand ROI	5	7	12	6	6
ILC vs. IDC	0	0	0	0	0

Figure 9. *The numbers of statistically different run-length matrix-based parameters ($p<0.05$) are presented, as analysed with the Wilcoxon signed-rank test for every tested imaging sequence between healthy tissue and cancer tissue (using standard and freehand ROIs) and invasive lobular carcinoma (ILC) and invasive ductal carcinoma (IDC).*

Again, when using freehand ROI, the number of significantly different parameters was more consistent than when using standard ROIs. However, the run-length matrix-based parameters seemed to perform rather well in discriminating cancer tissue from healthy tissue. None of the run-length matrix-based parameters were statistically different between ILC and IDC.

The numbers of statistically different run-length matrix-based parameters in the mesencephalon, in the WM in the level of the corona radiata between hemispheres and between segments of the CC in MTBI patients and healthy controls are presented in Figure 10.

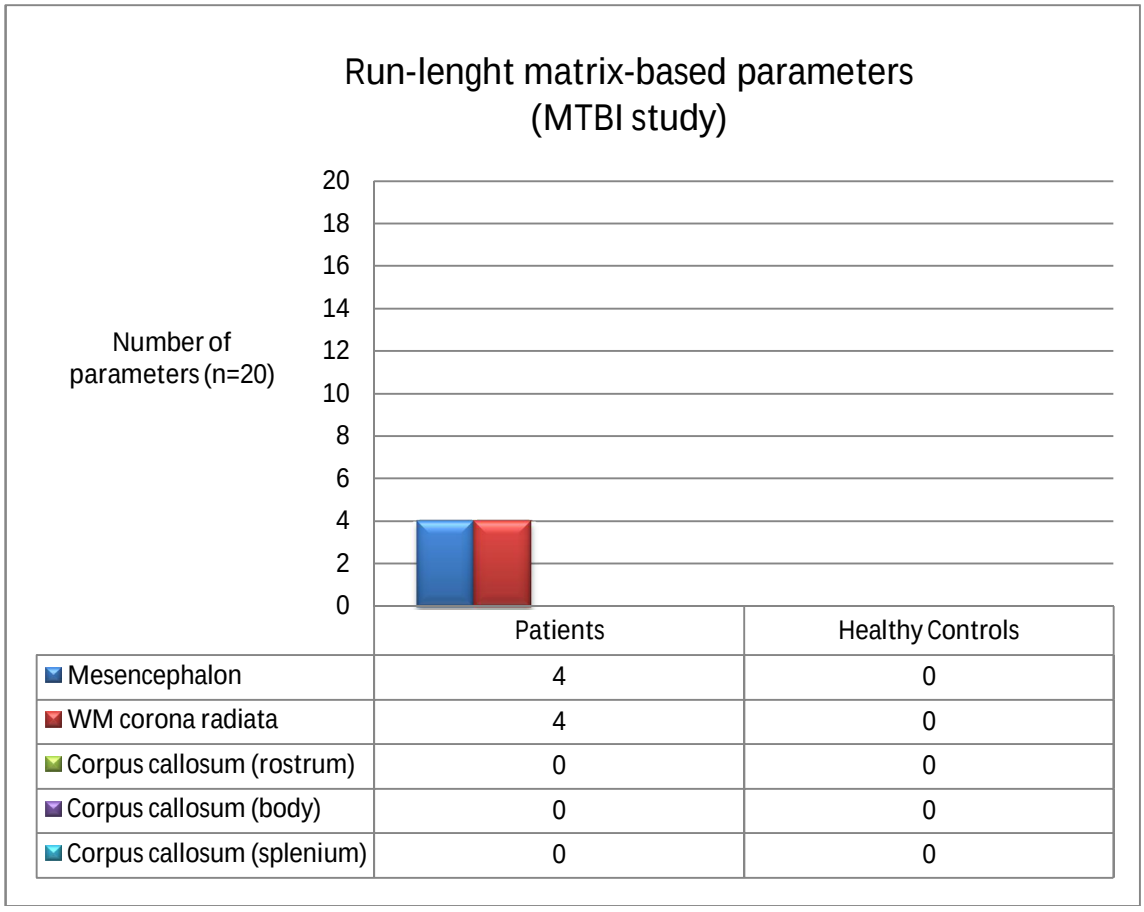

	Patients	Healthy Controls
Mesencephalon	4	0
WM corona radiata	4	0
Corpus callosum (rostrum)	0	0
Corpus callosum (body)	0	0
Corpus callosum (splenium)	0	0

Figure 10. *The numbers of statistically different run-length matrix-based parameters ($p<0.05$) are presented, as analysed with the Wilcoxon signed-rank test for patients and controls between hemispheres in the mesencephalic area and the WM in the level of the corona radiata and between segments of the CC.*

The run-length matrix-based parameters were statistically different only on patients and in the mesencephalic area and the WM in the level of the corona radiata. In analyses of the segments of the CC, there were no different run-length matrix-based parameters in patients or in healthy controls.

5.2.5 Autoregressive model-based parameters

Some of the autoregressive model-based parameters were statistically different in the breast cancer study, especially while using freehand ROI. Results of the evaluation of autoregressive model-based parameters between breast cancer lesions and healthy reference tissues using standard and freehand ROIs and the evaluation between IDC and ILC are presented in Figure 11.

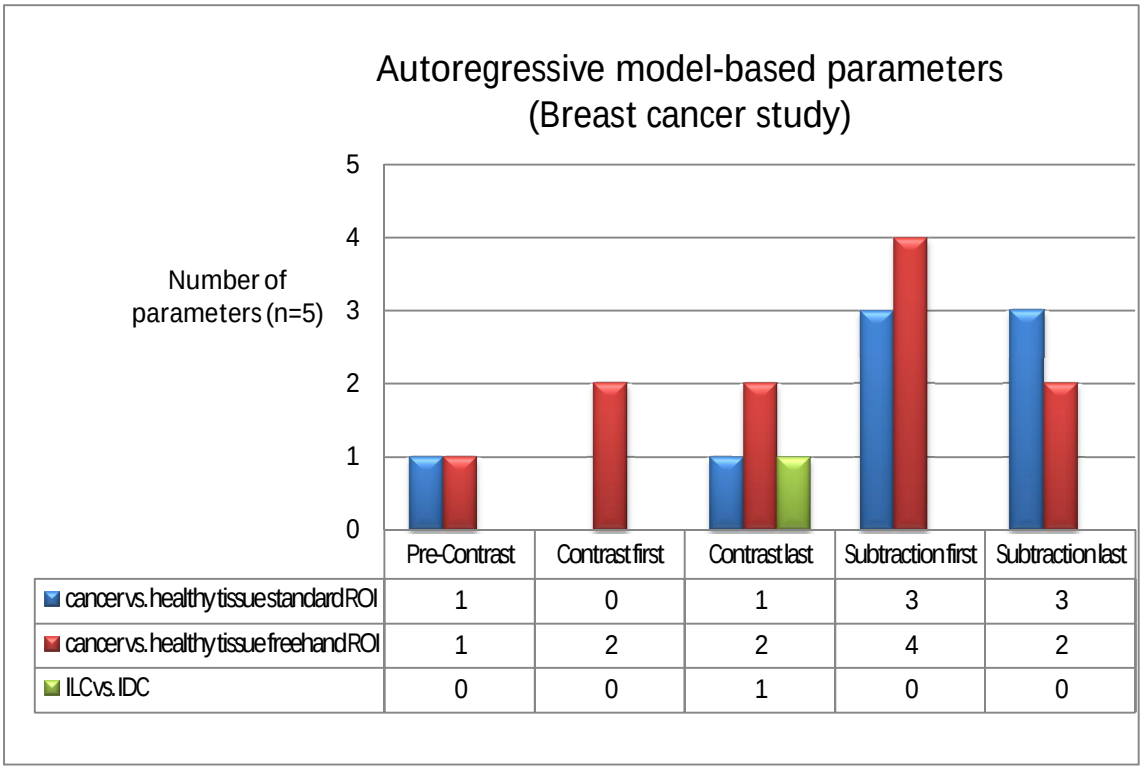

Figure 11. *The numbers of statistically different autoregressive model-based parameters ($p<0.05$) are presented, as analysed with the Wilcoxon signed-rank test for every tested imaging sequence between healthy tissue and cancer tissue (using standard and freehand ROIs) and invasive lobular carcinoma (ILC) and invasive ductal carcinoma (IDC).*

Once again, when using freehand ROI, the numbers of statistically different parameters were more consistent than when using standard ROIs. There were only five autoregressive model-based parameters calculated by the software. However, they performed rather well in discriminating cancer tissue from healthy tissue but not in discriminating between ILC and IDC.

There were no statistically different autoregressive model-based parameters in the mesencephalon or in the WM in the level of the corona radiata between hemispheres, either in patients or in controls. Only one parameter was statistically different in the body of the CC when assessing differences between segments of the CC in MTBI patients.

5.2.6 Wavelet-based parameters

Results of the evaluation of Wavelet-based parameters between breast cancer lesion and healthy reference tissue using standard and freehand ROIs and the evaluation between IDC and ILC are presented in Figure 12.

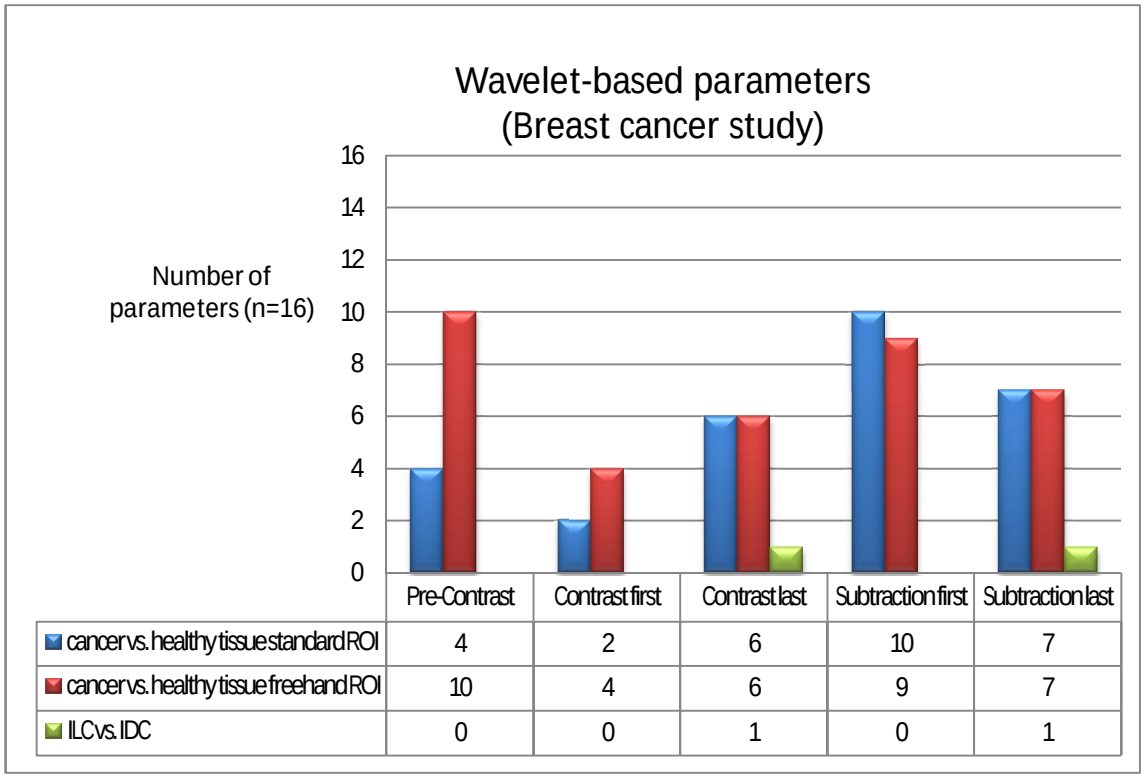

	Pre-Contrast	Contrast first	Contrast last	Subtraction first	Subtraction last
cancer vs. healthy tissue standard ROI	4	2	6	10	7
cancer vs. healthy tissue freehand ROI	10	4	6	9	7
ILC vs. IDC	0	0	1	0	1

Figure 12. *The numbers of statistically different wavelet-based parameters ($p<0.05$) are presented, as analysed with the Wilcoxon signed-rank test for every tested imaging sequence between healthy tissue and cancer tissue (using standard and freehand ROIs) and invasive lobular carcinoma (ILC) and invasive ductal carcinoma (IDC).*

Wavelet-based parameters showed rather good discrimination between cancer tissue and healthy tissue. Again, slightly better results were obtained using freehand ROI and subtracted images. Wavelet-based parameters did not seem to discriminate ILC and IDC.

The numbers of statistically different wavelet-based parameters in the mesencephalon, in the WM in the level of the corona radiata between hemispheres and between segments of the CC in MTBI patients and healthy controls are presented in Figure 13.

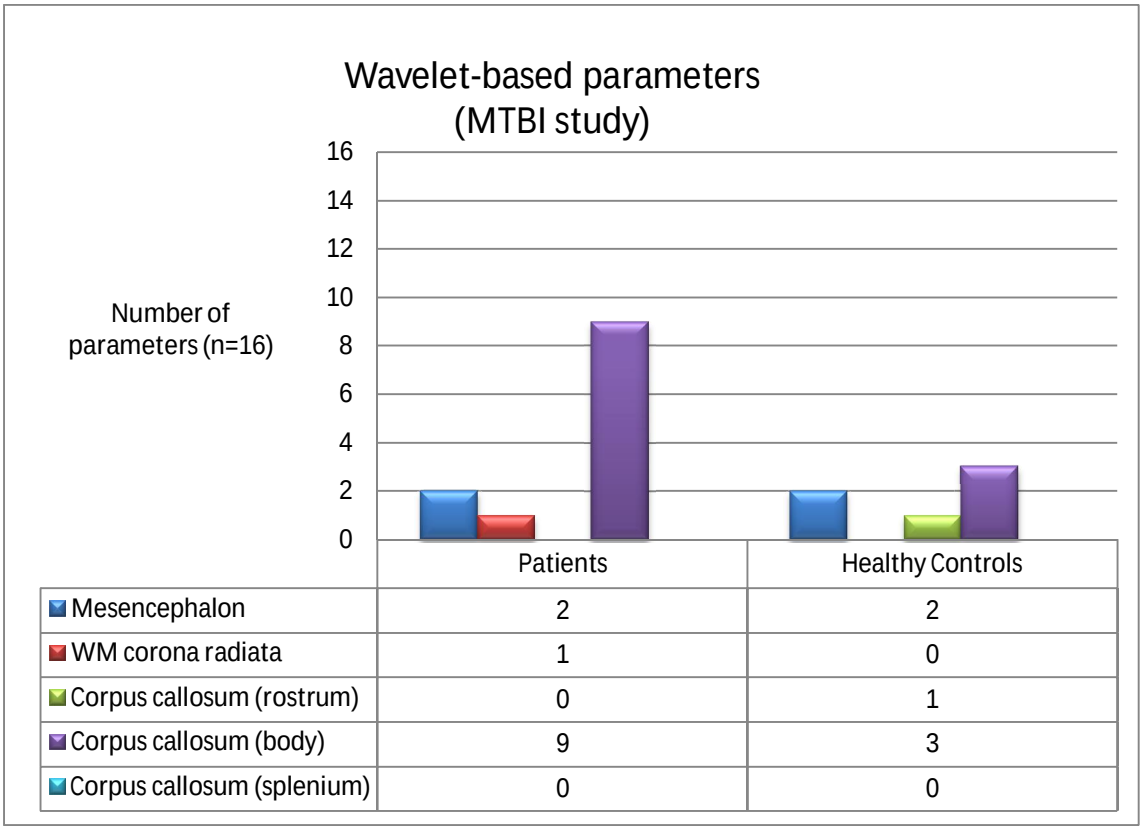

	Patients	Healthy Controls
Mesencephalon	2	2
WM corona radiata	1	0
Corpus callosum (rostrum)	0	1
Corpus callosum (body)	9	3
Corpus callosum (splenium)	0	0

Figure 13. *The numbers of statistically different wavelet-based parameters ($p<0.05$) are presented, as analysed with the Wilcoxon signed-rank test for patients and controls between hemispheres in the mesencephalic area and the WM in the level of the corona radiata and between segments of the CC.*

Wavelet-based parameters seemed to have discriminative power only when analysing segments of the CC. There were 9/16 statistically different wavelet-based parameters in the body of the CC in patients. In other analysed brain regions, the wavelet-based parameters did not perform well.

6. DISCUSSION AND CONCLUSIONS

The field of quantitative medical image analysis is in constant development. Imaging technologies, different image analysis methods and CAD systems are being developed to increase the information obtained from the images, to aid in the interpretation of medical images and to assist in decision-making processes for further examination or treatment planning. To implement these image analysis systems in clinical use, the methods should be made practical, fast, and as accurate as possible.

Because image texture is known to provide information that is not always visible to the human eye, the analysis of texture parameters may offer a useful way for increasing the information obtainable from medical images. This thesis concentrates on evaluating whether texture analysis could provide an additional tool for clinical medical MR image analysis in characterising abnormalities.

6.1 Additional value of texture analysis in the clinical context

6.1.1 Texture analysis of visible lesions

Studies I and II concentrated on texture analysis of breast cancer using breast MR images. Even though the MRI has a high sensitivity in diagnosing breast cancer, image interpretation is still challenging. These challenges include misinterpretation due to hormonal status of the patient (Kuhl et al., 1997), difficulties in interpretation from surgical (Cohen et al., 1996) or therapeutic interventions (Turnbull, 2009), overlap in the MRI appearance of some benign and malignant diseases and over- or underestimation of lesion size (Behjatnia et al., 2010; Onesti et al., 2008). Overestimation of lesion size is generally due to the presence of DCIS or LCIS and usually occurs with lesions over 20 mm. These overestimations occur in up to 10% of cases, while underestimation of lesion size occurs in equal proportion (Boetes et al., 1994; Boetes et al., 2004). Thus, while the location of the lesion and its margins can usually be rather well determined, the malignancy and the histopathology of the lesion may be difficult to characterize by conventional MRI alone.

The results of breast MRI TA studies demonstrated that TA with the combined set of

features succeeded in classifying normal breast tissue and breast cancer tissue with all applied analysis methods, all analysed sequences and all ROI settings. It should be noted, however, that only classification procedures that could be performed automatically with PCA, LDA and NDA were performed, as the number of samples was not large enough to be split into a training set and a validation set to run further neural network classifications. Many other studies have achieved promising results differentiating malignant and benign lesions using contrast-enhanced images in their texture analysis (Gibbs and Turnbull, 2003; Chen et al., 2007; Karahaliou et al., 2010; McLaren et al., 2009; Nie et al., 2008). In our studies, subtracted and pre-contrast images were also used to evaluate the effects of selected image series on the texture analysis results. Even though the overall classification accuracy was good, the analyses with pre-contrast and contrast series were slightly poorer than the subtracted series. Because the classification results were successful, the results indicate that the cancerous tissue has a different type of texture than healthy breast tissue and tissue near the cancerous tissue. Therefore, texture analysis might constitute a tool for evaluating the size of tumours that might be over- or underestimated by MRI by helping radiologists segment the tumour margins more accurately.

TA might be helpful for detecting and characterizing malignancy and the histopathological differences of lesions, thereby providing a solution for the reported problem of the relatively low specificity of breast MRI (Orel et al., 2006; Warren et al., 2005; Macura et al., 2006), as it is the overlap in the MRI appearance of some benign and malignant diseases that limits the specificity of breast MRI. As differences in enhancement patterns (Macura et al., 2006) and in texture features between malignant and benign diseases have been reported (Gibbs and Turnbull, 2003; Newell et al., 2010; Nie et al., 2008; Karahaliou et al., 2010; Woods et al., 2007), we also wanted to determine whether it was possible to identify texture differences between the two most common histological types of breast cancer. To the best of our knowledge, no other studies have undertaken differentiating histological types of breast cancer by TA. Typically, invasive ductal carcinoma (IDC) grows as a mass and produces a strong desmoplastic reaction in the surrounding tissue. In contrast, invasive lobular carcinoma (ILC) has a characteristic histopathologic appearance consisting of small, uniform tumour cells with round nuclei and scanty cytoplasms arranged in a classic single-file pattern and has a tendency to spread diffusely or between the collagen fibres of the breast (Tavassoli, 1999). Even though it has been reported that the enhancement profiles found for invasive lobular carcinoma are substantially lower and less specific (Lee et al., 1998) than with IDC, the dynamic and morphologic profiles overlap considerably (Dietzel et al., 2010). The hypothesis was that the different growth patterns of ILC and IDC might make it possible to differentiate between these two histological types by means of TA. Good classification accuracy in differentiating between ductal and lobular carcinoma was achieved. Therefore, TA might offer a tool for characterizing ILC, as it often presents more diagnostic difficulties than IDC in clinical examination and

conventional imaging due to its unique growth patterns (Yeh et al., 2003).

In Study V, the effectiveness of TA discrimination power in differentiating MS plaques from white matter and lesion-adjacent normal-appearing white matter (NAWM) was evaluated. Conventional MRI has enabled an earlier diagnosis of MS, but despite its increasing role in the clinical management and scientific investigation of MS, conventional MRI is limited by pathological specificity and sensitivity to diffuse damage in NAWM and normal-appearing grey matter. The development of modern imaging techniques for the early detection of brain inflammation and the characterisation of tissue-specific injury is an important objective and of increasing interest in MS research. Studies have demonstrated that TA has the potential to support the early diagnosis of MS, as it is particularly useful in detecting subtle tissue changes (Theocharakis P, 2009; Yu et al., 1999; Mathias et al., 1999; Zhang et al., 2008). The results of Study V showed rather accurate classification of MS plaques from white matter in three different MR sequences, with only a slight variation in classification accuracy depending on the feature selection method, classification method and the analysed sequence. The results showed that texture analysis has potential in the classification of MS plaques from WM and even from NAWM, which often presents difficulties in detection in conventional MRI. The lack of a control group is a limitation of this study, particularly when focusing on these non-visible changes in NAWM.

6.1.2 Texture analysis of non visible changes

The mild traumatic brain injury (MTBI) studies (Studies III and IV) concentrated on the texture analysis of non-visible diffuse changes. Even with new, improved imaging modalities, such as diffuse tensor imaging (DTI) and new MRI sequences, it is still difficult to detect damaged lesions and to make the diagnosis of MTBI on the basis of imaging findings. However, some studies have demonstrated abnormalities on DWI, ADC, or DTI without any structural damage seen in conventional MRI sequences such as T1, T2 (Rutgers et al., 2008; Chu et al., 2010). Textural properties of the MR image may capture direction and density of fibre bundles and the density and direction of vessels supplying the WM; therefore, TA may provide quantitative means for characterizing the changes in WM tracts caused by trauma in cases in which tissue changes cannot be detected by direct visual inspection. To the best of our knowledge, prior comparable studies have not been found in the literature.

Because our patient group all had radiologically normal MRI and CT scans, it proved to be very challenging to evaluate the texture changes potentially caused by the injury. Because there were no visible lesions in the MR images, it was not possible to categorise the patients according to which part of the head may have sustained the damage; therefore, the placement of the ROI was based only on the assumption of where damage might be located on the basis of reported imaging findings (Rutgers et

al., 2008; Chu et al., 2010; Gentry et al., 1988) and the clinical knowledge of typical sites of axonal injury. Therefore, no classification analyses were conducted. The results showed that there were significant differences between hemispheres in texture parameters in cerebral tissue in the mesencephalon, in the WM and in the segments of the CC in patients, but no considerable changes were observed in the healthy control group. The texture of the body of the CC seemed to be different than the texture in the rostrum/genu or the splenium. Conventional imaging and pathologic-anatomic studies have indicated that the posterior CC is more susceptible to fibre disruption than is the anterior CC (Gentry et al., 1988). Additionally, some DTI findings have been reported in segments of the CC. In the DTI of MTBI study, Rutgers et al. found that patients with mild TBI showed DTI abnormalities in the genu, without significant DTI changes in the body and splenium; in more severe TBI, DTI showed that the splenium was affected in addition to the genu (Rutgers et al., 2008). In the MTBI study by Wilde et al. (Wilde et al., 2008), decreased ADC and increased FA were identified within the mid-sagittal fibres traversing the CC in patients with acute MTBI relative to controls. Even though, there have been some previously reported imaging findings in the CC in MTBI, we cannot be sure that our textural findings are caused by trauma. Because the CC is the largest fibre bundle in the human brain, connecting the two cerebral hemispheres with more than 300 million fibres, different orientations or densities of fibres might yield different textures. The fibre composition in the CC has been studied (Aboitiz et al., 1992; Rabi et al., 2007), and it has been observed that there are fewer nerve fibres in the body of the CC per unit area, and more Glial cells occupied more of the body of the CC than other segments. Therefore, it is possible that the textural changes in the body of CC are caused by the different densities and numbers of fibres in different regions of the CC. However, we can note that such distinct textural differences in the healthy control group were not found.

In Study IV, significant correlations between texture parameters and memory composite scores were observed, especially in the mesencephalic area. Additionally, significantly correlating parameters between FA and ADC values were observed in the same region. These results might indicate that texture parameters could pinpoint an MTBI-damaged region that is otherwise non-visible in conventional MRI. Although statistically significant differences between hemispheres were found, and some of the findings correlated with the DTI findings and even neuropsychological tests, it is still difficult to tell if these findings actually result from trauma. In future studies, we would definitely need to have a larger control group to validate the significance of the findings.

6.2 Evaluation of the applied texture methods

The goals of feature selection are to improve classification performance, to reduce the computation time of the features and to provide a better understanding of the underlying

process (Guyon and Elisseeff, 2003). The challenge of feature selection is to determine which features must be selected for optimal classification. One goal of this thesis was to determine whether it was possible to identify some optimal feature sets for different applications to reduce the number of calculated texture parameters to use to extract the relevant information in each application, with the aim of making the whole texture analysis more approachable in clinical settings.

The co-occurrence matrix-based method appears to be the most commonly applied TA method, especially in the field of medical image analysis. In a review of the literature, we can observe that nearly all TA of breast MRI studies have used only this method (See Table 2). This has also been the trend in brain and neurological TA studies (See Table 3).

The TA software used in our studies calculated almost 300 texture parameters in all, using six different texture methods (histogram, COM-, RLM-, AR-, gradient-based and wavelets-based methods). In some cases, it might be optimal to calculate all these features from different texture methods to find the best combination for classification, but one must also consider the fact that the classification rates may start to degrade if too many texture methods are integrated due to the curse of dimensionality (Puig and Garcia, 2006). The MaZda software provides feature selection algorithms that are useful in classification tasks (Hajek et al., 2006). Most of the algorithms, however, might be insufficient in the sense that they depend on various dataset characteristics (Puig and Garcia, 2006). Because we are working with clinical images, the analyses do not depend only on the imaged target but also on the imaging parameters, the quality of achieved images and the size of the available data.

What we may observe from the statistical tests on the raw parameters calculated from breast MR images and brain MR images in the MTBI study is that there were a rather large number of statistically different parameters between analysed regions, regardless of the fact that the quality of the statistically different parameters seemed to be dependent on the application, the analysed sequence and other dataset characteristics.

6.2.1 Histogram-based method

The main advantage of the first-order histogram-based approach is its simplicity: it uses standard descriptors of the histogram distribution, such as mean brightness, variance, skewness, kurtosis and percentiles, to characterize the data. However, the power of the approach for discriminating between unique textures might be limited in certain applications because the method does not consider the spatial relationship or the correlations between pixels.

If we examine first-order histogram-based parameters in TA of breast MRI, we can see that no histogram-based parameters were significantly different in images from contrast sequences (Figure 5), while in images from subtraction sequences and pre-

contrast sequences, almost all histogram-based parameters yielded significantly different values when analysing parameters between the cancerous area and healthy tissue. In these sequences, the contrast and the grey level intensities were visibly different between analysed regions. If we were studying differences between two enhancing lesions, we would probably lose some information on the texture due to the enhancement patterns, which might be detected with some other texture parameters. Therefore, the histogram-based parameters do not seem to be the optimal choice in discriminating ILC from IDC.

In brain images, the histogram-based parameters showed potential in discrimination tasks between hemispheres in the mesencephalic area and in the segments of the CC in patients. They could not discriminate WM between hemispheres, in either patients or controls. This was expected because the analysed regions in the WM had very similar grey level intensities.

6.2.2 Gradient-based method

Based on the histogram of the image gradient, a similar feature set to the first-order histogram can be calculated for the distribution of image intensity. These features were not discriminated our studied regions in either study; therefore, this method cannot be considered a preferable choice for TA in the selected applications.

6.2.3 Co-occurrence matrix

The co-occurrence matrix is a second-order statistical measure of grey level variation. It indicates the joint probability of a grey level occurrence of two pixels at a certain displacement in an image. It is a useful method for enhancing details and is frequently used as an aid for interpretation of an image.

The co-occurrence matrix-based parameters showed good discriminatory power of raw parameters between tissues in all breast MR images from different sequences. The co-occurrence matrix is probably the most-used method for TA of breast MR images; it has enabled very promising results in discriminating malignant from benign lesions (See Table 2). Gibbs and associates (Gibbs and Turnbull, 2003) found the most discriminative features between benign and malignant lesions to be variance, sum entropy, and entropy, which are somewhat in line with our results, as most of the discriminative parameters in our study were angular second moment and entropy-based parameters. Because the angular second moment achieved higher values in the healthy tissue and the entropy-based parameters achieved higher values in cancerous tissue, we might assume that cancerous tissue has a more complex texture than does healthy tissue, given the fact that angular second moment is a measure of the homogeneity of an image, and a higher value of this feature indicates that its intensity varies less in an image. In

contrast, the sum entropy is a measure of randomness within an image; entropy is an indication of the complexity within an image, and complex images produce higher entropy values.

The significantly different parameters between the IDC and ILC lesions were also mainly those measuring the complexity and randomness of the image (e.g., entropy-based parameters). The fact that these texture parameters differ significantly between ILC and IDC might indicate that the texture of one lesion is more complex than that of the other, probably since ILC typically displays more diverse morphological appearances than does IDC, and TA was able to distinguish these subtle differences.

The co-occurrence matrix-based parameters showed good discriminative power of raw parameters between brain hemispheres and segments of the CC in our MTBI study. In the mesencephalic area, again, most of the discriminative parameters were parameters measuring homogeneity or randomness and complexity of the image. There were also similar discriminative parameters observed between hemispheres with the healthy controls; therefore, we can assume that some of these differences between hemispheres are normal and do not derive from the trauma. When the TA results were compared with the composite scores for verbal and visual memory, significant correlations in the mesencephalic area and in segments of the CC were observed. These results indicate that if the texture of the measured region is complex and heterogeneous, the patient will not perform as well on verbal memory tests when compared to an area found to be very homogeneous. Therefore, we might assume that if the texture in the mesencephalic area is random and heterogeneous, then MTBI has damaged this region, and the patient may have difficulty with the memory tests. In the area of the genu of the CC, correlations between entropy and angular second moment texture parameters and the visual memory composite score were found. In this case, entropy was negatively correlated, while the angular second moment was positively correlated, indicating that the area measured was likely to be heterogeneous, and the patient's performance on visual memory tests would be poor.

Significantly correlating parameters were observed in patients in the left side of the mesencephalon with FA and ADC values resulting from DTI. In a heterogeneous area, the entropy values increased, the inverse difference moment and the angular second moment decreased, the FA decreased, and the ADC increased. Some previous studies have shown that decreased FA and increased ADC follow MTBI (Lo et al., 2009; Kumar et al., 2009; Mayer et al., 2010); the DTI changes in the WM have also been found to correlate with post-concussion syndrome severity and emotional distress (Kumar, et al., 2009; Chu, et al., 2008).

6.2.4 Run-length matrix

Run-length statistics capture the coarseness of a texture in specified directions. A run is

defined as a string of consecutive pixels that have the same grey level intensity along a specific linear orientation. Fine textures are considered to contain more short runs with similar grey level intensities, while coarse textures tend to have more long runs with significantly different grey level intensities (Galloway, 1975). Run-length matrix-based parameters performed well in discriminating breast cancer tissue from healthy tissue but not in discriminating the two histological types. These results indicate that the breast cancer tissue would have a more coarse textural appearance than does the healthy tissue. Additionally, we found that the parameters discriminated brain tissue between hemispheres on the mesencephalic area and on the level of the corona radiata in patients.

6.2.5 Autoregressive-model

Autoregressive model-based parameters performed relatively well in discriminating breast cancer from healthy tissue, but no statistically different parameters were observed in the MTBI study in any given region. It seems that the autoregressive model was not even suitable for our breast cancer application, as only five texture features could be calculated; therefore, its usefulness is limited compared to the other methods.

6.2.6 Wavelet-based method

The transform method of texture analysis implemented in MaZda is based on a discrete Haar wavelet. The wavelet-based method is not widely used in texture medical applications; however, Jafari-Khouzani et al. achieved good results while studying lateralising mesial temporal lobe epilepsy (Jafari-Khouzani et al., 2010). The wavelet-based method seemed to discriminate well in both of our studies. In the breast cancer study, the wavelet-based features showed good discrimination between cancerous and healthy tissue; however, they did not discriminate ILC from IDC. In the MTBI study, the wavelet-based features were statistically different, particularly in the body of the CC. The wavelet-based features seemed efficient in our studies. Compared to co-occurrence matrix-derived features, Kociołek et al. (Kociołek et al., 2001) stated that DWT-derived features were more efficient. The main advantage of the wavelet-based method is a relatively small vector of features, which is sufficient for very good texture classification (Kociołek et al., 2001).

6.3 Texture analysis approach for clinical use

At this point, the complete analysis takes a long time, particularly due to the manual segmentation and setting the ROIs. Tools for semiautomatic segmentation would speed

up the analysis considerably. Semiautomatic or even automatic segmentation would work in applications in which there is a specific visible lesion, such as in our breast cancer and MS studies, but not in applications such as our MTBI study, where there is no visible lesion. Even in the cases of visible lesion, there would still be a need for the professional skill of a radiologist to visually evaluate normal and abnormal findings, because the texture measures of a target tissue or structure might be sensitive to ROI size, shape and placement. The differences between standard ROIs and freehand ROIs were evaluated in our studies to determine whether ROI selection has a notable effect on texture analysis results. Thus, ROIs with standard sizes and shapes would considerably speed the analysis process. Slightly better classification results were obtained with the freehand rather than standard ROI in the breast cancer study. It should be noted that a few of the tumours had areas of central necrosis that had some influence on our TA results, yielding some misclassifications when using the standard ROI box. Additionally, with the standard ROI, some of the misclassified results were due to the small size of the lesion compared to the ROI box. A standard-size ROI box may also overlap some pixels of other neighbouring tissues being investigated, thus causing partial volume pixels or even whole pixels representing neighbouring tissues, which would affect calculated parameter values. There were distinct differences between the hand-drawn and standard ROIs of MS plaques in intra-tissue texture parameter comparisons, but again, no great differences in classification results were observed. Standardised ROI on a lesion returned a slightly weaker classification from WM than did freehand ROI. Despite the fact that the selected ROI did not influence our classification result significantly, in our studies, there were some notable differences in the numbers of most discriminative parameters; thus, the freehand ROIs seemed to be slightly superior to the standard ROIs.

To use TA in daily clinical practice, more data must be collected from both patients and controls and analysed as a training set to build a texture model in each application, which could then be used in tissue discrimination. The efficacy of this type of pattern-recognition system is highly dependent on the training set used for pattern learning. The goal of the pattern recognition system is to be able to generalise well, so that patterns that the system has never encountered before are correctly classified. In a clinical setting, this provides a challenge. This study has shown that the discriminative texture parameters vary depending on the applied imaging sequence. In the breast cancer study, we could see that the classification results and discriminative parameters varied between pre-contrast, post-contrast and subtracted images. In the MS study, the parameters describing tissues did not change considerably in slice-to-slice comparisons. The differences between anatomical levels were also acceptably small, especially in T1-weighted MPR sequences without contrast agent. In all comparisons, there were some small differences between imaging sequences. Taking these into account, it is obvious that texture features are somewhat sensitive to the imaging sequence, slice thickness and other sequence characteristics. Consequently, one would always have new training data

if some of the imaging parameters or other technical points were changed. The gathering of sufficient training data could become a problem, especially in cases of breast cancer, as the different histological types of cancer yield differing discriminative parameters. Additionally, we would also have to take into account that even tissues such as benign fibrocystic lesions and blood vessels experience contrast enhancement, which can result in misclassification.

The applied texture analysis software provides numerous texture parameters that can be then used for classification. The software also provides feature selection algorithms for the selection of optimal feature sets for classification. The applied texture methods were evaluated to determine whether the number of calculated features could be narrowed down and if we could find some optimal method for clinical applications (if not to reduce the feature calculation time, then to make the process more understandable and approachable in clinical usage). The problem of selecting the optimal features derives partly from the fact that, if used in a clinical setting, there are numerous aspects that can affect the discriminative parameters. The images may suffer from artefacts of different origins, such as image thermal noise, image background non-uniformity from magnetic field inhomogeneities, and non-standardness of image greyscale intensity. Additionally, the involuntary movements of the patient (e.g., heartbeat, breathing, etc.) can cause artefacts in images. High image quality and minimisation of image artefacts are important, especially in quantitative analyses. Although numerous methods exist to correct some of these problems, such as intensity inhomogeneity artefacts (Vovk et al., 2007) and image intensity (Madabhushi and Udupa, 2005; Zhuge et al., 2009), many of the problems, especially those that are patient-oriented, cannot be fixed.

In our future studies, we plan to broaden our materials and concentrate on evaluating the effectiveness of specific characterizing parameters. Additionally, the 3D TA option, along with 2D TA, will be considered. The future aims of TA in the breast cancer study should be to discriminate malignant from benign changes, to further characterise histological types, to test the effectiveness of TA to detect in situ carcinomas and to try to make the texture application practical for clinical use. In the MTBI study, the future aim is to further evaluate TA findings with DTI to improve our chances of detecting early and subtle neuropathological changes, thereby facilitating better management of MTBI. In the MS study, we aim to further characterise MS lesion subtypes to assist in therapy decisions and to detect lesions before they have transformed from reversible to irreversible states.

Conclusions

1) On the basis of this study, it may be concluded that texture analysis performed well in differentiating visible lesions from healthy tissue in studies of breast cancer (Studies I and II) and in the MS study (Study V). It also performed well in discriminating non-visible differences between two histological types of breast cancer: invasive ductal carcinoma and invasive lobular carcinoma. The results indicate that TA could provide a reproducible quantitative method to aid radiologists in the detection and classification of pathological findings in breast MRI and in studying MS. TA also showed potential in the detection of non-visible diffuse changes in the MTBI studies (Studies III and IV) and the MS study (Study V). In future studies, more materials will be needed to validate the significance of our findings.

2) A single texture method that suits all clinical applications considered in this thesis could not be identified. However, based on the findings, a case-specific selection of the texture parameters from histogram-, co-occurrence-, run-length- and wavelet-based parameters would likely be the optimal solution.

3) For clinical usage, texture analysis must be simplified drastically and should be implemented in other CAD systems. With proper training sets and ROI setting methods, the system could be used to draw the radiologist's attention to suspicious regions. However, for reliability in correct classification and diagnosis, the system must be further evaluated with larger data sets.

7. REFERENCES

Aboitiz, F., Scheibel, A.B., Fisher, R.S. and Zaidel, E., 1992. Fiber composition of the human corpus callosum. *Brain Res*, 598(1), pp.143-53.

Allen, R.L. and Mills, D.W., 2004. *Signal analysis: Time, frequency, scale, and structure*. IEEE. Press (Wiley-Interscience), New York. E-book.

Dietzel M et al., 2010. Magnetic resonance mammography of invasive lobular versus ductal carcinoma: Systematic comparison of 811 patients reveals high diagnostic accuracy irrespective of typing. *J Comput Assist Tomog*, 34, pp.587-95.

Arfanakis, K. et al., 2002. Diffusion tensor MRI in temporal lobe epilepsy. *Magn Reson Imaging*, 20(7), pp.511-19.

Bader, W. et al., 2000. Does texture analysis improve breast ultrasound precision? *Ultrasound Obstet Gynecol*, 15(4), pp.311-16.

Bandettini, P., 2009. What's New in Neuroimaging Methods? *Ann N Y Acad Sci*, 1156, pp.260-93.

Basser, P.J. and Jones, D.K., 2002. Diffusion-tensor MRI: theory, experimental design and data analysis – a technical review. *NMR Biomed*, 15(7), pp.456-67.

Behjatnia, B. et al., 2010. Does size matter? Comparison study between MRI, gross, and microscopic tumor sizes in breast cancer in lumpectomy specimens. *Int J Clin Exp Pathol*, 3(3), pp.303-9.

Behrens, S. et al., 2007. Computer assistance for MR based diagnosis of breast cancer: present and future challenges. *Comput Med Imaging Graph*, 31(4-5), pp.236-47.

Belanger, H.G., Vanderploeg, R.D., Curtiss, G. and Warden, D.L., 2007. Recent neuroimaging techniques in mild traumatic brain injury. *J Neuropsychiatry Clin Neurosc*, 19(1), pp.5-20.

Bloch, F., 1952. *The principle of nuclear induction. Nobel Lecture, Physics*. [Online]. Available from: http://nobelprize.org/nobel_prizes/physics/laureates/1952/bloch-lecture.pdf [Accessed April 2011].

Bochar, S.A., 2001. Diffusion and perfusion-weighted magnetic resonance imaging of acute ischemic stroke. *Applied Radiology supplements*, 30.

Boetes, C. et al., 1994. MR characterization of suspicious breast lesions with a Gadolinium-enhanced Turbo- FLASH subtraction technique. *Radiolog*, 193(3), pp.777-81.

Boetes, C. et al., 2004. The role of MRI in invasive lobular carcinoma. *Breast Cancer Res Treat*, 86(1), pp.31-37.

Bonilha, L. et al., 2003. Texture analysis of hippocampal sclerosis. *Epilepsia*, 44(12), pp.1546-50.

Breast Imaging Reporting and Data System Atlas (BI-RADS Atlas). (2003). Reston: American College of Radiology (ACR).

Brown, M. and Semelka, R., 2010. *MRI: Basic Principles and Applications*. 4th ed. Wiley-Blackwell.

Buades, A., Coll, B. and Morel, J.M., 2005. A non-local algorithm for image denoising. In: *Proceedings of the 2005 IEEE Computer Society Conference (CVPR'05)*. 20-25 June 2005. IEEE Computer Society Washington, DC, USA. pp.60-65.

Bulacu, M. and Schomaker, L., 2007. Text-independent writer identification and verification using textural and allographic features. *IEEE TPAMI*, 29, pp.701-17.

CANTAB®, the Cambridge Neuropsychological Automated Testing Battery. (2004). Cambridge Cognition Ltd.

Carrol, L.J., Cassidy, J.D.H.L., Kraus, J. and Coronado, V.G., 2004. Methodological Issues and Research Recommendations for Mild Traumatic Brain Injury: The WHO Collaborating Centre Task Force on Mild Traumatic Brain Injury. *J Rehabil Med* , 43(suppl), pp.113-25.

Cassidy, J.D. et al., 2004. Incidence, risk factors and prevention of mild traumatic brain injury: Results of the WHO collaborating centre task force on mild traumatic brain injury. *J Rehab Med*, 43(suppl), pp.28-60.

Castellano, G., Bonilha, L., Li, L.M. and Cendes, F., 2004. Texture analysis of medical images. *Clin Radiol*, 59(12), pp.1061-69.

Castellino, R., 2005. Computer aided detection (CAD): an overview. *Cancer Imaging*, 23(5), pp.17-19.

Castillo, M., Smith, J., Kwock, L. and Wilbert, K., 2001. Apparent diffusion coefficients in the evaluation of high-grade cerebral gliomas. *ANJR*, 22(1), pp.60-64.

Cecil, K.M., Schnall, M.D., Siegelman, E.S. and Lenkinski, R.E., 2001. The evaluation of human breast lesions with magnetic resonance imaging and proton magnetic resonance spectroscopy. *Breast Cancer Res Treat*, 68(1), pp.45-54.

Chen, W.J., Giger, M.L., Bick, U. and Newstead, G.M., 2006. Automatic identification and classification of characteristic kinetic curves of breast lesions on DCE-MRI. *Med Phys*, 33(8), pp.2878-87.

Chen, W. et al., 2007. Volumetric texture analysis of breast lesions on contrastenhanced magnetic resonance image. *Magn Reson Med*, 58(3), pp.562-71.

Chen, D.R., Huang, Y.L. and Lin, S.H., 2001. Computer-aided diagnosis with textural features for breast lesions in sonograms. *Comput Med Imaging Graph*, 35(3), pp.220-26.

Chu, Z. et al. (2010). Voxel-Based Analysis of Diffusion Tensor Imaging in Mild Traumatic Brain Injury in Adolescents. *AJNR Am. J. Neuroradiol*, 31(2), pp.340-246.

Cohen, E.K. et al., 1996. Magnetic resonance imaging in potential postsurgical recurrence of breast cancer: pitfalls and limitations. *Can Assoc Radiol J*, 47(3), pp.171-76.

Dash, M. and Liu, H., 1997. Feature Selection for Classification. *Intelligent Data Analysis*, 1(3), pp.131-56.

de Oliveira M.S, et al., 2010. MRI-Texture Analysis of Corpus Callosum, Thalamus, Putamen, and Caudate in Machado-Joseph Disease. *J Neuroimaging*. Epub ahead of print.

de Oliveira, M.S. et al., 2011. MR imaging texture analysis of the corpus callosum and thalamus in amnestic mild cognitive impairment and mild Alzheimer disease. *AJNR Am J Neuroradiol*, 32(1), pp.60-6.

Desmond, K.L., Ramsay, E.A. and Plewes, D.B., 2007. Comparison of biphasic and reordered fat suppression for dynamic breast MRI. *J Magn Reson Imaging*, 25(6), pp.1293-98.

Dorrius, M.D. et al., 2011. Computer-aided detection in breast MRI: a systematic review and meta-analysis. *Eur Radiol*. (Epub ahead of print).

Duda, R., Hart, P. and Stork, D., 2001. *Pattern Classification.* New York: John Wiley and Sons.

Efros, A.A. and Leung, T.K., 1999. Texture Synthesis by Non-parametric Sampling. In: *IEEE International Conference on Computer Vision (ICCV'99)*. 20-27 September 1999. Corfu. pp. 1033–1038.

Esserman, L., Wolverton, D. and Hylton, N., 2002. Magnetic resonance imaging for primary breast cancer management: current role and new applications. *Endocr Relat Cancer*, 9(2), pp.141-53.

Farjam, R., Soltanian-Zadeh, H., Jafari-Khouzani, K. and Zoroofi, R.A., 2007. An image analysis approach for automatic malignancy determination of prostate pathological images. *Cytometry Part B: Clinical Cytometry*, 72B, pp.227-40.

Fischer, U., Kopka, L. and Grabbe, E., 1999. Breast carcinoma:effect of preoperative contrast-enhanced MR imaging on the therapeutic approach. *Radiology*, 213(3), pp.881-88.

Freeborough, P.A. and Fox, N.C., 1998. MR image texture analysis applied to thediagnosis and tracking of Alzheimer's disease. *IEEE Trans Med Imaging*, 17(3), pp.475-79.

Galloway, M.M. 1975. Texture analysis using gray level run lengths. *Computer Graphics Image Process*, 4, pp.172- 9.

Ganeshan, B. et al., 2011. Dynamic contrast-enhanced texture analysis of the liver: initial assessment in colorectal cancer. *Invest Radiol*, 46(3), pp.160-68.

Gentry, L.R., Godersky, J.C. and Thompson, B., 1988. MR imaging of head trauma: review of the distribution and radiopathologic features of traumatic lesions. *AJR Am J Roentgenol*, 150, pp.663–672.

Georgiadis, P. et al., 2009. Enhancing the discrimination accuracy between metastases, gliomas and meningiomas on brain MRI by volumetric textural features and ensemble pattern recognition methods. *Magn Reson Imaging 27:*, 27(1), pp.120-30.

Gibbs, P. and Turnbull, L.W., 2003. Textural analysis of contrast-enhanced MR Images of the breast. *Magn Reson Med*, 50(1), pp.92-98.

Gui, Y. and Ma, L., 2010. Periodic pattern of texture analysis and synthesis based on texels distribution. *Vis Comput*, 26, pp.951-64.

Guo, Y. et al., 2002. Differentiation of clinically benign and malignant breast lesions using diffusion weighted imaging. *J Magn Reson Imaging*, 16(2), pp.172-78.

Guo, Q., Shao, J. and Ruiz, V.F., 2009. Characterization and classification of tumor lesions using computerized fractal-based texture analysis and support vector machines in digital mammograms. *Int J Comput Assist Radiol Surg*, 4(1), pp.11-25.

Gupta, R. and Undrill, P.E., 1995. The use of texture analysis to delineate suspicious masses in mammography. *Phys Med Biol*, 40(5), pp.835-55.

Guyon, I. and Elisseeff, A., 2003. An introduction to variable and feature selection. *J of Machine Learning and Research*, 3, pp.1157–1182.

Hajek, M., Dezortova, M., Materka, A. and Lerski, R.,eds., 2006. *Texture analysis for magnetic resonance imaging*. Prague: Med4publishing.

Haralick, R.M., 1979. Statistical and structural approaches to texture. *Proceedings of the IEEE*, 67(5), pp.786-804.

Haralick, R.M., Shanmugam, K. and Dinstein, I., 1973. Textural features for image classification. *IEEE Transactions on SMC*, 3, pp.610-12.

Harms, S. and Flamig, D., 1993. MR imaging of the breast: technical approach and clinical experience. *Radiographics*, 13(4), pp.905- 912.

Harrison, L. et al., 2008. Non-Hodgkin lymphoma response evaluation with MRI texture classification. *J Exp Clin Cancer Res*, 28, pp.87-100.

Hendrick, R. 2008. *Breast MRI; Fundamentals and Technical Aspects*. New York: Springer.

Herlidou-Meme, S. et al., 2003. MRI texture analysis on texture test objects, normal brain and intracranial tumors. *Magn Reson Imaging*, 21(9), pp.989-93.

Heywang, S. et al., 1986. MR imaging of the breast: comparison with mammography and ultrasound. *J Comput Assist Tomogr*, 10(4), pp.615-20.

Heywang-Köbrunner, S.H. et al., 2001. International investigation of breast MRI: results of a multicentre study (11 sites) concerning diagnostic parameters for contrastenhanced MRI based on 519 histopathologically correlated lesions. *Eur Radiol*, 11(4), pp.531-46.

Heywang-Köbrunner, S.H., Viehweg, P., Heinig, A. and Kuchler, C., 1997. Contrast enhanced MRI of the breast: accuracy, value, controversies, solutions. *Eur J Radiol*, 24(2), pp.94-108.

Heywang, S.H. et al., 1989. MR imaging of the breast with Gd-DTPA: use and limitations. *Radiolog*, 171(1), pp.95-103.

Hofmann, T., Puzicha, J. and Buhmann, J.M., 1998. Unsupervised texture segmentation in a deterministic annealing framework. *IEEE TPAMI*, 20, pp.803-18.

Hori, M. et al., 2003. T1-Weighted Fluid-Attenuated Inversion Recovery at Low Field Strength: A Viable Alternative for T1-Weighted Intracranial Imaging. *AJNR Am J NeuroRadiol*, 24(4), pp.648-51.

Hornak, J.P., 2002. *The Basics of MRI*. [Online] Available from http://www.cis.rit.edu/htbooks/mri/. [Accessed April 2011]

Jacobs, M.A. et al., 2005. Combined dynamic contrast enhanced breast MR and proton spectroscopic imaging: a feasibility study. *J Magn Reson Imaging*, 21(1), pp.23-28.

Jafari-Khouzani, K. et al., 2010. FLAIR signal and texture analysis for lateralizing mesial temporal lobe epilepsy. *Neuroimage*, 49(2), pp.1559-71.

Jain, A.K., 1989. *Fundamentals of digital image processing*. Englewood Cliffs: Prentice-Hall.

Jain, A.K. and Zhong, Y., 1996. Page segmentation using texture analysis. *Pattern Recognition*, 29, pp.743-70.

James, D., Clymer, B.D. and Schmalbrock, P., 2001. Texture detection of simulated microcalcification susceptibility effects in magnetic resonance imaging of breasts. *J Magn Reson Imaging*, 13(6), pp.876-81.

Jansen, S. et al., 2008. Differentiation between benign and malignant breast lesions detected by bilateral dynamic contrast-enhanced MRI: A sensitivity and specificity study. *Magnetic Resonance in Medicine*, 59(4), pp.747-54.

Jolliffe, I., 2005. Principal Component Analysis. In *Encyclopedia of Statistics in Behavioral Science*. New York: John Wiley and Sons. p.1580–1584.

Julesz, B., Gilbert, E.N., Shepp, L.A. and Frisch, H.L., 1973. Inability of humans to discriminate between visual textures that agree in second order statistics: Revisited. *Perception*, 2(4), pp.391-405.

Kaiser, W. and Zeitler, E., 1989. MR imaging of the breast: fast imaging sequences with and without Gd-DTPA. Preliminary observations. *Radiology*, 170(3 Pt 1), pp.681-86.

Karahaliou, A.N. et al., 2008. Breast cancer diagnosis: analyzing texture of tissue surrounding microcalcifications. *IEEE Trans Inf Technol Biomed*, 12(6), pp.731-38.

Karahaliou, A.N. et al., 2010. Assessing heterogeneity of lesion enhancement kinetics in dynamic contrast-enhanced MRI for breast cancer diagnosis. *Br J Radiol*, 83(988), pp.296-309.

Kelcz, F., Santyr, G.E., Cron, G.O. and Mongin, S.J., 1996. Application of a quantitative model to differentiate benign from malignant breast lesions detected by dynamic contrast-enhanced MRI. *J Magn Reson Imaging*, 6(5), pp.743–52.

Kociołek, M., Materka, A., Strzelecki, M. and Szczypiński, P., 2001. Discrete wavelet transform – derived features for digital image texture analysis. In: *Proc. of Interational Conference on Signals and Electronic Systems*. 18-21 September 2001. Lodz. pp. 111-116.

Konyer, N.B., Ramsay, E.A., Bronskill, M.J. and Plewes, D.B., 2002. Comparison of MR imaging breast coils. *Radiolog*, 222(3), pp.830-34.

Kovalev, V. and Kruggel, F., 2007. Texture anisotropy of the brain's white matter as revealed by anatomical MRI. *IEEE Trans Med Imaging*, 26(5), pp.678-85.

Kovalev, V.A., Kruggel, F. and von Cramon, D.Y., 2003. Gender and age effects in structural brain asymmetry as measured by MRI texture analysis. *Neuroimage*, 19(3), pp.895-905.

Kudo, M. and Sklansky, J., 2000. Comparison of algorithms that select features for pattern classifiers. *Pattern Recogn*, 33(1), pp.25-41.

Kuhl, C.K. et al., 1997. Healthy premenopausal breast parenchyma in dynamic contrast-enhanced MR imaging of the breast: normal contrast medium enhancement and cyclical-phase dependency. *Radiology*, 203(1), pp.137-44.

Kuhl, C. et al., 1999. Dynamic breast MR imaging: are signal intensity time course data useful for differential diagnosis of enhancing lesions? *Radiology*, 211(1), pp.101-10.

Kumar, R. et al., 2009. Comparative evaluation of corpus callosum DTI metrics in acute mild and moderate traumatic brain injury: its correlation with neuropsychometric tests. *Brain Inj*, 23(7), pp.675-85.

Larsson, H.B.W. et al., 1992. In vivo magnetic resonance diffusion measurements in the brain of patients with multiple sclerosis. *Magn Reson Imaging*, 10(1), pp.7-12.

Lee, A.H., Dublin, E.A., Bobrow, L.G. and Poulsom, R., 1998. Invasive lobular and invasive ductal carcinoma of the breast show distinct patterns of vascular endothelial growth factor expression and angiogenesis. *J Pathol*, 185(4), pp.394-401.

Lerski, R.A. et al., 1993. MR image texture analysis—an approach to tissue characterisation. *Magn reson imaging*, 11, pp.873-87.

Lezak, M., Hovieson, D. and Loring, D., 2004. *Neuropsychological assessment*. 4th ed. New York: Oxford University Press.

Lo, G.G. et al., 2009. Diffusion-weighted magnetic resonance imaging of breast lesions: first experiences at 3 T. *J Comput Assist Tomogr*, 33(1), pp.63-69.

Lo, C. et al., 2009. Diffusion tensor imaging abnormalities in patients with mild traumatic brain injury and neurocognitive impairment. *J Comput Assist Tomogr*, 33(2), pp.293-297.

Lucht, R.E., Knopp, M.V. and Brix, G., 2001. Classification of signal-time curves from dynamic MR mammography by neural networks. *Magn Reson Imaging*, 19(1), pp.51-57.

Macura, K.J., Ouwerkerk, R., Jacobs, M.A. and Bluemke, D.A., 2006. Patterns of enhancement on breast MR images: interpretation and imaging pitfalls. *Radiographics*, 26(6), pp.1719-34.

Madabhushi, A. and Udupa, J.K., 2005. Interplay between intensity standardization and inhomogeneity correction in MR images. *IEEE Trans Med Imaging* , 24(5), p.561–576.

Mahmoud-Ghoneim, D., Alkaabi, M.K., de Certaines, J.D. and Goettsche, F.M., 2008. The impact of image dynamic range on texture classification of brain white matter. *BMC Med Imaging*, 23, pp.8-18.

Mahmoud-Ghoneim, D., Toussaint, G., Constans, J. and de Certaines, J.D., 2003. Three dimensional texture analysis in MRI: A preliminary evaluation in gliomas. *Magn Reson Imaging*, 21(9), pp.983-87.

Mandelbrot, B.B., 1977. *Fractals: Form, chance and dimension.* San Francisco: Freeman.

Manjunath, B.S. and Chellappa, R., 1991. Unsupervised texture segmentation using markov random field models. *IEEE TPAMI*, 13(5), pp.478-82.

Manjunath, B.S. and Ma, W.Y., 1996. Texture features for browsing and retrieval of image data. *IEEE TPAMI*, 18, pp.837-42.

Mao, J. and Jain, A.K., 1992. Texture classification and segmentation using multiresolution simultaneous autoregressive models. *Pattern Recogn*, 25, pp.173-88.

Marini, C. et al., 2007. Quantitative diffusion weighted MR imaging in the differential diagnosis of breast lesion. *Eur Radiol*, 17(10), p.2646–2655.

Martel, A.L., Chan, R.W., Ramsay, E. and B, P.D., 2008. Removing Undersampling Artifacts in DCE-MRI Studies Using Independent Components Analysis. *Magnetic Resonance in Medicine*, 59(4), pp.874-78.

Ma, L., Tan, T., Wang, Y. and Zhang, D., 2003. Personal Identification Based on Iris Texture Analysis. *IEEE TPAMI*, 25(12), pp.1519-33.

Mathias, J.M., Tofts, P.S. and Losseff, N.A., 1999. Texture analysis of spinal cord pathology in multiple sclerosis. *Magn Reson Med*, 42(5), pp.929-35.

Mavroforakis, M.E. et al., 2006. Mammographic masses characterization based on localized texture and dataset fractal analysis using linear, neural and support vector machine classifiers. *Artif Intell Med*, 37(2), pp.145-62.

Ma, J. et al., 2006. Fat-suppressed threedimensional dual echo Dixon technique for contrast agent enhanced MRI. *J Magn Reson Imaging*, 23(1), pp.36-41.

Mayer, A.R. et al., 2010. A prospective diffusion tensor imaging study in mild traumatic brain injury. *Neurology*, 74(8), pp.643-50.

McDonald, W.I. et al., 2001. Recommended diagnostic criteria for multiple sclerosis: Guidelines from the international panel on the diagnosis of multiple sclerosis. *Ann Neurol* , 50(1), pp.121-27.

McLaren, C.E., Chen, W.P., Nie, K. and Su, M.Y., 2009. Prediction of malignant breast lesions from MRI features: a comparison of artificial neural network and logistic regression techniques. *Acad Radiol*, 16(7), pp.842-51.

Miller, P. and Astley, S., 1992. Classification of breast tissue by texture analysis. *Image Vis Comput*, 10, p.277–283.

Mori, S. and Barker, P.B., 1999. Diffusion magnetic resonance imaging: its principle and applications. *Anat Rec*, 257(3), pp.102-09.

Mori, S. and Van Zijl, P.C., 2002. Fiber tracking: principles and strategies- a technical review. *NMR Biomed*, 15(7-8), pp.468-80.

Morrell, R.G., 2006. Rapid fat suppression in MRI of the breast with short binomial pulses. *J Magn Reson Imaging*, 24(5), pp.1172-76.

Morrow, L.A. and Ryan, C., 2002. Normative data for a working memory test: the four word short-term memory test. *Clin Neuropsychol*, 16(3), pp.373-80.

Muralidhar, G.S. et al., 2011. Computer-aided diagnosis in breast magnetic resonance imaging. 78(2), pp.280-90.

Newell, D. et al., 2010. Selection of diagnostic features on breast MRI to differentiate between malignant and benign lesions using computer-aided diagnosis: differences in lesions presenting as mass and non-mass-like enhancement. *Eur Radiol*, 20(4), pp.771-81.

Nie, K. et al., 2008. Quantitative analysis of lesion morphology and texture features for diagnostic prediction in breast MRI. *Acad Radiol*, 15(12), pp.1513-25.

Noseworthy, J.H., Lucchinetti, C., Rodriguez, M. and Weinshenker, B.G., 2002. Multiple sclerosis. *N Engl J Med*, 343(13), pp.938-52.

Ojala, T., Pietikainen, M. and Harwood, D., 1996. A comparative study of texture measures with classification based on feature distributions. *Pattern Recogn*, 21(1), pp.51-59.

Ojala, T. and Pietikäinen, M., 1999. Unsupervised texture segmentation using feature distributions. *Pattern Recogn*, 32, pp.477-86.

Ojala, T., Pietikäinen, M. and Mäenpää, T., 2002. Multiresolution Gray-scale and Rotation Invariant Texture Classification with Local Binary Patterns. *IEEE TPAMI*, 24(7), pp.971-87.

Ojala, T., Valkealahti, K., Oja, E. and Pietikäinen, M., 2001. Texture discrimination with multidimensional distributions of signed gray level differences. *Pattern Recogn*, 34(3), pp.727-39.

Onesti, J.K., Mangus, B.E., Helmer, S.D. and Osland, J.S., 2008. Breast cancer tumor size: correlation between magnetic resonance imaging and pathology measurements. *Am J Surg*, 196(6), pp.844-50.

Orel, S.G., Schnall, M.D., LiVolsi, V.A. and Troupin, R.H., 2006. Suspicious breast lesions:MRimaging with radiologic-pathologic correlation. *Radiology*, 190(2), pp.485-93.

Padhani, A., 2002. Dynamic contrast-enhanced MRI in clinical oncology: Current status and future directions. *J Magn Reson Imaging*, 16(4), pp.407-22.

Partridge, S.C. et al., 2009. Quantitative diffusion- weighted imaging as an adjunct to conventional breast MRI for improved positive predictive value. *AJR*, 193(6), pp.1716-22.

Partridge, S.C. et al., 2010. Differential diagnosis of mammographically and clinically occult breast lesions on diffusion- weighted MRI. *J Magn Reson Imaging*, 31(3), pp.562-70.

Peng, Q., McColl, R.W., Wang, J. and Weatherall, P.T., 2005. Novel rapid fat suppression strategy with spectrally selective pulses. *Magn Reson Med*, 54(6), pp.1569-74.

Pentland, A.P., 1984. Fractal-based description of natural scenes. *IEEE TPAMI*, 6(6), pp.661-74.

Pereira, F.P., Martins, G. and Carvalhaes de Oliveira, R.V., 2011. Diffusion magnetic resonance imaging of the breast. *Mgn Reson Imaging Clin N Am*, 19(1), pp.95-110.

Peters, N.H. et al., 2008. Meta-analysis of MR imaging in the diagnosis of breast lesions. *Radiology*, 246(1), pp.116-24.

Polman, C.H. et al., 2005. Diagnostic criteria for multiple sclerosis: 2005 revisions to the "McDonald criteria". *Ann Neurol*, 58(6), pp.840-46.

Puig, D. and Garcia, M.S., 2006. Automatic texture feature selection for image pixel classification. *Pattern Recogn*, 39(11), pp.1996-2009.

Purcell, E., 1952. *Research in nuclear magnetism. Nobel lecture, Physics*. [Online] Available from: http://nobelprize.org/nobel_prizes/physics/laureates/1952/purcelllecture.pdf [Accessed April 2011].

Qian, S. and Chen, D., 1993. Discrete Gabor transform. *IEEE Transactions on Signal Processing*, 41(7), pp.2429 - 38.

Rabi, S., Madhavi, C., Antonisamy, B. and Koshi, R., 2007. Quantitative analysis of the human corpus callosum under light microscopy. *Eur J Anat*, 11, pp.95-100.

Rangayyan, R.M., Banik, S. and Desautels, J.E.J., 2010. Computer-aided detection of architectural distortion in prior mammograms of interval cancer. *Digit Imaging*, 23, pp.611-31.

Rausch, D.R. and Hendrick, R.E., 2006. How to optimize clinical breast MR imaging practices and techniques on your 1.5-T system. *RadioGraphics*, 26(5), pp.1469-84.

Reed, T.R. and Dubuf, J.M.H., 1993. A Review of Recent Texture Segmentation and Feature Extraction Techniques. *VGIP: Image Understanding*, 57(3), pp.359-72.

Rodenko, G.N. et al., 1996. MR Imaging in the management before surgery of lobular carcinoma of the breast: correlation with pathology. *Am J Roentgenol*, 167(6), pp.1415-19.

Rosen, P.P., 2001. Invasive lobular carcinoma. In P.P. Rosen, ed. *Rosen's Breast Pathology*. 2nd ed. Philadelphia: Lippincott Williams and Wilkins. p.627–652.

Russ, J.C., 2002. *The image processing handbook*. 4th ed. Boca Raton: CRC Press.

Rutgers, D.R. et al., 2008. White matter abnormalities in mild traumatic brain injury: a diffusion tensor imaging study. *AJNR Am J Neuroradiol*, 29(3), pp.514-19.

Sardanelli, F. et al., 2010. Magnetic resonance imaging of the breast: recommendations from the EUSOMA working group. *Eur J Cancer*, 46(8), pp.1296-316.

Saslow, D. et al., 2007. American Cancer Society Guidelines for Breast Screening with MRI as an Adjunct to Mammograph. *CA Cancer J Clin* , 57(2), p.75–89.

Schelfout, K. et al., 2004. Preoperative breast MRI in patients with invasive lobular breast cancer. *Eur Radiol*, 14(7), pp.1209-16.

Schnall, M.D. et al., 2001. A combined architectural and kinetic interpretation model for breast MR images. *Acad Radiol*, 8(7), pp.591-97.

Sharma, N. and Aggarwal, L.M., 2010. Automated medical image segmentation techniques. *J Med Phys*, 35, pp.3-14.

Simoncelli, E., 1997. Statistical Models for Images: Compression, Restoration and Synthesis. In *31st Asilomar Conference on Signals Systems, and Computers*. Pacific Grove, 1997.

Singh, S. and Gupta, R., 2011. Identification of components of fibroadenoma in cytology preparations using texture analysis: a morphometric study. *Cytopathology*. [Epub ahead of print].

Sinha, S., Bastin, M.E., Whittle, I.R. and Wardlaw, J.M., 2002. Diffusion tensor imaging of high-grade cerebral gliomas. *ANJR*, 23(4), pp.520-27.

Skaane, P., 1999. The additional value of US to mammography in the diagnosis of breast cancer. *Acta Radiol*, 40(5), p.486–490.

Strauss, E., Sherman, E.M.S. and Spreen, O., 2006. A compendium of neuropsychological tests. In *Administration, Norms, and Commentary*. 3rd ed. New York: Oxford University Press.

Sundgren, P.C. et al., 2004. Diffusion tensor imaging of the brain: review of clinical applications. *Neuroradiology*, 46(5), pp.339-50.

Tavassoli, F.A., 1999. Invasive lobular carcinoma. In F.A. Tavassoli, ed. *Pathology of the Breast*. 2nd ed. Stamford: CN: Appleton and Lange. pp.426–36.

Taylor, J. et al., 1999. MR imaging of tumor microcirculation: Promise for the new millennium. *J Magn Reson Imagin*, 10(6), pp.903–7.

Teasdale, G. and Jennett, B., 1973. Assessment of coma and impaired consciousness.A practical scale. *Lancet*, 2(7872), pp.81-84.

Theocharakis P, et al., 2009. Pattern recognition system for the discrimination of multiple sclerosis from cerebral microangiopathy lesions based on texture analysis of magnetic resonance images. *Magn Reson Imaging*, 27(3), pp.417-22.

Tofts, P., 2003. *Quantitative MRI of the Brain: Measuring Changes Caused by Disease*. John Wiley and Sons.

Tozaki, M. and Fukuma, E., 2009. 1H MR spectroscopy and diffusion-weighted imaging of the breast: are they useful tools for characterizing breast lesions before biopsy? *AJR*, 193(3), pp.840-49.

Tuceryan, M. and Jain, A.K., 1998. Texture Analysis. In Chen, C.H., Pau, L.F. and Wang, P.S.P. *The Handbook of Pattern Recognition and Computer Vision*. World Scientific Publishing Co. pp.207-48.

Turnbull, L., 2009. Dynamic contrast-enhanced MRI in the diagnosis and management of breast cancer. *NMR Biomed*, 22(1), pp.28-39.

Twellmann, T., Lichte, O. and Nattkemper, T.W., 2005. An adaptive tissue characterization network for model-free visualization of dynamic contrast-enhanced magnetic resonance image data. *IEEE Trans Med Imaging* , 24(10), pp.1256-66.

Tzacheva, A.A., Najarian, K. and Brockway, J.P., 2003. Breast Cancer Detection in Gadolinium-Enhanced MR Images by Static Region Descriptors and Neural Networks. *J Magn Reson Imaging*, 17, p.337–342.

Vainio, H. and Bianchini, F., eds., 2002. Breast Cancer Screening. In *IARC Handbooks of Cancer Prevention*. Lyon: IARC. p.248.

Varma, M. and Zisserman, A., 2003. Texture classification: are filter banks necessary? *CVPR03 II*, 2, pp.691-98.

Warren, P.A. and Mamassian, P., 2010. Recovery of surface pose from texture orientation statistics under perspective projection. *Biol Cybern*, 103(3), pp.199-212.

Warren, R.M.L. et al., 2005. Reading protocol for dynamic contrast-enhanced MR images of the breast: sensitivity and specificity analysis. *Radiology*, 236(3), pp.779-88.

Weishaupt, D., Köchli, V. and Marincek, B., 2008. *How does MRI work? An introduction to the Physics and Function of Magnetic Resoanance Imaging*. 2nd ed. Berlin Heidelberg: Springer.

Wellings, S.R., 2008. Development of human breast cancer. *Advances in cancer research*, 31, pp.287-314.

Wenkel, E. et al., 2007. Diffusion weighted imaging in breast MRI: comparison of two different pulse sequences. *Acad Radiol*, 14(9), pp.1077- 83.

Weszka, J.S. and Rosenfeld, A., 1976. An application of texture analysis to materials inspection. *Pattern Recognition*, 8(4), pp.195-200.

Wilde, E.A. et al., 2008. Diffusion tensor imaging of acute mild traumatic brain injury in adolescents. *Neurology* , 70(12), pp.948-55.

Wood, C., 2005. Computer Aided Detection (CAD) for breast MRI. *Technol Cancer Res Treat*, 4(1), pp.49-53.

Woods, B.J. et al., 2007. Malignant-lesion segmentation using 4D co- occurrence texture analysis applied to dynamic contrast-enhanced magnetic resonance breast image data. *J Magn Reson Imaging*, 25(3), pp.495-501.

Vovk, U., Pernus, F. and Likar, B., 2007. A review of methods for correction of intensity inhomogeneity in MRI. *IEEE Trans Med Imaging* , 26(3), p.405–421.

Xie, X., 2007. A Review of Recent Advances in Surface Defect Detection using Texture analysis Techniques. *ELCVIA*, 29, pp.701-17.

Yeatman, T.J. et al., 1995. Tumor biology of infiltrating lobular carcinoma: implications for management. *Ann Surg*, 222(4), p.549–559.

Yeh, E.D. et al., 2003. Invasive Lobular Carcinoma: Spectrum of Enhancement and Morphology on Magnetic Resonance Imaging. *The Breast Journal*, 9(1), pp.13-18.

Yuan, W. et al., 2007. Diffusion tensor MR imaging reveals persistent white matter alteration after traumatic brain injury experienced during early childhood. *AJNR Am J Neuroradiol*, 28(10), pp.1919-25.

Yu, O., Mauss, Y., Namer, I.J. and Chambron, J., 2001. Existence of contralateral abnormalities revealed by texture analysis in unilateral intractable hippocampal epilepsy. *Magn reson imaging*, 19(10), pp.1305-10.

Yu, O. et al., 1999. Distinct patterns of active and non-active plaques using texture analysis on brain NMR images in multiple sclerosis patients: preliminary results. *Magn Reson Imaging*, 17(9), pp.1261-67.

Zacharaki, E.I. et al., 2009. Classification of brain tumor type and grade using MRI texture and shape in a machine learning scheme. *Magn Reson in Medicine*, 62(6), pp.1609-18.

Zhang, J., Tong, L., Wang, L. and Li, N., 2008. Texture analysis of multiple sclerosis: a comparative study. *Magn Reson Imaging*, 26(8), pp.1160-66.

Zhang, D., Wong, A., Indrawan, M. and Lu, G., 2000. Content-based Image Retrieval Using Gabor Texture Features. *IEEE TPAMI*, pp.13-15.

Zhonker, D. and Jain, A., 1996. Algorithms for feature selection: an evaluation. In *13th International Conference of Pattern Recognition*. Vienna, 1996. IEEE Computer Society Press.

Zhuge, Y., Udupa, J.K., Liu, J. and Saha, P.K., 2009. Image background inhomogeneity correction in MRI via intensity standardization. *Comp Med Imaging Graph*, 33(1), pp.7–16.

8. APPENDIX 1

Histogram-based features:

Within defined ROI a histogram distribution of the image is computed. Assuming that p(i) is a normalized histogram value for a grey level i and N denotes number of grey levels in the image – nine features are calculated: Mean, Variance, Skewness, Kurtosis, Perc.1%, Perc.10%, Perc.50%, Perc.90% and Perc.99%.

Mean: $$\mu = \sum_{i=1}^{N} ip(i)$$

Variance: $$\sigma^2 = \sum_{i=1}^{N} (i-\mu)^2 p(i)$$

Skewness: $$\mu_3 = \sigma^{-3} \sum_{i=1}^{N} (i-\mu)^3 p(i)$$

Kurtosis: $$\mu_4 = \sigma^{-4} \sum_{i=1}^{N} (i-\mu)^4 p(i) - 3$$

Perc. K%: $$[k] = \left\{ k \left(\sum_{i=1}^{k} p(i) \right) \left(\sum_{i=1}^{N} p(i) \right)^{-1} = K\% \right\}$$

Gradient-based features:

For the gradient feature calculation the following neighbourhood for image pixel $x(i,j)$ is defined:

A	B	C	D	E
F	G	H	I	J
K	L	$x(i,j)$	N	O
P	Q	R	S	T
U	V	W	Y	Z

The absolute value of image gradient $(ABSV(i,j))$ is calculated for each 5x5 pixel neighbourhood:

$$ABSV(i,j) = \sqrt{(W-C)^2 + (O-K)^2}$$

Based on this matrix, the gradient features are defined:

Mean absolute gradient $$g_1 = \frac{1}{x(i,j)} \sum_{i,j \in ROI} ABSV(i,j)$$

Variance of absolute gradient: $$g_2 = \frac{1}{x(i,j)} \sum_{i,j \in ROI} (ABSV(i,j) - g_1)^2$$

Skewness of absolute gradient: $$g_3 = \frac{1}{\left(\sqrt{g_2}\right)^3} \frac{1}{x(i,j)} \sum_{i,j \in ROI} (ABSV(i,j) - g_1)^3$$

Kurtosis of absolute gradient: $$g_4 = \frac{1}{\left(\sqrt{g_2}\right)^4} \frac{1}{x(i,j)} \sum_{i,j \in ROI} (ABSV(i,j) - g_1)^4 - 3$$

Run- length matrix based features:

The 5 run-length matrix parameters are calculated for four directions providing 20 parameters. The elements of run-length matrix represent the number of times there is a run of length *j* having grey level *i*. N_g is the number of grey levels and N_r is the number of runs.

Short run emphasis inverse moments: $$r_1 = \left(\sum_{i=1}^{N_g} \sum_{j=1}^{N_r} \frac{p(i,j)}{j^2} \right) / C$$

Long run emphasis moments: $$r_2 = \left(\sum_{i=1}^{N_g} \sum_{j=1}^{N_r} j^2 p(i,j) \right) / C$$

Grey level nonuniformity: $$r_3 = \left(\sum_{i=1}^{N_g} \left(\sum_{j=1}^{N_r} p(i,j) \right)^2 \right) / C$$

Run length nonuniformity: $$r_4 = \left(\sum_{j=1}^{N_r} \left(\sum_{i=1}^{N_g} p(i,j) \right)^2 \right) / C$$

Fraction of image in runs: $$r_5 = \left(\sum_{i=1}^{N_g} \sum_{j=1}^{N_r} j(i,j) / \sum_{i=1}^{N_g} \sum_{j=1}^{N_r} jp(i,j) \right)$$

The coefficient C is defined as $$C = \sum_{i=1}^{N_g} \sum_{j=1}^{N_r} p(i,j)$$

Co-occurrence matrix based features:

The second-order histogram is defined as the co-occurrence matrix $P_{d\theta}(i,j)$ where d is distance (d = 1, 2 3, 4, 5) and θ is angle (0, 45°, 90°, 135°) between two pixels.

The given the image $f(x,y)$ with a set of N_g discrete intensity levels, the matrix $P_{d\theta}(i,j)$ is defined such that its (i,j)th entry is equal to the number of times that

$f(x_1, y_1) = i$ and $f(x_2, y_2) = j$,

where $(x_2, y_2) = (x_1, y_1) + (d\cos\theta, \sin\theta)$.

$R(d,\theta)$ is the total number of neighbouring pixels in ROI.

The (i,j)th entry in a normalized co-occurrence matrix $p(i,j) = P(i,j)$/R.

Marginal-probability matrices

$$p_x(i) = \sum_{j=1}^{N_g} P(i, j),$$

$$p_y(j) = \sum_{i=1}^{N_g} P(i, j)$$

Means of the p_x, p_y are μ_x, μ_y and standard deviations are σ_x, σ_y.

$$p_{x+y}(k) = \sum_{\substack{i=1 \\ i+j=k}}^{N_g} \sum_{j=k}^{N_g} p(i, j) \qquad k = 2,3....,2N_g$$

$$p_{x+y}(k) = \sum_{\substack{i=1 \\ |i+j|=k}}^{N_g} \sum_{j=k}^{N_g} p(i, j) \qquad k = 0,1,....,N_g - 1$$

Means of the p_{x+y}, p_{x-y} are μ_{x+y}, μ_{x-y} and standard deviations are σ_{x+y}, σ_{x-y}.

Angular second moment:

$$f_1 = \sum_{i=1}^{N_g}\sum_{j=1}^{N_g} p(i,j)^2$$

Contrast:

$$f_2 = \sum_{n=0}^{N_g-1} n^2 \sum_{\substack{i=1 \\ |i-j|=n}}^{N_g}\sum_{j=1}^{N_g} p(i,j)$$

Correlation:

$$f_3 = \frac{\sum_{i=1}^{N_g}\sum_{j=1}^{N_g} ijp(i,j) - \mu_x\mu_y}{\rho_x\rho_y}$$

Sum of squares:

$$f_4 = \sum_{i=1}^{N_g}\sum_{j=1}^{N_g} (i-\mu_x)^2\, p(i,j)$$

Inverse difference moment:

$$f_5 = \sum_{i=1}^{N_g}\sum_{j=1}^{N_g} \frac{1}{1+(i-j)^2}\, p(i,j)$$

Sum average:

$$f_6 = \sum_{i=1}^{N_g}\sum_{j=1}^{N_g} ip_{x+y}(i)$$

Sum variance:

$$f_7 = \sum_{i=1}^{N_g}\sum_{j=1}^{N_g} (i-f_6)^2\, p_{x+y}(i)$$

Sum entropy:

$$f_8 = -\sum_{i=1}^{N_g} p_{x+y}(i)\log\left(p_{x+y}(i)\right)$$

Entropy:

$$f_9 = -\sum_{i=1}^{N_g}\sum_{j=k}^{N_g} p(i,j)\log\left(p(i,j)\right)$$

Difference variance: $$f_{10} = \sum_{i=0}^{N_g-1} \left(i - \mu_{x-y}\right)^2 p_{x-y}(i)$$

Difference entropy: $$f_{11} = -\sum_{i=1}^{N_g-1} p_{x+y}(i) \log\left(p_{x+y}(i)\right)$$

Wavelet-based features:

At the present, only a simple Harr wavelet transform is considered in MaZda software and only one feature (Energy) is calculated. The Energy feature is computed for each subband.

$$E_{subband,scale} = \sum_{x,y \in ROI} \left(i_{x,y}^{subband}\right)^2 / n$$

where the parameter $i_{x,y}$ is a resulting matrix element. Summation is performed for every pixel (x,y) located in the defined ROI and where *n* is the number of pixels.

Autoregressive model parameters:

The autoregressive (AR) model assumes a local interaction between image pixels in that pixel intensity is a weighted sum of neighbouring pixel intensities. Assuming image *f* is a zero-mean random field, an AR causal model can be defined as:

$$f_s = \sum_{r \in N_s} \theta_r f_r + e_s$$

where f_s is the image intensity at site *s*
e_s denotes an independent and identically distributed noise
σ is the standard deviation of the driving noise e_s
N_s is a neighbourhood of *s*
θ = [Teta1, Teta2, Teta3, Teta4] is a vector of model parameters.
Local neighbourhood of image element f_s

O	O	O	O	O
O	O^{θ_2}	O^{θ_3}	O^{θ_4}	O
O	O^{θ_1}	O^{s}	O	O
O	O	O	O	O

The parameters can be estimated by minimizing the sum of squared error,

$$\sum_S e_S^2 = \sum \left(f_S - \hat{\theta} w_s \right)^2$$

which leads to the following linear equations:

$$\hat{\theta} = \left(\sum_s w_s w_s^T \right)^{-1} \left(\sum_s w_s f_s \right) \qquad \sigma^2 = N^{-2} \sum \left(f_s - \theta \hat{w}_s \right)^2$$

where w_s = col[f_i, $i \in N_s$], and the square $N \times N$ image is assumed.

ORIGINAL PUBLICATIONS

Tampereen teknillinen yliopisto
PL 527
33101 Tampere

Tampere University of Technology
P.O.B. 527
FI-33101 Tampere, Finland

ISBN 978-952-15-2656-5
ISSN 1459-2045